Universidad Nacional Autónoma de México
Programa de Posgrado en Ciencias Fisicas
Departamento de Gravitación y Teoría de Campos,
Instituto de Ciencias Nucleares

Non-linear analysis of solar system tests in $f(R)$ gravity

T E S I S

que para optar por el grado de

Maestro en ciencias físicas

PRESENTA:
Hodek Mealstrom García Tavera

Tutor Principal:
Dr. Marcelo Salgado Rodríguez
Instituto de Ciencias Nucleares - UNAM

Comité Tutor
Dr. Miguel Alcubierre Moya
Instituto de Ciencias Nucleares - UNAM
Dr. Juan Carlos Degollado Daza
Instituto de Ciencias Físicas - UNAM

Ciudad Universitaria, CDMX, Febrero, 2023

Atarse a algo.
A una huerta, un bosque, una planta, una palabra.
Atarse a algo que tenga raíz, anudarse para no perderse
en el viento que sopla sobre la pampa y llama.
Los Llanos, Federico Falco

Abstract

Several modifications to the standard theory of General Relativity (GR) have been proposed to explain the currently observed accelerated expansion of the Universe, which is a major challenge to cosmology. In this thesis, we study $f(R)$ gravity which is a class of metric theories of gravity that offers viable models for dark energy. In particular we focus on the proposed models by Hu-Sawicki and Starobinsky. These theories, apart from the extra scalar degree of freedom with respect to GR, necessarily contain a built in scale of the order of the observed cosmological constant. Thus, they suffer from an inherent contrast problem due to the abysmal difference of curvature scales when confronted in scenarios such as the solar system and neutron stars. These models claim to pass both the solar system and the laboratory tests by means of an *a priori* assumptions about mechanisms that screen their effects in high density environments. For this regard, we explore numerically the solution space of static and spherical symmetric spacetimes by taking into account the modified $f(R)$ equations for stellar structure.

We start by calibrating our code by reproducing the well known results of hydrostatic equilibrium in GR through an incompressible fluid and a variety of polytropic equations of state (EoSs). Thereafter we analyze and check the solutions for constant density objects within the $f(R)$ field equations without resorting to the usual scalar-tensor transformation. To deal in the best manner possible with the curvature scale difference, which translates itself into a numerical contrast, we implement arbitrary precision arithmetic and higher order Runge-Kutta methods with adaptive size. Although some stellar configurations can be constructed, we argue that is not possible to find solutions for any of the $f(R)$ gravity models considered that have the density and pressure of the Sun. Our results thus rais serious doubts about the non-linear studies of $f(R)$ gravity with respect the solar system tests.

Finally, we elaborate on R-squared $f(R)$ model which does not suffer from the numerical contrast since it is not a cosmological motivated model. We perform the same analysis and find mass-radius diagrams for static neutron star models. However, although is not as difficult to obtain solutions as in the cosmological motivated $f(R)$ models, we advocate that the built in scale assumed in this $f(R)$ models is rather artificial and presumably selected in an *ad-hoc* manner in order to avoid the contrast problem alluded above. Moreover, it is not clear that this quadratic $f(R)$ models pass the solar system tests or other tests.

Resumen

Se han propuesto múltiples modificaciones a la teoría estándar de la Relatividad General (RG) con el objetivo de explicar la expansión acelerado del Universo, la cual representa un gran desafío para la cosmología actual. En esta tesis se analiza la teoría $f(R)$ que es una teoría modificada de la gravedad métrica. Dicha teoría provee un modelo alternativo para explicar a la energía oscura. En particular, se analizan los modelos propuestos por Hu-Sawicki y Starobinsky. Estas teorías, además de contar con grado escalar extra de libertad con respecto a RG, necesariamente contienen una escala de curvatura intrínseca que es del orden de la constante cosmológica observada. Por lo tanto, sufren de un inherente problema de contraste debido a la diferencia abismal entre las escalas de curvatura cuando se confrontan en escenarios como el sistema solar y las estrellas de neutrones. Estos modelos pretenden pasar las pruebas tanto del sistema solar como de laboratorio por medio de mecanismos que ocultan sus efectos en entornos de alta densidad estelar. Para este propósito, se explora numéricamente el espacio de soluciones de espacios-tiempo estáticos y simétricamente esféricos para estos modelos teniendo en cuenta las ecuaciones modificadas de la teoría $f(R)$ para la estructura estelar.

Para calibrar el código numérico desarrollado se reproducen los resultados bien conocidos del equilibrio hidrostático en RG a través de un fluido incompresible y una variedad de ecuaciones de estado politrópicas. Posteriormente se analizan y verifican las soluciones para objetos con densidad constante dentro de las ecuaciones de campo de los modelos $f(R)$ sin recurrir a la transformación escalar-tensorial habitual. Para tratar de la mejor manera posible con la diferencia de la escala de curvatura, que se traduce en un contraste numérico, se implementa aritmética de precisión arbitraria y métodos de Runge-Kutta de orden superior con paso adaptativo. Si bien es posible construir algunas configuraciones estelares, no es posible encontrar soluciones para ninguno de los modelos de gravedad $f(R)$ considerados que tengan la densidad y la presión del Sol. Los resultados plantean serias dudas sobre los estudios no lineales de la gravedad $f(R)$ en el contexto de las pruebas del sistema solar.

Finalmente, se elabora sobre el modelo de gravedad *R-squared* $f(R)$ que no sufre del contraste numérico antes mencionado ya que no es un modelo motivado por la cosmología. Se realiza el mismo análisis y además se obtienen las curvas radio-masa para modelos estáticos de estrellas de neutrones. Sin embargo, aunque no es tan difícil obtener soluciones como en los modelos $f(R)$ motivados cosmológicamente, se concluye que la escala incorporada asumida en estos modelos $f(R)$ es más bien artificial, presumiblemente seleccionada de manera *ad-hoc*. Con lo anterior, no es posible esclarecer como estos modelos cuadráticos $f(R)$ pasan las pruebas del sistema solar u otras pruebas de escalas similares.

Contents

Chapter 1

Introduction

Since the discovery of the accelerated expansion of the universe by several independent observations [3, 111, 120, 149] a plethora of studies in cosmology have been devoted to understand and explain this late-time acceleration era.[1] The current paradigm appeals to the existence of a cosmological constant Λ, better known as the *dark energy* component, along with the introduction of the so called *dark matter*. Both account for the dark sector of the universe which has been thoroughly modeled by many proposals [46, 131] and has been measured to a tremendous accuracy. In particular, if General Relativity (GR), which is widely accepted as the fundamental theory of gravity [148], is assumed, a flawed picture of the universe emerges. The dark sector accounts for approximately the 96% of its material content, 70% given by the dark energy fluid of negative pressure, whose origin is currently unable to be explained, and the rest by cold dark matter (CDM), whose origin is also unclear. The resulting description has become known as the concordance ΛCDM Model [15]. Although this candidate matches cosmological observations well it is plagued by several theoretical and epistemological issues including the well known fine-tuning problem related to the vacuum energy scale [38].

In rough terms, there are two main lines of thought to explain the accelerated expansion aiming to avoid the need of dark components. The first one being looking for possible candidates in the realm of particle physics, those that encompasses cosmic fluids with exotic equations of state. On the other hand, if one assumes that GR cannot describe in a suitable manner the universe at large scales without resorting to Λ, then it is always permissible to propose new theories purely in the gravitational sector.

Within the vast realm of modifications to GR, $f(R)$ gravity stands as one of the simplest and most extensively studied metric theories, which is a particular class of higher derivative gravity theories where the Einstein-Hilbert action is replaced by an *a priori* arbitrary function of the curvature scalar, while the matter part of the action is left unchanged, at least the part of the matter sector aimed to explain the dark energy (see e.g. [32, 35, 50, 52, 104, 134] for extensive reviews). Such theories have some important cosmological implications [75, 79, 137, 140]. For instance, several of these theories naturally admit a phase of late-time accelerated expansion.

[1] Not to mention the other phase of cosmic acceleration which is believed to have occurred prior to the radiation domination era, i.e., during the stages of evolution of the universe also known as the *inflation* epoch (see [93] and references therein).

Therefore, it can be thought that dark energy has a geometric origin. Indeed, it has been shown that for many choices of the function $f(R)$, acceptable cosmological solutions appear. Also, many of these $f(R)$ models show several interesting observational signatures such as the modification to the spectra of galaxy clustering, gravitational weak lensing, CMB, etc [31, 60, 74, 81, 98, 106, 131, 132].

In this way, $f(R)$ provides a nontrivial alternative to the ΛCDM and more specifically an alternative to dark energy or the cosmological constant. However, it turns out that to construct a self-consistent theory that is not only compatible with the cosmological observation but also with the laboratory and astrophysical local system tests (e.g. solar-system tests, binary pulsar phenomenology) is not an easy task. That is, a consistent theory of gravity should be equally applicable to all gravity regimes. Notwithstanding, many of the early $f(R)$ models were ruled out by observational evidence and some theoretical arguments (e.g. presence of ghosts and tachions). After several detours, it has been clear that for a viable $f(R)$, certain conditions and constraints must be satisfied in order to preserve stability and feasibility under a variety of theoretical and experimental tests. A handful of models which we focus on this thesis have been carefully constructed to meet these requirements [75, 96, 137].

The obvious difficulty of explaining the dark sector relying on modifications of GR, such as $f(R)$ gravity, lies precisely in the tremendous agreement between local observables and GR, including the recent detection of gravitational waves [19, 81, 151]. In this way, testing $f(R)$ models in our local environment while leaving the large scale behavior unaffected, besides helping to constraint viable theories beyond Einstenian gravity in this regime, leads to investigate whether the GR stringent local bounds (solar system tests) are sufficient to rule out modified gravity scenerios, since there is no *a priori* fundamental principle to single out a particular model.

As argued by Weinberg [150], modifications to GR necessarily introduces additional degrees of freedom. However, introducing these dynamical quantities to drive modifications to gravity at cosmological scales without any consequences in dramatically different curvature scales has proven a subtle issue. In this context, it is well known that the entire class of $f(R)$ models are dynamically equivalent to a specific kind of scalar-tensor theory (see e.g. [30, 134, 146] for a review). Thus, $f(R)$ gravity has an extra single scalar degree of freedom with respect to GR. In this vein, most of the analysis has followed at least three distinct, but equivalent, approaches under the metric formalism.[2] Among these, two of them consist of recasting the $f(R)$ action into a Brans-Dicke (BD) theory with BD parameter, $\omega = 0$. One can discuss the theory in terms of the original metric g_{ab} or alternatively makes use of a conformal transformation to reveal a scalar field coupled nonminimally to matter via a Weyl rescaling of the metric. The former viewpoint is known as the Jordan Frame (JF) and the latter as the Einstein Frame (EF). However, several misconceptions have arisen in the past regarding the transformations used to redefine the fields. Recently, a third more robust approach has been proposed by Jaime et al. [78] which consists in leaving the original $f(R)$ action functional as it is, without mapping it to their BD counterpart, maintaining the Ricci scalar R as the independent degree of freedom. The advantages respect to JF and EF viewpoints are that the third approach is a more straightforward and cleaner way to perform calculations and draw numerical conclusions avoiding the common complications of going back and forth between different schemes. In this thesis we follow this approach.

[2] Equivalent at least under certain conditions. We will expand on this subject in Chapter 3 and briefly mention the Palatini formalism of $f(R)$ gravity which is at some point a completely different theory.

Notwithstanding, in all the aforementioned approaches, the scalar degree of freedom has a non-linear potential that depends on the form of the $f(R)$ model considered and whose effective mass depends on the local matter density through the trace of the energy-momentum tensor. It is precisely this nontrivial potential responsible for possible deviations to GR in high density regions, such as Milky way or our sun. Indeed, the metric around stars such as the Sun might be different in this class of theories.

As emphasized by some authors [61, 78], the failure to find a unique exterior solution for a stellar object that matches an asymptotic Schwarzschild-de Sitter spacetime could be a decisive factor to rule out $f(R)$ models that are cosmologically viable. As we will explain later in further detail, studies of the physics of these theories are hampered by the complexity of the field equations, making it difficult to obtain exact and numerical solutions, even in highly symmetric spacetimes.

In fact, since the beginning of the study of $f(R)$ theories, the existence of the scalar degree of freedom has been a subject of debate. On the earlier controversial studies regarding the existence of relativistic extended objects within $f(R)$ gravity the analysis done by Kobayashi and Maeda [88] stands because of his main conclusions. It was claimed that relativistic stars are unable to exist in the $f(R)$ model proposed by Starobinsky [137]. They point to a *cuvature singularity* developed within the object[3] which is the same anticipated by Frolov [66]. However, subsequent works showed explicitly that this claim does not hold [12, 78, 145] and was unphysical due to numerical instabilities. As shown by [78, 79], the singular behavior is not intrinsic to the theory, but mainly due to specific formulations of $f(R)$ gravity. Moreover, the viability of $f(R)$ models regarding solar system constraints has been unclear, to the extent that some authors simply thought it as dependent on the point of view [41, 64]. More specifically, as we mentioned before, when mapping $f(R)$ gravity to a BD theory, $\omega = 0$ while the observations lead to a value where $\omega \sim 40000$. Therefore, apparently $f(R)$ gravity fails four orders of magnitude. Nonetheless, the caveat is an argument when one does not consider the scalar potential associated with the $f(R)$ theory.

When trying to obtain stellar like solutions numerically, the main difficulty encountered lies on the fact that two completely different density (or curvature) scales are involved. Indeed, the central density of our Sun ($\rho_\odot \sim 10^3 \mathrm{kg/m}^3$) is enormously bigger compared to the density associated with the cosmological constant ($\rho_\Lambda \sim 10^{-27} \mathrm{kg/m}^3$). The situation is even more dramatic when neutron stars are considered ($\rho_{\mathrm{NS}} \sim 10^{14} \mathrm{kg/m}^3$). In the past, the numerical challenges were usually overcomed by restricting the central densities to that of unrealistic stars with $\rho_c \sim 10^2 \rho_\Lambda$, which are far from sun like densities $\rho_\odot \sim 10^{30} \rho_\Lambda$ and way off typical neutron star densities $\rho_c \sim 43 \rho_\Lambda$ [12, 77, 78, 88, 145].

Given this density difference, one usually resort to a mechanism to suppress its potential signature on observable parameters. To this end, several theories of gravity that introduce an extra scalar degree of freedom rely on precisely on *screening mechanisms* which act like suppressors to deviations from GR (for a detailed review see Refs. [19, 82]) in order to be able to pass solar system tests. However, as Negrelli et al. [103] point out, screening effects depend crucially on the shape of the scalar-field potential, which directly depends on the $f(R)$ model at hand and not the approach taken to specify the additional scalar degree of freedom. Moreover, those screening effects are independent of the chosen frame and therefore one can use the robust approach

[3] A similar singularity is found in a cosmological setting [66] associated with an ill-defined potential.

put forwarded by Jaime et al. [78]. Thus, the metric obtained after numerical integration of the hydrostatic equilibrium equations in $f(R)$ gravity with realistic central densities must reflect this condition. However, no such full numerical solutions are found anywhere in literature, as far as the author is concerned.

The goal of this thesis is to analyze numerically the full non-linear equations of $f(R)$ gravity with realistic central densities, using novel numerical integrators and high-precision numerical arithmetic, and explore the viability of these theories with a handful of the most studied $f(R)$ models presented in literature. The thesis layout is as follows. In Chapter 2, we review stellar solutions under GR. We also obtain numerical solutions of neutron stars given polytropic equations of state. In Chapter 3, the formalism of $f(R)$ gravity is presented, we briefly expand and elaborate on its cosmological implications. In Chapter 4, the spherical and symmetrical solutions in $f(R)$ gravity are derived and integrated numerically, and we discuss and compare our results with other studies. Finally, in Chapter 5 we elaborate on the R-squared $f(R)$ model and draw some conclusions.

Notations and Conventions

Throughout this thesis, units where $c = 1$ are assumed unless specified otherwise. We follow the conventions and notation of Wald [148]. In particular, the metric signature is $(-,+,+,+)$ and the Einstein summation convention is used given the abstract index notation (latin characters $a, b, c, \cdots$). The spacetime is represented by a 4-dimensional manifold M with lorentzian metric g_{ab} associated with the covariant derivative ∇_a (i.e., $\nabla_a g_{bc} = 0$).

Chapter 2

Stars in General Relativity

In this chapter we review the most relevant aspects of GR for stellar applications. We refer the reader to Refs. [112, 129, 139] for more detailed treatments. We obtain numerical solutions for the equations of stellar structure for an incompressible fluid and polytropic models for the Sun and neutron stars. The goal of this preliminary study is to calibrate the code that is later generalized for $f(R)$ gravity.

2.1 Spherical bodies in hydrostatic equilibrium

A non-rotating spherical star is considered a *self-gravitating fluid* configuration in hydrostatic equilibrium. It is assumed as an isolated body which consist of a fluid-filled interior region and a vacuum exterior region. Both regions are solution of the Einstein field equations[1] and therefore satisfy the conservation of rest mass, energy and momentum

$$R_{ab} - \frac{1}{2} g_{ab} R = \kappa T_{ab}, \tag{2.1a}$$

$$\nabla_a T^{ab} = 0, \tag{2.1b}$$

where T_{ab} is the energy-momentum tensor for a perfect fluid given by

$$T_{ab} = (p + \rho) u_a u_b + g_{ab} p. \tag{2.2}$$

We recall that ρ, p and u^a are the total mass-energy density, the pressure and the fluid four-velocity, respectively. The exterior solution is already known and is provided by *Birkhoff's Theorem*: The only vacuum, spherically symmetric gravitational field is static and is called the Schwarzschild metric [148], given in area coordinates by

$$ds^2 = -\left(1 - \frac{R_s}{r}\right) dt^2 + \left(1 - \frac{R_s}{r}\right)^{-1} dr^2 + r^2 d\Omega^2, \tag{2.3}$$

[1] We use units where $c = 1$ so $\kappa = 8\pi G$.

with r_s being the Schwarzschild radius

$$R_s := \frac{2GM}{c^2} \approx 3\left(\frac{M}{M_\odot}\right)\text{km}. \tag{2.4}$$

where $M_\odot$ is the mass of the Sun and M is the mass of the source. Thus, the Schwarzschild metric applies everywhere outside a spherical star, right up to its surface. Let us briefly mention the weak field limit of the Schwarzschild solution. The transformation

$$r = r_{\rm iso}\left(1 + \frac{R_s}{4r_{\rm iso}}\right), \tag{2.5}$$

takes the Schwarzschild metric (2.3) into isotropic coordinates

$$ds^2 = -\left(\frac{1 - R_s/4r_{\rm iso}}{1 + R_s/4r_{\rm iso}}\right)^2 dt^2 + \left(1 + \frac{R_s}{4r_{\rm iso}}\right)^4 \left[dr_{\rm iso}^2 + r_{\rm iso}^2 d\Omega^2\right]. \tag{2.6}$$

We note that the spatial part of Eq. (2.6) is conformal to an euclidean metric. Knowing that the gravitational potential generated by our Sun is small $U \sim GM_\odot/r$ (for $r \geq r_\odot$) the metric can be expanded in powers of U, since $r_{\rm iso}$ is large compared to the Schwarzschild R_s. The components take the form

$$g_{00} = -1 + \frac{R_s}{r_{\rm iso}} - \frac{1}{2}\left(\frac{R_s}{r_{\rm iso}}\right)^2 + \cdots = -1 + 2U - 2U^2 + \cdots \tag{2.7}$$

$$g_{jk} = \delta_{jk}\left(1 + \frac{R_s}{r_{\rm iso}} + \frac{3}{8}\left(\frac{R_s}{r_{\rm iso}}\right)^2 + \cdots\right) = \delta_{jk}(1 + 2U + \cdots). \tag{2.8}$$

As we will discuss later, in the case of solar system tests, deviations from GR account for departures from the metric (2.6) and can be parametrized as follows

$$g_{00} = -1 + 2U - 2\beta U^2 + \cdots \tag{2.9}$$

$$g_{jk} = \delta_{jk}(1 + 2\gamma U + \cdots), \tag{2.10}$$

where $\gamma = \beta = 1$ are the only two non-zero post-Newtonian parameters in GR and are in very good agreement with current experimental bounds [112, 151]. For instance, the current measured γ value is found to be [20],

$$|\gamma - 1| \lesssim 2.3 \times 10^{-5}. \tag{2.11}$$

2.1.1 Equations of stellar structure

We turn our attention to the properties of hydrostatic equilibrium inside the star. The interior metric needs to be determined from Eqs. (2.1). Because of hydrostatic equilibrium, the interior of the metric is time-independent. Also, since it is spherically symmetric, we already know that

such spacetime is of the same form as (2.3) [2], specifically

$$ds^2 = -e^{2\Phi}dt^2 + e^{2\lambda}dr^2 + r^2 d\Omega^2 \tag{2.12}$$

where Φ and λ are functions of r. Following the treatment given by Rezzolla and Zanotti [119], we take the operator $h_{ab} = g_{ab} + u_a u_b$, which projects any tensor onto the hypersurface orthogonal to the fluid four-velocity, on Eq. (2.1b), keeping T_{ab} as in given previously in Eq. (2.2). Thus,

$$(\rho + p)u^a \nabla_a u_b = -h_b^c \partial_c p, \tag{2.13}$$

which are the general-relativistic Euler equations. Finally, if the conditions of staticity and spherical symmetry are imposed, Eqs. (2.13) reduces to

$$\frac{dp}{dr} = -(\rho + p)\frac{d\Phi}{dr}. \tag{2.14}$$

On the other hand, inserting the metric (2.12) in the GR field equations (2.1a), we obtain, for the tt- component

$$\frac{1}{r^2}\frac{d}{dr}(r(1 - e^{2\lambda})) = 8\pi\rho, \tag{2.15}$$

from where it follows

$$e^{2\lambda} = \left[1 - \frac{2G\mu(r)}{r}\right]^{-1}, \tag{2.16}$$

where

$$\mu(r) := 4\pi \int_0^r \rho(r') r'^2 dr'. \tag{2.17}$$

Recalling that outside a star the solution needs to match the Schwarzschild metric (2.3), $\mu(r)$ represents the gravitational mass-energy inside a sphere of radius r. On the other hand, the remaining components of the Einstein field equations lead to

$$\frac{d\Phi}{dr} = \frac{\mu(r) + 4\pi r^3 p}{r(r - 2G\mu(r))}. \tag{2.18}$$

Eqs. (2.15), (2.18), (2.14) together with an equation of state (EoS)[3] completely determine the entire structure of a compact star and are called the Tolman Oppenheimer-Volkoff (TOV) equations. Written in this form, it is straightforward to see that in the Newtonian limit, that is when $r^3 P \ll \mu(r)$ and $G\mu(r) \ll r$, Eq. (2.18) reduces to $d\Phi/dr \approx \mu(r)/r^2$, which is of the same form as the equation for the Newtonian gravitational potential. Thus, Φ is a general relativistic analog of the Newtonian potential. For a given EoS $p = p(\rho)$, the TOV equations can be integrated outward from the center with the boundary conditions, $\mu(0) = 0$ after specifying central density $\rho(0) = \rho_c$, to the stellar surface at a some radius R defined where the pressure vanishes. As a further consequence, we see that, for vanishing pressure the TOV solution is indeed given by

[2] Indeed, one can show that the most general spherically symmetric metric $ds^e = -Adt^2 + Bdr^2 + Cdtdr + Dd\Omega^2$ reduce to Eq. (2.12) [129, 148].

[3] In general, an EoS relates the pressure of the object to its density, temperature, and chemical composition. However, if the EoS does not depend on the temperature, the hydrostatic equilibrium equations decouple from energy transport equations and can be solved separately [112].

the Schwarzschild solution with the following boundary conditions at the surface

$$e^{-2\lambda(R)} = 1 - \frac{R_s}{R}, \qquad e^{2\Phi(R)} = 1 - \frac{R_s}{R}, \tag{2.19a}$$

$$\mu(R) = M, \qquad p(R) = 0. \tag{2.19b}$$

in order to have a smooth transition to the Schwarzschild metric for $r > R$.

The TOV equations must typically be integrated numerically. In order to do so, we shall parametrize the metric (2.12) in the following form:

$$ds^2 = -n(r)dt^2 + m(r)dr^2 + r^2 d\Omega^2. \tag{2.20}$$

Thus, the following useful relations hold

$$\Phi = \frac{1}{2}\ln n, \qquad \lambda = -\frac{1}{2}\ln m. \tag{2.21}$$

With this variables, the TOV equations take a more symmetric form

$$\frac{dm}{dr} = \frac{m}{r}\left[(1-m) - mr^2\kappa\rho\right], \tag{2.22a}$$

$$\frac{dn}{dr} = \frac{n}{r}\left[mr^2\kappa p + (m-1)\right], \tag{2.22b}$$

$$\frac{dp}{dr} = -(p+\rho)\frac{1}{2n}\frac{dn}{dr}. \tag{2.22c}$$

For the following sections of this chapter we will keep the parametrization given by Eqs. (2.22b) and (2.22c) but leave the mass $\mu(r)$ as a variable instead of $m(r)$. Therefore the set of the stellar structure equations can be written as

$$\frac{d\mu}{dr} = 4\pi\rho r^2, \tag{2.23a}$$

$$\frac{dn}{dr} = \frac{2nG}{c^2}\left[\frac{4\pi c^{-2} r^3 p + \mu}{r(r - 2G\mu c^{-2})}\right], \tag{2.23b}$$

$$\frac{dp}{dr} = -\left(\frac{p}{c^2} + \rho\right)\frac{c^2}{2n}\frac{dn}{dr}. \tag{2.23c}$$

where we have restored the c's. On the other hand, for comparison purposes, it is useful to define the PPN γ parameter

$$\gamma = \left|\frac{1-m(r)}{1-n(r)}\right|. \tag{2.24}$$

However, due to numerical systematic errors in the direct implementation of the above expression in GR due to the division of small numbers (n and m are expected to be of the order $\sim 10^{-6}$), it is easier to simplify (2.24).[4] Using $n = m^{-1}$ the γ parameter becomes

$$\gamma = |n^{-1}|, \tag{2.25}$$

[4] Strictly speaking, in GR the γ parameter is exactly one, that is the reason Eq. (2.24) fails to be evaluated numerically. The definition (2.24) is more suitable to measure deviations from GR that are expected in alternatives theories of gravity such as $f(R)$ theories.

so in the limit $r \to \infty$, $\gamma \to 1$.

2.1.2 Numerical considerations

Before proceeding to specific solutions of the TOV equations, it is worth to introduce a dimensionless form of the Eqs. (2.23). One can define the following dimensionless quantities

$$\bar{\mu} = \frac{\mu}{M_\star}, \qquad \bar{r} = \frac{r}{r_\star}, \qquad \bar{\rho} = \frac{\rho}{\rho_\star}, \qquad \bar{p} = \frac{p}{p_\star}, \tag{2.26}$$

in order to measure the mass, the radius and the energy-density, respectively, which are carefully selected within each further astrophysical object considered. For instance, when treating with neutron stars or the Sun, we choose $\rho_\star$ as the nuclear density $\rho_n = 1.66 \times 10^{17}\text{kg m}^{-3}$ or as $\rho_\odot = 1408$ kg m^{-3}, respectively. In terms of these quantities, the system (2.23) becomes

$$\frac{d\bar{\mu}}{d\bar{r}} = \alpha\bar{\rho}\bar{r}^2, \tag{2.27a}$$

$$\frac{dn}{d\bar{r}} = \beta n\left[\frac{\alpha b\bar{r}^3\bar{p} + \bar{\mu}}{\bar{r}(\bar{r} - \beta\bar{\mu})}\right], \tag{2.27b}$$

$$\frac{d\bar{p}}{d\bar{r}} = -(\bar{p} + \bar{\rho})\frac{1}{2n}\frac{dn}{d\bar{r}}, \tag{2.27c}$$

where the dimensionless factors are defined as

$$\alpha = \frac{4\pi r_\star^3\rho_\star}{M_\star}, \qquad b = \frac{p_\star}{\rho_\star c^2}, \qquad \beta = \frac{2GM_\star}{c^2 r_\star}. \tag{2.28}$$

We use $G = 6.670\ 10^{-11}$ m^{3}kg^{-1}s^{-2}, $c = 3.0\ 10^8$ms^{-1}, $M_\odot = 2.0\ 10^{30}$kg. Notice that for each choice of $_\star$ variables, the parameters of Eq. (2.28) will change. In this way, the system of differential equations takes the form of $dy^i/dr = \mathcal{F}^i(\bar{r}, y^i)$, where $y^i = (\mu, n, p)$. To solve the system, boundary conditions must be supplied. Above we mentioned the conditions that are met at the surface of the star (Eq. (2.19)). The local flatness condition implies that we could choose $n(0) = 1$ and $\bar{\mu}(0) = 0$, i.e. $m(0) = 1$.[5] Taking $\bar{\rho}(0) = \bar{\rho}_c$, the dimensionless pressure $\bar{p}$ is fixed with help of the EoS $\bar{p} = \bar{p}(\bar{\rho})$. The integration proceeds up until the dimensionless pressure vanishes at some $\bar{r} = R$, which defines the stellar radius, where the following conditions are verified

$$n(R) = -\frac{1}{2}\ln\left(1 - \frac{R_s}{R}\right), \qquad \rho(R) = 0, \tag{2.29a}$$

$$\mu(R) = M, \qquad p(R) = 0. \tag{2.29b}$$

Aided by the considerations above, we can now compute numerical solutions using a robust integration method such as the RK4 routine [114].[6] We analyze three different kind of solutions for the TOV equations in GR.

[5] At the end of the numerical integration the variable is normalized by dividing over max n.

[6] In GR, there is no crucial drawback regarding numerical systematics as happens in $f(R)$ gravity (cf. chapter 4).

2.2 The Sun

The Sun is considered a main sequence star,[7] which indicates that is assumed to be in hydrostatic equilibrium and powered mainly by the fusion of H ($\sim$ 75%) into He ($\sim$ 23%). Due to its proximity it has been the most analyzed star so far. The most precise and complex model that describes the Sun's interior and fits the observables with high accuracy is known as the Standard Solar Model (SSM) [14], which uses input parameters such as nuclear paramaters, solar luminosity, solar age, elemental abundances, radiative opacity, etc., to construct a very complex EoS for the Sun. However, one can obtain a good representation for the Sun, by using an incompressible fluid or a polytropic EoS.

2.2.1 Incompressible Fluid

The simplest stellar configuration in hydrostatic equilibrium is given by a spherically symmetric star with uniform density ρ_0. For this case, an analytic integration is permitted. Such an object is defined by

$$\rho = \begin{cases} \rho_0 & \text{for } 0 \leq r \leq R \\ 0 & \text{for } r > R \end{cases} \tag{2.30}$$

where R is the star radius. The mass function is easily computed performing the integral (2.17), giving $M = 4\pi\rho_0 R^3/3$. It is straightforward to show that the metric functions for this case are

$$m(r) = \begin{cases} \left(1 - \frac{2GMr^2}{R^3}\right)^{-1} & \text{for } 0 \leq r \leq R \\ \left(1 - \frac{2GM}{r}\right)^{-1} & \text{for } r \geq R \end{cases} \tag{2.31}$$

and

$$n(r) = \begin{cases} \frac{1}{4}\left[3\left(1 - \frac{2GM}{R}\right)^{1/2} - \left(1 - \frac{2GMr^2}{R^3}\right)\right]^2 & \text{for } 0 \leq r \leq R \\ \left(1 - \frac{2GM}{r}\right) & \text{for } r \geq R. \end{cases} \tag{2.32}$$

Although the density is constant thorough the stellar interior, the pressure equation (2.23c) is easily integrated to give

$$p(r) = \rho_0 \left[\frac{(1 - 2GMr^2/R^3)^{1/2} - (1 - 2GM/R)^{1/2}}{3(1 - 2GM/R)^{1/2} - (1 - 2GMr^2/R^3)^{1/2}}\right]. \tag{2.33}$$

We note that the pressure function (2.33) decreases with r; its largest value is at the center of the star,

$$p_c := p(0) = \rho_0 \left[\frac{(1 - (1 - 2GM/R)^{1/2}}{3(1 - 2GM/R)^{1/2} - 1}\right]. \tag{2.34}$$

This equation tells us that, for a fixed density, the central pressure increases with the ratio M/R, that is, the body becomes increasingly compact if the stellar compactness is defined as $C := GM/R$). Note that the central pressure becomes infinite when $R = 9/4GM$, or alternatively, when the critical compactness $C_{\text{crit}} := 4/9$ is reached. In other words, to support compact star against its own weight more pressure is required. Above the critical compactness threshold, the

[7] According to the Hertzsprung–Russell diagram which shows the relationship between mass, luminosity and radius [40].

body will collapse to produce a black hole. This result is also known as the Buchdahl's limit [148]. Although it was deduced from a constant density star, it holds for any EoS. For instance, in a neutron star, $C \sim 0.3$ while for a star like the Sun, $C \sim 10^{-6}$.

As a final remark, let us solve numerically the TOV system (2.27) for an incompressible fluid that mimics the Sun, to calibrate our code. We choose $\rho_\star = \rho_\odot$, so the dimensionless parameters (2.28) of the system (2.27) become

$$\alpha \approx 0.0088 \qquad b = 1 \qquad \beta \approx 2.9 \times 10^{-5}. \tag{2.35}$$

Notice that we took the pressure in units of the Sun density, $p_\star = \rho_\odot c^2$. Since strictly speaking for a constant density star no EoS is supplied, we need to fix the central pressure *a priori*. Fortunately, we can use Eq. (2.34) using the known Sun mass and radius, which gives the value $p_c/\rho_c \approx 1.06028 \times 10^{-6}$ and check if our code gives the correct mass and radius.

Fig. 2.1 depicts the decreasing behavior of the pressure for the star and the constant density profile in the same units. Numerically, the radius is found to be $r_\odot \approx 6.9581959 \times 10^5$km, which coincides with the actual Sun radius [148]. Meanwhile, Fig. 2.2 shows the mass profile which increases up until the constant value of one solar mass $M_\odot$. In both cases, the largest gradients of $p(r)$ and $\mu(r)$ occur near the surface of the star.

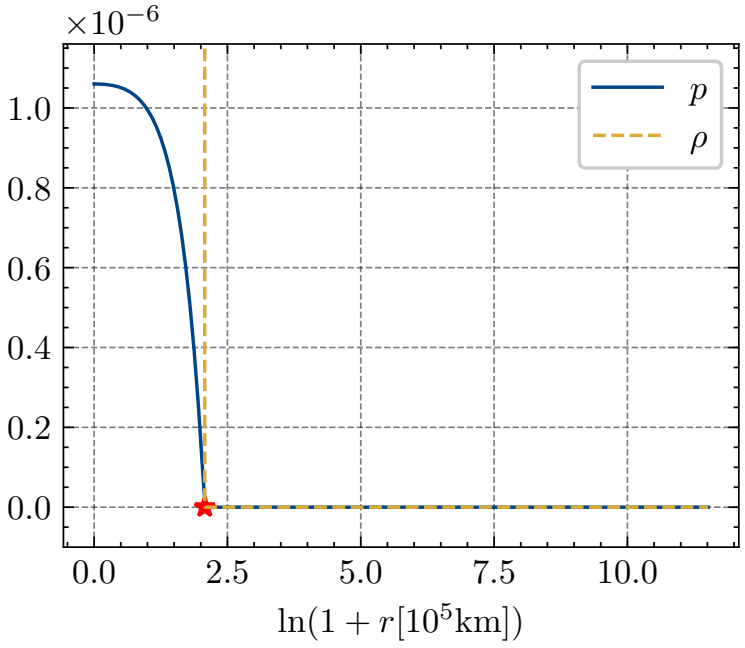

FIGURE 2.1: Pressure function $p(r)$ (blue solid line) for an incompressible fluid that mimics the Sun in units of the Sun density $\rho_\odot = 1408$ kg/m^3 (yellow dashed line). The radial coordinate is given in units of 10^5 km and the red star represents the radius of the Sun.

Fig. 2.3 depicts the behavior of the metric functions (left panel) and the gamma parameter (right panel) defined by Eq. (2.24). Notice that m and n are close to one inside and outside the star which indicates that the sun is not a compact star. Contrary to the solution for $n(r)$, there is a discontinuity in $m(r)$ which implies that is non-differentiable. This can be understood by looking at Eq. (2.23a), which, when integrated, implies $\mu(r) = 4\pi/3\rho r^3$. The discontinuity

appears in both $\mu(r)$ and $m(r)$ due to their implicit dependence on the density which happens to be a discontinuous at the radius $r_\odot$. Hence, the product $n(r)m(r)$ reaches (abruptly) the value one at the star surface. This non-differentiable behavior does not occur when a continuous EoS is considered (cf. section 2.2.2). Finally, note that the deviations of the γ parameter remain small as $\log_{10}|\gamma - 1| \lesssim -5$, which is in agreement with the experimental bound of Eq. (2.11).

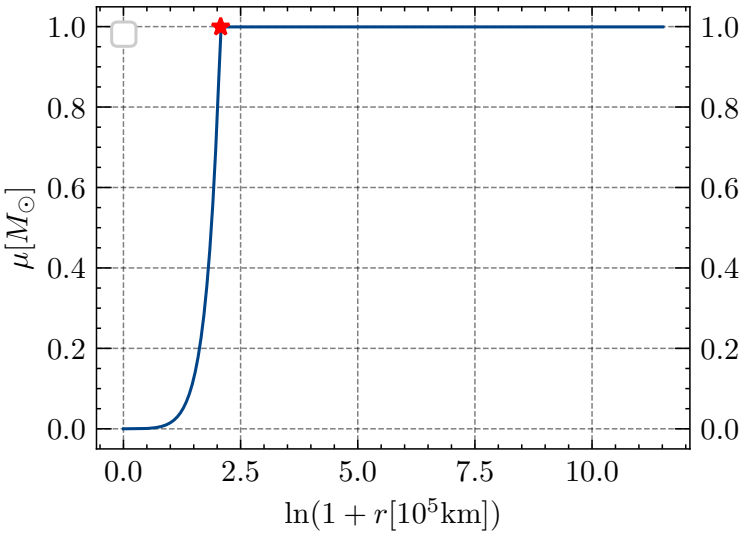

FIGURE 2.2: Mass function $\mu(r)$ for an incompressible fluid that mimics the Sun in units of $M_\odot$. The radial coordinate is in units of 10^5 km.

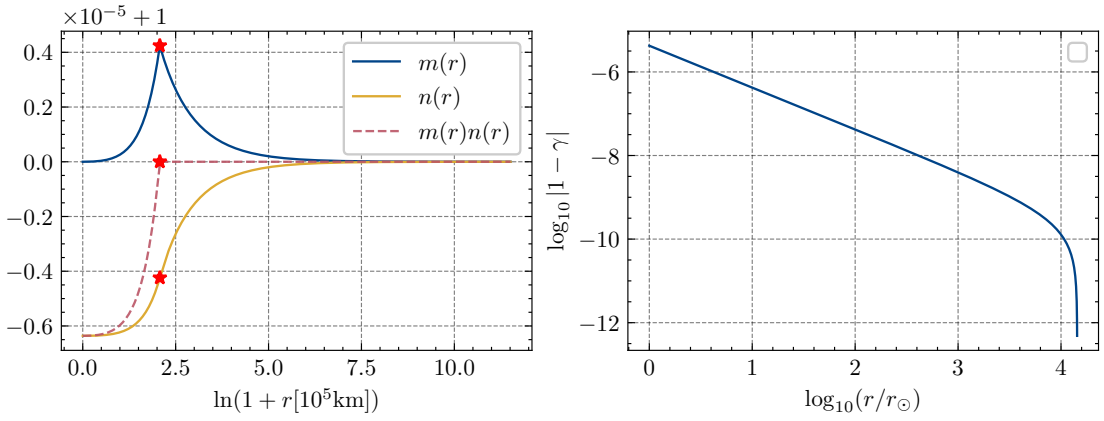

FIGURE 2.3: Metric functions $m(r)$ and $n(r)$ for an incompressible fluid that mimics the Sun (right panel). The red star is the Sun radius. γ parameter as function of the radial coordinate measured in $r_\odot$ units as defined in Eq (2.25) outside the Sun (right panel).

2.2.2 Non-relativistic polytrope

Let us improve now the consideration of a constant density star by taking into account the case where the EoS for the Sun is a smooth function given by a polytrope. The main characteristic of

this kind of EoS is that the pressure p and the density ρ are related through a power law:

$$p = K\rho^{\Gamma}, \qquad \Gamma = \frac{N+1}{N}, \tag{2.36}$$

where K is the adiabatic constant and N is the adiabatic index. Usually, the selected value N accounts for the description of the stellar model. In particular, main-sequence stars like our Sun are well modeled by $N = 3$ ($\Gamma = 4/3$). This choice was first introduced by Eddington (see e.g. [40]). However, Hendry [72] introduced a more refined choice for the adiabatic index, $N = 3.35$ ($\Gamma = 1.2985$). We shall compare both cases (see Table 2.1).

Before getting started with the integration of the equations of hydrostatic equilibrium, Eqs. (2.27), it is useful to introduce the parametric form of the polytrope (2.36) as

$$\rho = \rho_c\theta^N, \qquad p = p_c\theta^{N+1}. \tag{2.37}$$

with ρ_c the central density and $p_c := K\rho_c^{\Gamma}$, the central pressure. Notice that we have adopted θ as the dimensionless function for the density.

As in the case of a constant density star, we introduce a set of suitable scales for Eq. (2.26), $\rho_\star = \rho_c$, $p_\star = p_c$, $M_\star = 4\pi\rho_c r_0$, and $r_0^2 = (n+1)p_c/(4\pi G\rho_c^2)$. Hence, the quantities of Eq. (2.28) for the polytropic case are given by

$$\alpha = 1, \qquad b = \frac{p_c}{\rho_c c^2}, \qquad \beta = 2(N+1)b. \tag{2.38}$$

At this point, it is worth noting that b measures how relativistic the object is, i.e., when $b \ll 1$, the star is in the non-relativistic regime, and when $b > 1$ is considered relativistic. By using Eq. (2.38) and (2.37), the differential equation for the pressure, Eq. (2.27c), can be recasted in terms of θ as

$$\frac{d\theta}{d\bar{r}} = -\left(\frac{\bar{\mu}}{\bar{r}^2} + b\bar{r}\theta^{N+1}\right)\frac{1+\theta b}{1-\beta\bar{\mu}/\bar{r}}. \tag{2.39}$$

In this parametric form, Eq (2.39), together with the differential equation for the mass, are known as the relativistic Lane-Emden equations of stellar structure.[8] Thus, the system of equations to solve numerically takes the form $dy^i/dr = \mathcal{F}^i(\bar{r}, y^i)$, where $y^i = (\mu, n, \theta)$.

Finally, let us return to the polytropic paramaters for the Sun. Table 2.1 shows the parameters for two polytropic EoS that represents a star of $1M_\odot$ and $1r_\odot$. However, notice that the central values differ among the two EoSs when compared to the SSM values for the central pressure and density in the last row. This tell us that, even when two different polytropic EoSs match the desired boundary conditions at the surface, the satisfactory model is the one that has realistic values at the center that accurately math the observations. Nevertheless, we obtain solutions to the stellar evolution equations for both polytropes.

The right panel of Fig. 2.4 shows the pressure and density profiles according to Eq. (2.37) for the parameters given in Table 2.1. The dashed and solid lines correspond to $N = 3$ and $N = 3.35$, respectively. Contrary to the case of the incompressible fluid (cf. Fig. 2.1), in which the density is a step function, we see that in the case of the polytrope the density is a smooth

[8] Indeed, taking $b \to 0$, Eq. (2.39) takes the form $d\theta/d\bar{r} = -\bar{\mu}/\bar{r}^2$ together with the mass equation $d\bar{\mu}/\bar{r} = \bar{r}^2\theta^N$, which are the equations of hydrostatic equilibrium in Newtonian gravity [112].

N	Γ	$\rho_c[\mathrm{kgm}^{-3}]$	$p_c[\mathrm{Nm}^{-2}]$
3	4/3	7.646×10^4	1.2461×10^{16}
3.35	1.2985	1.53×10^5	3.00×10^{16}
SSM values		1.48×10^5	2.29×10^{16}

TABLE 2.1: Parameters for two polytropic models representing a star with of $1M_\odot$ and $1r_\odot$. The first and second columns list the the polytropic index N and $\Gamma = 1 + 1/N$, respectively. The third column lists the central density ρ_c. The fourth column lists the central pressure. For each polytropic EoS K is calculated through $K = p_c/\rho_c^\Gamma$. The last row corresponds to the standard central values for the density and the pressure taken from the SSM [14].

function. The radius for both models is found to be $r_\odot \approx 6.9825442017601 \times 10^5$ km, which coincides with the actual Sun's radius [14]. The mass profiles are shown in the left panel of Fig. 2.4. Notice that, indeed, the achieved constant mass outside of the object is that of the Sun ($M_\odot = 1.988409870698051 \times 10^{30}$).

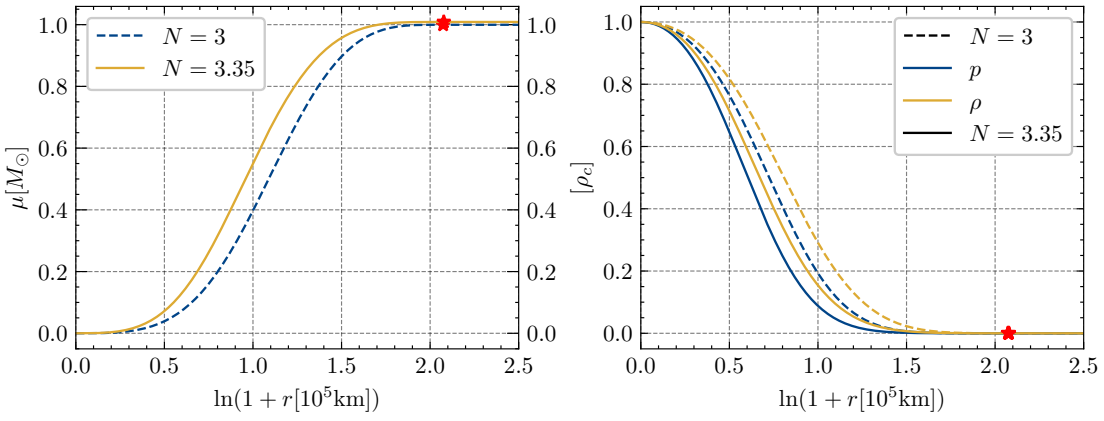

FIGURE 2.4: Metric components as a function of the radial coordinate for the polytropic EoSs of Table 2.1 that represent a star of $1M_\odot$ and $1r_\odot$ (left panel). Gamma parameter outside the star (right panel). The radial coordinate is given in units of 10^5 km.

The left panel of Fig. 2.5 exhibits the behavior of the metric components which smoothly transition from the center outwards. Meanwhile, the right panel shows the γ parameter as a function of the radial coordinate. As in the incompressible fluid for the Sun presented in Section 2.2.1, the variation of the γ parameter remains under the reported bounds ($|\gamma - 1| < 10^{-5}$) for both polytropic models. Notice that immediately outside the star, the product $m(r)n(r) = 1$ as $r \to \infty$ meaning that the exterior metric is Schwarzschild.

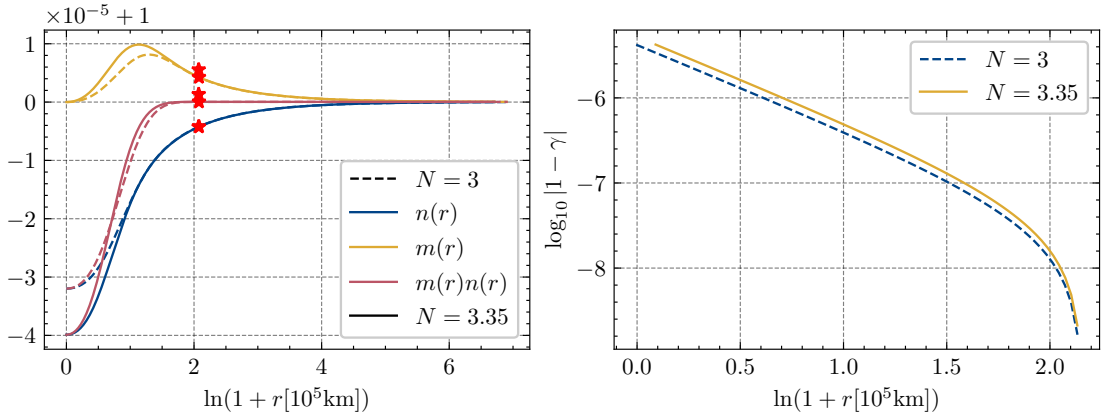

FIGURE 2.5: Metric components as a function of the radial coordinate of a polytrope that mimics the Sun (left panel). Gamma parameter outside the Sun (right panel). The radial coordinate is given in units of 10^5 km.

Most interestingly, the two polytropes match the requirements of a star with the mass and radius of the Sun. In order to discern between the two models we have to look for the assumed values at the center. In this way, the polytrope with $N = 3.35$ is a satisfactory solar model. As a final remark, it is worth to mention that, all the profiles for the polytropes (Fig. 2.4 and Fig. 2.5) are smooth. This can be contrasted with the incompressible fluid case where the discontinuity of the density function reflects the non-differentiable character of $p(r)$, $m(r)$ and $\mu(r)$.

With the introduction of the polytropic EoS we can expand the analysis to study solutions for more relativistic objects such as neutron stars.

2.3 Neutron stars

Neutron stars (NS) are compact stars which are known to contain matter under extreme physical conditions [1, 70, 90]. Their internal structure ranges from a few $\sim$ g/cm^3 on the surface to $\sim 10^{15}$g/cm^3 at the center. They typically have radii $R \sim 10$ km and masses $M \sim 1.4M_\odot - 2.0M_\odot$. Thus, they differ vastly from a main sequence star like the Sun. Accordingly, the composition of a NS depends heavily on its density which, at the moment, cannot be constrained by terrestrial experiments. Despite the continuous efforts of modern astrophysical observations, they can only look for the macroscopic properties of NSs such as the radius or the mass. In consequence, the true EoS inside NS is uncertain at densities beyond nuclear saturation $\rho_n = 2.8 \times^{14}$ g/cm^3.[9]

The constituent particles within the different layers of a NS are assumed to be formed mainly by neutrons, protons, electrons and other baryons and leptons. Several candidates for a *realistic* EoSs have been proposed in literature and involve large numbers of fundamental parameters, which are interpolated [117]. However, it has been shown that, although its simplicity, polytropic EoSs can give a very good description of the properties of a NS.

[9] It can be said also that due to the lack of knowledge of the strong nuclear interactions, the EoS for the *liquid interior* ($\rho > \rho_n$) is uncertain [122].

2.3.1 Relativistic polytrope

A clever way to model the internal structure of a NS with one polytrope was introduced by Bonazzola et al. [22] (see also [47, 54, 122]). In the same way as Eq. (2.37), the polytrope is parametrized by the baryon density n_b:

$$\frac{p(n_b)}{c^2} = K m_b n_0 \left(\frac{n_b}{n_0}\right)^{\Gamma}, \tag{2.40}$$

$$\rho(n_b) = m_b n_b + \frac{p}{c^2\Gamma - 1}, \tag{2.41}$$

where $m_b = 1.66 \times 10^{27}$ kg is the mean baryon mass and $n_0 = 0.1$ fm^{-3}. The above equations represent a two parameter family of a stiff or soft EoSs given different values of K and Γ which can be seen as

$$\rho = \left(\frac{p}{K}\right)^{1/\Gamma} + \frac{p}{\Gamma - 1}. \tag{2.42}$$

The lower the value of the polytropic index Γ, the stiffer the EoS becomes.[10] Following [47, 122] we consider two pairs of parameters (Γ, K) that mimic two different NS models. The model DIAZII corresponds to $\Gamma = 2.34$ and $K = 0.0195$ to fit the EoS II of Ref. [55], and the model ARNA corresponds to $\Gamma = 2.46$ and $K = 0.00936$ to fit the EoS A of Ref. [9].

Using dimensionless variables the EoS takes the form

$$\bar{p} = K \bar{n}_b^{\Gamma}, \qquad\qquad \bar{\rho} = \bar{n}_b + \frac{K \bar{n}_b^{\Gamma}}{\Gamma - 1}. \tag{2.43}$$

Also, instead of $\bar{p}$ as the third dynamical variable, we write it in terms of $\bar{n}_b$ using

$$\frac{d\bar{n}_b}{d\bar{r}} = \frac{\bar{n}_b}{\bar{p}\Gamma}\frac{d\bar{p}}{d\bar{r}}. \tag{2.44}$$

Then, the system of equations to implement in the code is

$$\frac{d\bar{\mu}}{d\bar{r}} = \alpha \bar{\rho} \bar{r}^2 \tag{2.45a}$$

$$\frac{dn}{d\bar{r}} = \beta n \left[\frac{\alpha \bar{r}^3 \bar{p} + \bar{\mu}}{\bar{r}(\bar{r} - \beta\bar{\mu})}\right] \tag{2.45b}$$

$$\frac{d\bar{n}_b}{d\bar{r}} = -\frac{\bar{n}_b}{\bar{p}\Gamma}(\bar{p} + \bar{\rho})\frac{1}{2n}\frac{dn}{d\bar{r}} \tag{2.45c}$$

where the dimensionless factors α and β are defined as in Eq. (2.28). We choose to measure the density, mass, and radius in units of the nuclear density $\rho_\star = \rho_n := m_b n_0$, solar mass $M_\star = M_\odot$ and one kilometer $r_\star = 1$km, respectively. This choice gives rise to the following values

$$\alpha \approx 0.00105, \qquad\qquad \beta \approx 2.954. \tag{2.46}$$

[10] A stiffer EoS usually means that for a given change in density, the pressure increases a lot more, contrary to the softer EoS where a small change in pressure happens.

Another quantity of physical interest is the baryonic mass of the star

$$\mu_A(r) = 4\pi m_b \int_0^r n_b(r') r'^2 \left(1 - \frac{2G\mu(r')}{c^2 r_0}\right)^{-1/2} dr', \tag{2.47}$$

which can be written as a differential equation independent from the system (2.45) as

$$\frac{d\bar{\mu}_A}{d\bar{r}} = \alpha \frac{\mu_\odot}{m_b} \bar{n}_b \bar{r}^2 \left(1 - \frac{\beta\bar{\mu}}{\bar{r}}\right)^{-1/2}, \tag{2.48}$$

where the adimensional baryonic mass $\bar{\mu}_A = \mu_A/m_b$ was defined. In this way, the solutions of the TOV equations ((2.45) and (2.48)) form a single-parameter family, where the free parameter labeling the different solutions is commonly set by the central density ρ_c.

Representative sequences of equilibrium models of neutron stars are plotted in Figure 2.6 which shows different mass profiles as a function of ρ_c, the density at the center of the star. Each choice of ρ_c generates a pair of (μ, R) where μ is its gravitational mass and R is the radius of the star. The variation of this parameter gives us a mass-radius relation for every EoS.

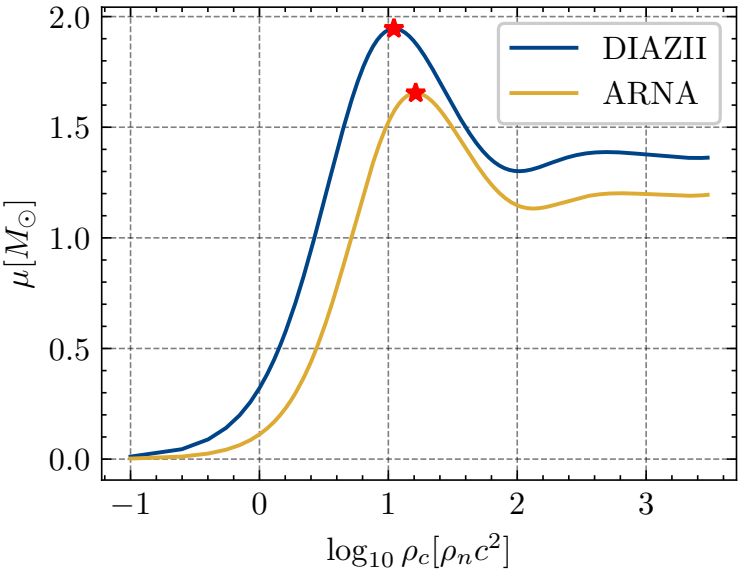

FIGURE 2.6: Neutron star mass (in $M_\odot$) as a function of the central value of the (mass) density for a range of equilibrium configurations for DIAZII (dashed line) and ARNA (solid line) models. The red star indicates the maximal configuration in each model.

In Fig. 2.7, the mass-radius relation is plotted. We see that the maximal mass (red stars) for the DIAZII and ARNA EoS are about $1.927M_\odot$ and $1.6M_\odot$, respectively. The maximal masses obtained are consistent with those reported in previous analyses [122].

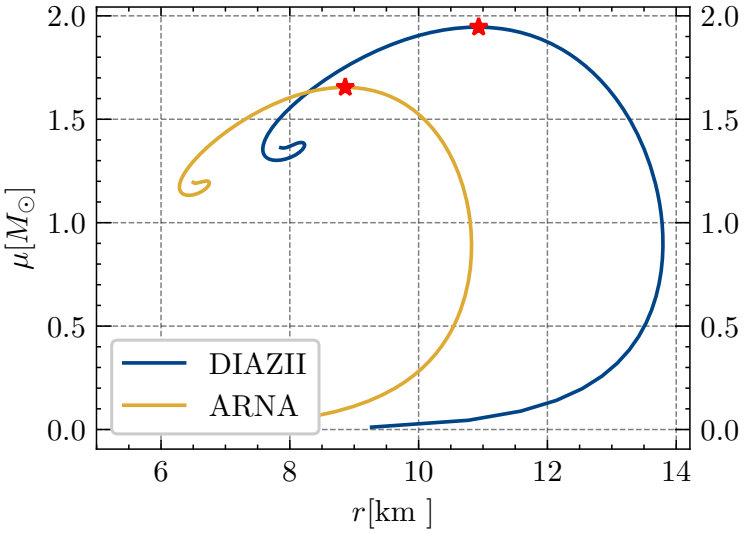

FIGURE 2.7: Neutron star mass (in $M_\odot$) as a function of the radius (in km) for a range of equilibrium configurations for DIAZII (blue line) and ARNA (yellow line) models. The red stars indicates the maximal configurations of each model.

In particular, the solutions for the DIAZII and ARNA maximal masses configurations are shown in Figures 2.8-2.10. For instance, Fig. 2.8 depicts the behavior of the metric functions of both EoSs for these particular configurations. We observe a smooth profile in the same way as in the polytopic EoS for the Sun. Fig. 2.9 shows the total baryon mass and the total gravitational mass for both configurations. Finally, in Fig. 2.10 we see the decreasing of pressure function as the star surface is approached.

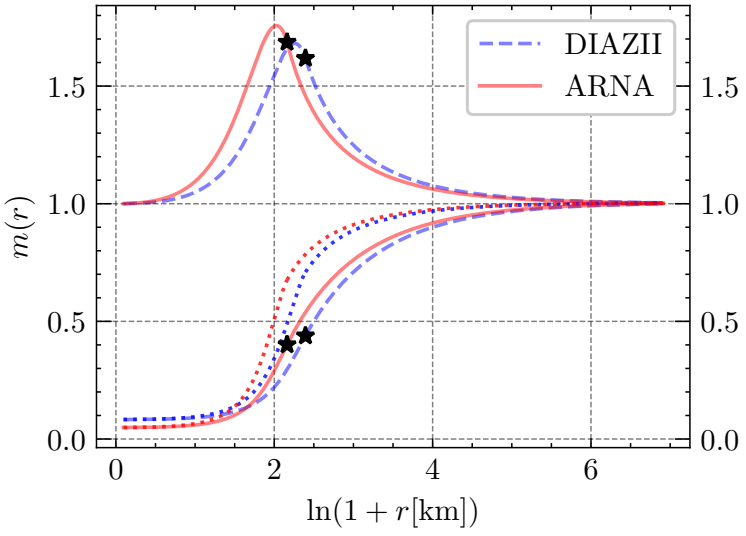

FIGURE 2.8: Metric functions $m(r)$, $n(r)$ and their product (dotted lines) for the two models, DIAZII (blue lines) and ARNA (red lines). The black star indicates the value where the pressure and density vanish (i.e., the surface of the star). The radial coordinate is given in units of 10^5 km.

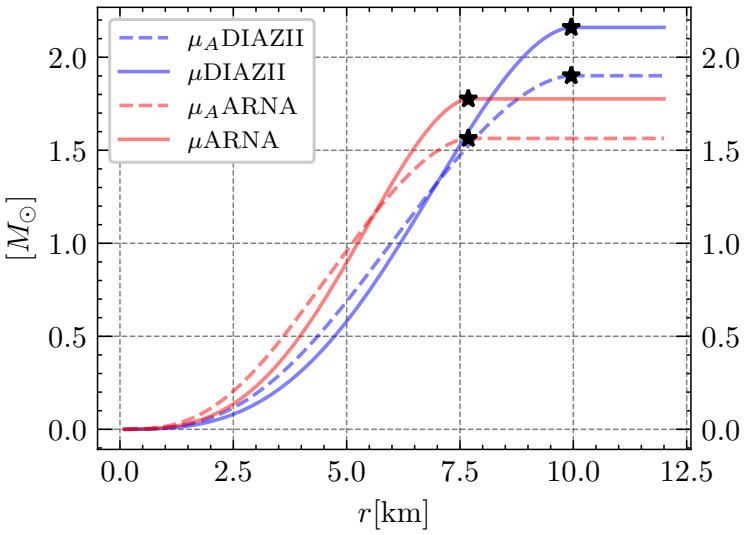

FIGURE 2.9: Baryonic mass $\mu_A(r)$ and gravitational mass $\mu(r)$ measured in solar mass units $M_\odot$ for the two models, DIAZII (dashed line) and ARNA (solid line). The black star indicates the surface of the star R. Notice that μ_A and μ converges to the total baryon mass and the total gravitational mass respectively.

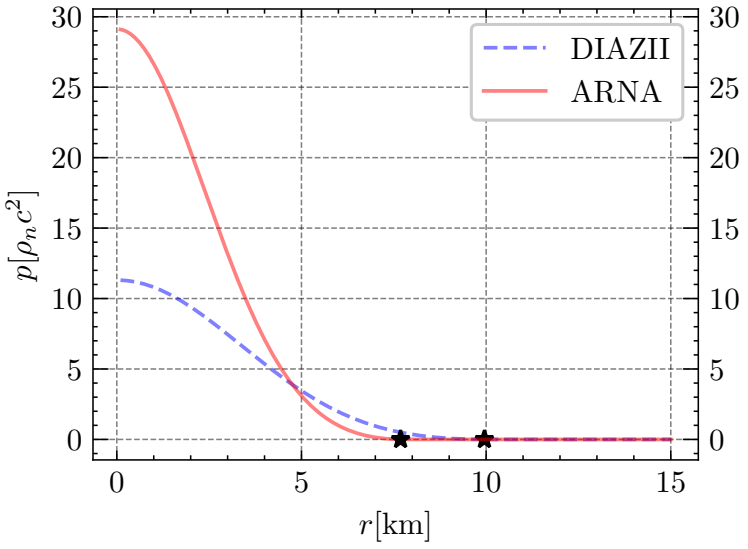

FIGURE 2.10: Pressure function $p(r)$ for the two models considered, DIAZII (dashed line) and ARNA (solid line).The units are given in terms of the nuclear density $\rho_n = 1.66 \times 10^{17}$ kg/m^3.

2.3.2 Piecewise polytrope

As we stated before, the EoS of a NS is uncertain. Strictly speaking, the whole density range of a NS cannot be accurately approximated with only one polytrope, but only a specific range. To this regard, a few more complex parametrizations than that of the prior section have been proposed in the literature to accurately reproduce feature of realistic EoS. The one we are interested in is based on a Piecewise Polytropic (PP) EoS with three free parameters, developed by Read et al.

[117].[11] This parametrization consists of stitching together polytropic EoSs (as in Eq. (2.36)) with different fixed adiabatic index Γ and K, for a different range of densities. It has been shown that this form of EoS is able to reproduce macroscopic observables for a wide range of candidate EoSs [118]. It has also been used extensively in gravitational-wave parameter estimation and NS in alternative theories of gravity. In particular, in the R-squared $f(R)$ model (cf. chapter 5).

In this approach, the energy density that appears in the energy-momentum tensor is decomposed as $\rho c^2 + \epsilon$, i.e., the proper rest-mass density ρ plus the proper internal (thermodynamic) energy density ϵ [117, 118]. For a set of dividing densities $\rho_{i-1} \leq \rho \leq \rho_i$, the polytropic relation is satisfied

$$p(\rho) = K_i \rho^{\Gamma_i}, \tag{2.49}$$

where i labels each segment of the polytrope. To obtain an expression for ϵ in terms of the rest-mass density ρ we use the first law of thermodynamics, which implies the following relation

$$d\left(\frac{\epsilon}{\rho}\right) = -p d\rho^{-1}, \tag{2.50}$$

where it follows, after integration, that

$$\epsilon(\rho) = (1+\alpha_i)\rho + \frac{K_i}{\Gamma_i - 1}\rho^{\Gamma_i}, \qquad \alpha_i = \frac{\epsilon(\rho_{i-1})}{\rho_{i-1}} - 1 - \frac{K_i}{\Gamma_i - 1}\rho_{i-1}^{\Gamma_i - 1}. \tag{2.51}$$

The rest mass density zero limit, $\lim_{\rho\to 0} \epsilon/\rho = 1$, ensures that $\epsilon = \rho$ thus, Eq. (2.42) is recovered. Each polytropic segment is specified by the initial density ρ_{i-1}, the coefficient K_i, and the adiabatic index Γ_i. However, if another EoS is supplied at lower densities than that of the segment, continuity implies that at the fixed matching density ρ_i, $p(\rho_i) = p(\rho_{i+1})$, thus $K_{i+i} = p(\rho_i)/\rho_i^{\Gamma_{i+1}}$. Following [118], a PP EoS is divided in two density regimes linked by a density ρ_0. Three individual polytropes in the high-density ($\rho \geq \rho_0$) portion of the EoS are anchored to a fixed low-density EoS ($\rho < \rho_0$).

For the high-density, part each density interval $\rho_{i-1} \leq \rho \leq \rho_i$, is joined by a polytrope. In this way, the model requires four parameters $\{\log(p_1), \Gamma_1, \Gamma_2, \Gamma_3\}$. The first polytrope with adiabatic index Γ_1 is anchored at pressure $p_1 = p(\rho_1)$ and a fixed matching density $\rho_1 = 10^{14.7}$ g/cm^3. A second polytrope follows with adiabatic index Γ_2 is defined from (p_1, ρ_1) to the second fixed density $\rho_2 = 10^{15.0}$ g/cm^3. Finally, the third polytrope with adiabatic index Γ_3 is joined at (p_2, ρ_2). In particular, the diagram for this parametrization in the high-density part is shown in Fig. 2.11 for the model MPA1. Similar profiles are obtained for the other models considered in Table 2.2.

[11] Other parametric models include the *spectral* and a direct pamaretrization of the *speed of sound* (see e.g. [91]).

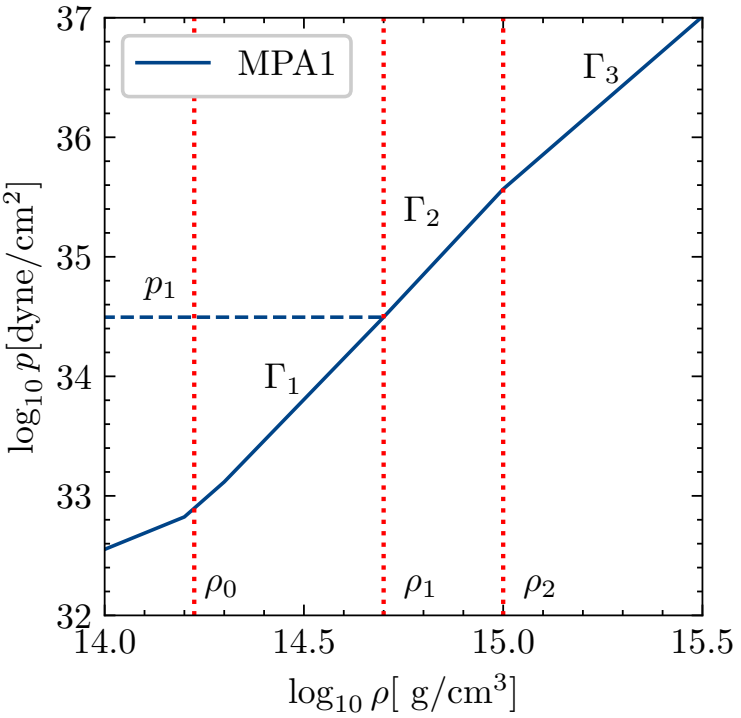

FIGURE 2.11: High-density region part of the PP EoS ($\rho > \rho_0$) for the *MPA*1 model given by three joined polytropes parametrized by the adiabatic indexes $\{\Gamma_1, \Gamma_2, \Gamma_3\}$ and the pressure p_1.

On the other hand, since NS observables, such as the mass, are not very sensitive below nuclear saturation density for the low-density part ($\rho < \rho_0$), we adopt the SLy analytic representation [69], which was approximated by four polytropic pieces by Read et al. [117]. In the same notation described above, Table 2.3 shows the values $\{\Gamma_i, K_i, \rho_i\}$ for each piece. Both density regions are connected by equating the first polytrope of the high-density region with the last polytrope of the low-density SLy EoS.

For simplicity, we consider four distinct EoS for the high-density part which are widely studied in literature. These are: APR4, SLy, H4 and MPA1 (see section II of [117] for the origin of each EoS).

EoS	$\log P_1(\mathrm{dyne/cm^2})$	Γ_1	Γ_2	Γ_3	Approach
APR4	34.269	2.830	3.445	3.348	Variational-method
SLy	34.348	3.005	2.988	2.851	Effective-one-body potential
H4	34.669	2.909	2.246	2.144	Relativistic mean field
MPA1	34.495	3.446	3.572	2.887	BruecknerHartree-Fock method

TABLE 2.2: Parameters of high-density part for the APR4, SLy, H4 and MPA1 PP EoS. The maximal mass of spherical neutron stars, $M_{\max}$, for each EOS obtained. Composition means strongly interacting components (n=neutron, p=proton, H=hyperon, Q=quark, π^0=pion) and SLy, H4 include leptonic components.

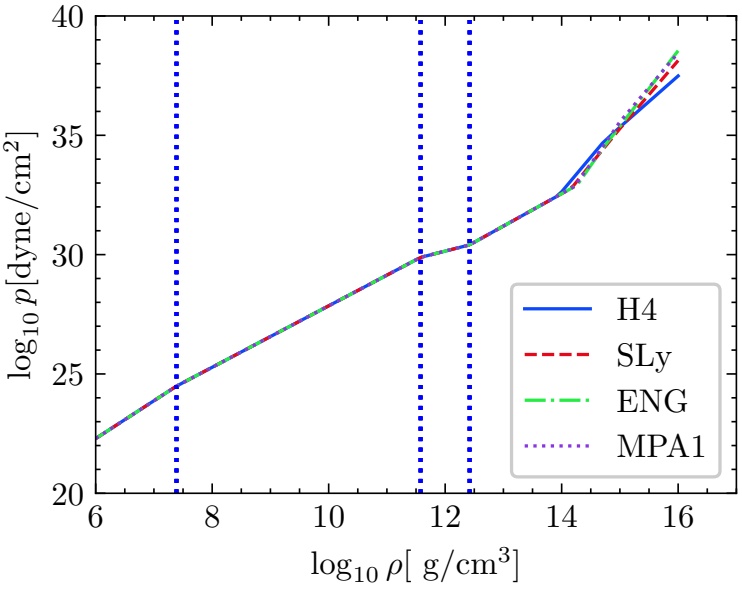

FIGURE 2.12: Density profile for the four EoS of Table 2.2. The vertical dotted blue lines corresponds to the dividing densities for the low-density region given in Table 2.3.

Fig. 2.12 shows the pressure profile as a function of the density for the EoS of Table 2.2. Both density regions are plotted. Because of the construction of this parametrization all EoS coincide in the low-density regime by the SLy PP EoS of Table 2.3.

K_i	Γ_i	ρ_i
6.80110e-09	1.58425	2.44034e+07
1.06186e-06	1.28733	3.78358e+11
5.32697e+01	0.62223	2.62780e+12
3.99874e-08	1.35692	–

TABLE 2.3: Parameters for the SLy EoS below nuclear density which is given by four polytropes specified by Γ_i, ρ_i (in $\mathrm{g/cm^3}$) and K_i (in cgs units) The corresponding value of p is in units of $\mathrm{dyne/cm^2}$. The values are taken from Appendix 1 of [117]. The last dividing density which does not appear in the table is the density where the low density EoS matches the high density EoS and depends on the parameters p_1 and Γ_1 of the high density EoS for each model listed in Table 2.2.

After specifying the PP EoS, we solved numerically the system (2.27) choosing units such that

$$r_\star = r_g \qquad \rho_\star = M_\odot / r_g^3 \qquad p_\star = M_\odot c^2 / r_g^3 \tag{2.52}$$

where we set $r_g = GM_\odot/c^2 \approx 1.47473$ km, that is the sun's half Schwarzschild radius. Thus, the coefficients (4.31) are set to $\alpha = 8\pi$ and $\beta = 1$. The dimensionless factors (2.28) are $\alpha = 4\pi$, $\beta = 1$ and $b = 1$.

The mass as a function of the stellar radius is shown in Figure 2.13 for the four EoSs of Table 2.2. The maximal mass configurations are highlighted by the red stars. These masses, which are shown in Table 2.4, were obtained numerically and coincide with the reported masses in [117]. In Fig. 2.14, we plot the mass as a function of the central density for the same PP EoSs. The differences between the maximal masses that occur roughly at the same density are due solely to the EoS. All the masses are above $\sim 2M_\odot$, contrary to the EoS used in Section 2.3.1.

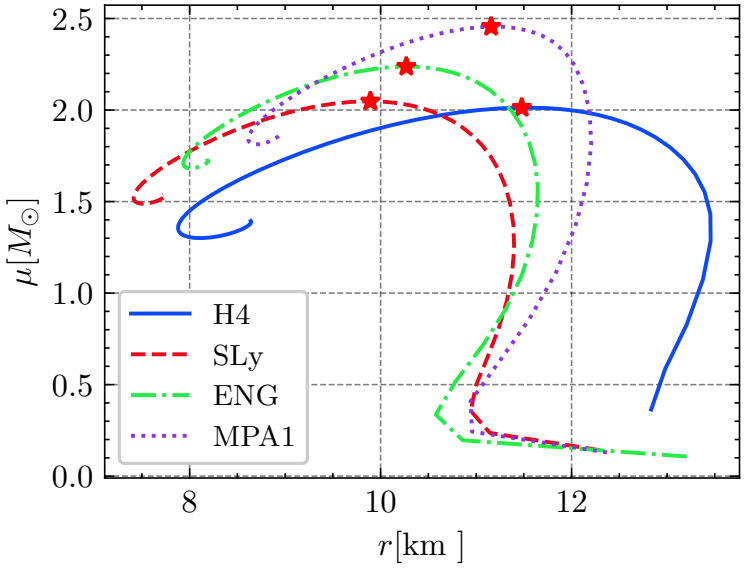

FIGURE 2.13: Neutron star mass (in $M_\odot$) as a function of the radius (in km) for a range of equilibrium configurations for the models depicted in Table 2.2. The red stars indicates the maximal configurations of each model.

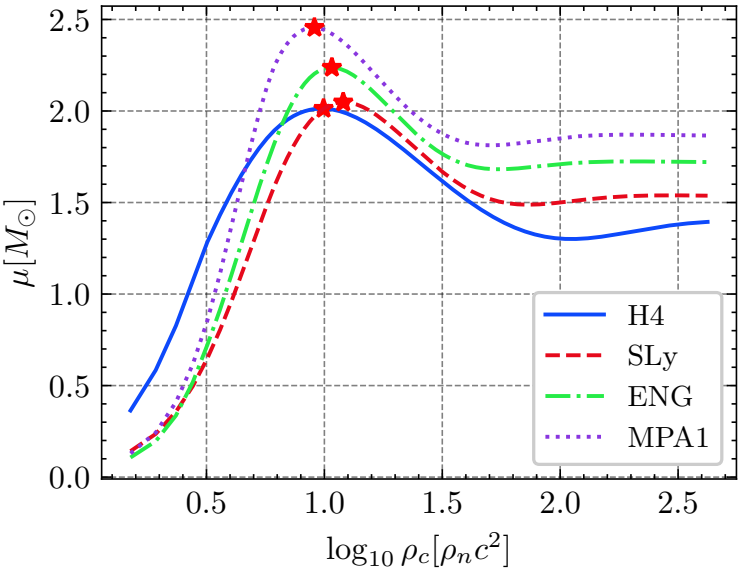

FIGURE 2.14: Neutron star mass (in $M_\odot$) as a function of the central value of the (mass) density for a range of equilibrium configurations for the models depicted in Table 2.2. The red stars correspond to the maximal mass configurations.

EoS	$M_{\max}(M_\odot)$
APR4	2.213
SLy	2.049
H4	2.032
MPA1	2.461

TABLE 2.4: Maximal masses obtained for the four different PP EoSs specified in Table 2.2.

As a closing remark for this chapter, the analysis of previous sections makes it clear that the implemented numerical code functions fairly well for a variety of well-known EoSs, including the case of a constant density object that mimics the Sun. We have managed to reproduce the Sun within two different models. We have also found solutions for NS within GR. With this in hand, in the next chapter, the $f(R)$ metric theories of gravity will be introduced.

Chapter 3

$f(R)$ Theories

In the previous chapter we have established the fact that equilibrium of spherically symmetric stars in General Relativity (GR) is governed by the Tolman-Oppenheimer-Volkoff (TOV) equations. We now turn to consider the case of star-like objects in $f(R)$ theory. For that, we review the metric $f(R)$ theories.

Among the countless (inequivalent) ways to modify GR, $f(R)$ gravity stands as one of the simplest and most straightforward paths to circumvent the Lovelock's theorem by adding an extra degree of freedom.[1] They are part of a more general class of gravity theories based on modifications of the Einstein-Hilbert Lagrangian which have a long history of development (see [50, 134] for detailed reviews). However, a natural question arises: why is the $f(R)$ function chosen as a function of only the Ricci Scalar instead of high-order curvature invariants such as $R_{ab}R^{ab}$, $R_{abcd}R^{abcd}$, $R_{abcd}R^{ab}R^{cd}\ldots$, or combinations of those such as the Gauss-Bonnet invariant.[2] The fact is that $f(R)$ theories are one of the theories which can prevent the Ostrogradsky instability [152]. Hereafter, we will focus our attention in $f(R)$ gravity models as functions only of the Ricci Scalar R.

As widely discussed in Chapter 1, the existence of two eras of accelerated expansion of the universe boosted the interest in these kind of theories. The earlier phase of expansion being the cosmic inflation which was addressed by the original Starobinsky model of inflation [136]. On the other hand, the observed phenomenon of late time cosmic acceleration, which is considered the puzzle of the millennium [15, 82, 95, 123, 149], has also stimulated the idea of dark energy models based on $f(R)$ theories [4, 98, 105, 131]. One of the advantages of $f(R)$ models in the cosmological regime is the property of a potentially disappearing cosmological constant.[3] It was thought as a natural step trying to explain the late time expansion by the same mechanism (at much lower energies than in the earlier universe). Earlier $f(R)$ models were proved wrong since they were plagued by matter instabilities and were unable to produce the late time acceleration

[1] Lovelock's theorem says the following: *In four spacetime dimensions the only divergence-free symmetric rank-2 tensor constructed solely from the metric g_{ab} and its derivatives up to second differential order, and preserving diffeomorphism invariance, is the Einstein tensor plus a cosmological term [19, 43].*

[2] In this regard recall that the Gauss-Bonnet invariant is defined by $\mathcal{G} = R^2 - 4R_{ab}R^{ab} + R_{abcd}R^{abcd}$ and itself is an object of study known as Gauss-Bonet gravity (see e.g. section 12 of [50]).

[3] Not all $f(R)$ have this property, see for e.g. [77].

together with a viable cosmic expansion. In this way, the main interest was shifted to construct cosmological viable $f(R)$ models.

In this Chapter we review the general properties of $f(R)$ gravity, derive its field equations and analyze its experimental and theoretical constraints. Several approaches to treat the field equations have been proposed. In section 3.1 we review those approaches to formulate metric $f(R)$ gravity. In section 3.3 the TOV equations for $f(R)$ gravity are discussed. Section 3.4 addresses the constraints that $f(R)$ is subject to. For completeness the discussion in Section 3.2 is briefly dedicated to the actual status of cosmology in $f(R)$ gravity.

3.1 Metric $f(R)$ gravity formulations

As in GR, the field equations from $f(R)$ gravity can be extracted from a variation principle. However, we must point out that there are actually two main formalism for deriving the field equations. The first is the standard metric formalism where variation to the action respect to the metric tensor g_{ab} leads to the field equations. The second is the Palatini formalism [26] in which the affine connection Γ^a_{cd} is allowed to be a variable independent of the metric (see [17, 18, 83, 84, 108] for the application of this formalism to spherical symmetric solutions). These two formalism are not equivalent unless $f(R) = R$. We shall focus on the theory obtained through the metric formalism and discuss below its different formulations.[4]

3.1.1 JPS formalism

In this section we present the robust approach to $f(R)$ gravity developed by Jaime, Patiño and Salgado (JPS) [78]. The general action for an $f(R)$ theory of gravity in a 4-dimensional manifold is given by

$$S[g_{ab}, \Psi] = \int \frac{f(R)}{2\kappa} \sqrt{-g} d^4x + S_M[g_{ab}, \Psi], \tag{3.1}$$

where $\kappa = 8\pi G_0/c^4$. Varying the action with respect to the metric gives

$$f_R R_{ab} - \frac{1}{2} f g_{ab} - (\nabla_a \nabla_b - g_{ab}\Box) f_R = \kappa T_{ab}, \tag{3.2}$$

where $f_R := \partial_R f$ and $\Box := g^{ab}\nabla_a\nabla_b$ and, as usual,

$$T_{ab} = \frac{-2}{\sqrt{-g}} \frac{\delta S_M}{\delta g^{ab}}, \tag{3.3}$$

is the energy-momentum tensor of matter. Is straightforward to write Eq. (3.2) in the following way

$$\begin{aligned} f_R G_{ab} - f_{RR}\nabla_a\nabla_b R - f_{RRR}(\nabla_a R)(\nabla_b R) \\ + g_{ab}\left[\frac{1}{2}(Rf_R - f) + f_{RR}\Box R + f_{RRR}(\nabla R)^2\right] = \kappa T_{ab}, \end{aligned} \tag{3.4}$$

[4] There is actually a third version of $f(R)$ gravity: *metric-affine* $f(R)$ gravity. In this case, matter depends explicitly on the connection Γ and the Palatini variation is used. The interested reader is referred to [32, 135].

where $G_{ab} = R_{ab} - g_{ab}R/2$ is the Einstein tensor, $(\nabla R)^2 := g^{ab}(\nabla_a R)(\nabla_b R)$, $f_{RR} := \partial_R^2 f$ and $f_{RRR} := \partial_R^3 f$. Since Eq. (3.4) contains the second derivative of R the field equations are fourth order in the metric, but avoid Ostrogradsky instabilities because the theory is equivalent to a Scalar-Tensor Theory with second order equations of motion, as we will see in Section 3.1.2. Moreover, the trace of Eq. (3.4) yields

$$\Box R = \frac{1}{3f_{RR}}\left[\kappa T - 3f_{RRR}(\nabla R)^2 + 2f - Rf_R\right], \tag{3.5}$$

where $T := T^a_{\ a}$. Thus, we have explicitly obtained a scalar equation for R. Furthermore, using Eq (3.5) in Eq. (3.4) we obtain

$$G_{ab} = \frac{1}{f_R}\left[f_{RR}\nabla_a\nabla_b R + f_{RRR}(\nabla_a R)(\nabla_b R) - \frac{g_{ab}}{6}(Rf_R + f + 2\kappa T) + \kappa T_{ab}\right], \tag{3.6}$$

which tell us the clear modifications to GR. Eqs. (3.6) and (3.5) are the fundamental equations of the robust approach to $f(R)$ gravity. In this way, $f(R)$ gravity can be written as two second order equations. One for the metric (3.6) and one for the Ricci Scalar (3.5). Viewed in this approach the theory has an extra scalar degree of freedom represented by the Ricci Scalar itself. Unlike GR, where R and T are algebraically constrained by $R = \kappa T$, in $f(R)$ gravity exists a dynamical, differential relation between the matter sources and R itself given by Eq. (3.5). Notice that if $f(R) = R - 2\Lambda$, GR with Λ is recovered. In the latter form, the field equations allow us to treat $f(R)$ gravity in a more cleaner way instead of transforming them as a Scalar-Tensor Theory.

One very important implication of Eq. (3.5) comes from a suggestive reading of its right-hand side. An effective potential can be defined from part of the trace of the field equations in such a way that it can be calculated as an integral. Lets discuss in more detail the algebraic structure of this potential.

First thing to note is that, aside from the GR case, one is to look for monotonically growing and convex $f(R)$ functions, such that $f_{RR}, f_R > 0$. Second, when the energy-momentum tensor is traceless ($T \equiv 0$), Eq. (3.5) admits $R = R_1 = const$ as a particular solution provided R_1 is an algebraic root of the implicitly defined *potential* $\mathcal{V}_{\rm JPS}(R)$ via its derivative

$$\frac{d\mathcal{V}_{\rm JPS}(R)}{dR} := \frac{2f - Rf_R}{3f_{RR}}. \tag{3.7}$$

In general,[5] if $f_{RR}(R_1) \neq 0$, R_1 is a root of the alternative potential (the factor $1/3$ is kept for convention),

$$\frac{dV(R)_{\rm JPS}}{dR} := \frac{2f - Rf_R}{3}. \tag{3.8}$$

Once an $f(R)$ model is provided, the explicit expression either $V(R)_{\rm JPS}$ or $\mathcal{V}(R)_{\rm JPS}$ can be computed as follows

$$V(R)_{\rm JPS} = -\frac{Rf(R)}{3} + \int^R f(x)dx. \tag{3.9}$$

On the other hand, when the energy-momentum tensor trace does not vanish, the potentials are redefined. The effective potentials $\mathcal{V}^{\rm eff}_{\rm JPS}(R,T)$ and its counterpart $V^{\rm eff}_{\rm JPS}(R,T)$ inside the stellar

[5] There are some exceptional cases where where both the numerator $2f - Rf_R$ and the denominator vanish at R_1, e.g. the R^n model [80], which has been disproved as a cosmological viable model.

object are as follows,

$$\frac{d\mathcal{V}^{\rm eff}_{\rm JPS}(R,T)}{dR} := \frac{\kappa T + 2f - Rf_R}{3f_{RR}}, \qquad \frac{dV^{\rm eff}_{\rm JPS}(R,T)}{dR} := \frac{\kappa T + 2f - Rf_R}{3}. \tag{3.10}$$

Thus, Eq. (3.5) is rewritten as a standalone scalar equation with an effective potential,

$$\Box R + \frac{f_{RRR}}{f_{RR}}(\nabla R)^2 = \frac{d\mathcal{V}^{\rm eff}_{\rm JPS}(R,T)}{dR}. \tag{3.11}$$

The effective potential $V^{\rm eff}_{\rm JPS}(R,T)$ has an extremum at

$$2f - Rf_R\Big|_{R_{min}} = -\kappa T. \tag{3.12}$$

This relies upon the specific value R_{min} which is constant and it is related to the effective cosmological constant associated with the assigned value that comes from the $f(R)$ cosmology. At such minimum value, that is where Eq. (3.10) vanishes, the effective mass associated with R is defined as

$$m^2_{\rm eff} := \frac{d^2V_{\rm eff}}{dR^2}\Big|_{R_{min}} = \left[\frac{f_R - Rf_{RR}}{3f_{RR}} - \frac{f_{RRR}}{f_{RR}}\frac{dV_{\rm eff}}{dR}\right]\Big|_{R_{min}} = \frac{f_R - Rf_{RR}}{3f_{RR}}\Big|_{R_{min}}. \tag{3.13}$$

As pointed out by Jaime et al. [78], the potential $V(R)_{\rm JPS}$ is well defined as far as $f(R)$ is. The usefulness of introducing this potential is that it reveals the possible critical points that R can reach asymptotically (in time and space). Other than that, this potential has no fundamental meaning whatsoever. As we will see in the following section, the behavior of the associated scalar potential in the Scalar-Tensor formulation does not enable the insight that the JPS formalism naturally provides. It raises questions of ill defined mappings and pathological features. It leads to rather questionable results and conclusions.

3.1.2 Scalar-Tensor Formalism of $f(R)$ Theory

In the previous subsection we have written down the field equations of $f(R)$ gravity and seen that the new propagating degree of freedom is encompassed in the R equation. In this section we further show the two alternative approaches that have been used to analyze stars in $f(R)$ gravity, exploiting the equivalence between $f(R)$ theory and a Scalar-Tensor theory.

Jordan-Frame

Among many authors there is the widespread idea that one should *always* recast $f(R)$ gravity as a *chameleon theory* [86]. This procedure starts by considering the theory as a Brans-Dicke (BD) theory which belongs to the Scalar-Tensor class. In the context of spherically symmetric spacetimes, this approach was used by Kobayashi and Maeda (KM) [88], and later on by Upadhye and Hu [145] (UH) (and many other authors [66, 68, 96]). The analysis of both groups will play an interesting role in the following sections. Hereafter, KM is going to be used as subscript for this formulation.

Note that one can rewrite the action (3.1) by introducing a new auxiliary field χ (a Lagrange multiplier). Let us consider the action

$$S = \frac{1}{2\kappa}\int d^4x\sqrt{-g}[f(\chi) + f_\chi(\chi)(R-\chi)] + S_{\rm M}[g_{ab},\Psi], \tag{3.14}$$

where f is an arbitrary function of the auxiliary field χ. Varying the action with respect to $f_\chi = \phi$ gives the constraint condition $f_{\chi\chi}(\chi)(R-\chi) = 0$. Hence, $\chi = R$, provided $f_{\chi\chi}(\chi) \neq 0$. Thus the action (3.14) is dynamically equivalent to (3.1). Redefining the field χ by

$$\phi := f_\chi(\chi) = f_R(R), \tag{3.15}$$

the action (3.14) becomes

$$S_{JF} = \int d^4x\sqrt{-g}\left[\frac{1}{2\kappa}\phi R - U(\phi)\right] + S_{\rm M}[g_{ab},\Psi], \tag{3.16}$$

where the potential $U(\phi)$ is given by

$$U(\phi) = \frac{\chi(\phi)\phi - f(\chi(\phi))}{2\kappa}. \tag{3.17}$$

Note that, in order for transformation (3.15) to be regular (invertible), we need the condition that $f_{\chi\chi}(\chi) \neq 0$, which is already satisfied by the assumption. Consider the original BD gravity action in the Jordan frame given by [146],

$$\mathcal{S}_{JF}^{BD} = \int d^4x\sqrt{-g}\left[\phi R + \omega_{BD}\frac{1}{\phi}\nabla_a\phi\nabla^a\phi\right]. \tag{3.18}$$

We see that the action (3.16) is equivalent to a BD with the parameter $\omega_{\rm BD} = 0$[6] where the quantity ϕ is taken as a single field with no kinetic term. However, it must be pointed out that such an equivalence holds partially since the action (3.18) has no scalar field potential. Thus $f(R)$ gravity is equivalent to a BD theory with parameter $\omega_{BD} = 0$ with the presence of a non-trivial self-interaction potential [33, 107, 141]. Such subtle consideration is crucial since such a value for ω_{BD} in these theories gives rise to a post-Newtonian (PPN) parameter $\gamma = 1/2$ which vastly differs from the value $\gamma \sim 1$ required by Solar System tests. Whether this was concluded directly from the action or from the equations of motion themselves makes no difference. As we shall see in Section 3.4.2 only by virtue of the proper equivalence between $f(R)$ gravity and BD theory the correct PPN limit is achieved. This limit is professedly enforced thanks to the chameleon mechanism [86].

Inverting the relation (3.15), the Ricci scalar can be expressed in terms of ϕ. In practice, it is not obvious to invert the scalar degree of freedom explicitly ($\phi = f_R(R)$). So a parametric form is

[6]Note that the $f(R)$ theory in the Palatini formalism is equivalent to the case $\omega_{\rm BD} = -3/2$ [84].

used.[7] Varying the action (3.16) respect to the metric and the scalar field ϕ leads to

$$G_{ab} = \frac{\kappa}{\phi}\left(T_{ab} - g_{ab}U(\phi)\right) + \frac{1}{\phi}\left(\nabla_a\nabla_b\phi - g_{ab}\Box\phi\right), \tag{3.19a}$$

$$R = 2\kappa\frac{dU(\phi)}{d\phi}. \tag{3.19b}$$

The right hand side of Eq. (3.19a) can now be seen as the source terms for the metric. It is also important to mention that these equations could have been derived directly from Eq. (3.2). We recognize in Eq. (3.19b) the expression that the scalar curvature satisfies, which is just the trivial identity $\chi = R$. As in the JPS formalism we take the trace of Eq. (3.19a) in order to replace R. Hence, we obtain the relation $R\phi = 3\Box\phi - \kappa(T - 4U(\phi))$ which, using Eq. (3.19b), yields

$$3\Box\phi + 2\kappa\left(U(\phi) - \phi\frac{dU(\phi)}{d\phi}\right) = \kappa T. \tag{3.20}$$

This makes strikingly clear that it is indeed a BD theory with null kinetic term and with a non-trivial potential $V(\phi)$. One can rewrite the equations using an alternative notation for the potential which leaves the equations of motion as (3.16):

$$\phi R_{ab} - \frac{1}{2}f g_{ab} - (\nabla_a\nabla_b - g_{ab}\Box)\phi = \kappa T_{ab}, \tag{3.21a}$$

$$\Box\phi = \frac{1}{3}\left[\kappa T + 2f - Rf_R\right] := \frac{\kappa T}{3} + \frac{dV_{\rm KM}}{d\phi}, \tag{3.21b}$$

where $V_{\rm KM} := Rf_R - f$ (i.e. a re-scaled version of Eq. (3.17)) and f is now function of $R(\phi)$. As is evident, we can assign to the scalar field a mass. An examination of Eq. (3.20) tells us that the dynamics of ϕ are regulated by the combination $U(\phi) - \phi\frac{dU(\phi)}{d\phi}$. In fact, one may go even further and realize that the mass considered in the classic STT is given by the second derivative of $V_{\rm KM}(\phi)$. So we have,

$$\frac{dV_{\rm KM}}{d\phi} = \frac{1}{3}(2f(R(\phi)) - \phi R(\phi)), \qquad m^2_{\rm KM} := \left.\frac{d^2V_{\rm KM}}{d\phi^2}\right|_{\phi=\phi_{min}} = \frac{1}{3}\left(\frac{\phi}{f_{RR}(R(\phi))} - R(\phi)\right). \tag{3.22}$$

This result has been derived from a variety of analysis such as perturbations to a de-Sitter background and studies of stability [30, 62]. Eqs. (3.21) are the field equations written in the so called Jordan-frame, a reminiscent terminology of the standard STT (see e.g. [19, 104]). It is interesting to see that ϕ now contains the Ricci scalar R degree of freedom.

Einstein Frame

By means of a conformal transformation, the action (3.16) can be transformed into the so called Einstein frame, in which a redefined field $\Phi \sim \ln\phi$ has a canonical kinetic term and is minimally coupled to the Ricci scalar. This approach was used by Babichev and Langlois (BL) in the context of compact stars [12] (see also [23, 36, 42, 64, 85, 94] for works which use the same formulation and [50, 104, 133, 134] for detailed analysis).

[7] For example, given a arbitrary function g of ϕ it can be written as $\frac{dV}{dR} = \frac{dV}{d\phi}\frac{d\phi}{dR}$.

Under the conformal transformation $\tilde{g}_{ab} = \Omega^2 g_{ab}$ we get the following relation for the Ricci scalars R and $\tilde{R}$ [148],

$$R = \Omega^2(\tilde{R} + 6\tilde{\Box}\omega - 6\tilde{g}^{ab}\partial_a\omega\partial_b\omega), \tag{3.23}$$

where a tilde represents quantities in the Einstein frame and

$$\omega = \ln\Omega, \qquad \tilde{\Box}\omega = \frac{1}{\sqrt{-\tilde{g}}}\partial_a(\sqrt{-\tilde{g}}\tilde{g}^{ab}\partial_b\omega). \tag{3.24}$$

We can rewrite the action (3.1) as

$$S[g_{ab}, \Psi] = \int \sqrt{-g}d^4x\left(\frac{FR}{2\kappa} - U(R)\right) + S_{\rm M}[g_{ab}, \Psi], \tag{3.25}$$

where we have defined $U = (FR - f(R))/2\kappa$ and set $F := f_R$ to keep the distinction from Eq. (3.16), although they are essentially the same action. By using Eq. (3.23), this action can be more easily transformed in to

$$S[g_{ab}, \Psi] = \int \sqrt{-\tilde{g}}d^4x\left[\frac{1}{2\kappa}F\Omega^{-2}(\tilde{R} + 6\tilde{\Box}\omega - 6\tilde{g}^{ab}\partial_a\omega\partial_b\omega) - U\Omega^{-4}\right] + S_{\rm M}[\Omega^{-2}\tilde{g}_{ab}, \Psi], \tag{3.26}$$

where we have used $\sqrt{-g} = \Omega^{-4}\sqrt{-\tilde{g}}$. Since we are looking for a linear action in $\tilde{R}$ we observe that the choice $F = \Omega^2$ gives us $\tilde{R}$ in the first term inside the square brackets. On the other hand, to change the kinetic term in to a standard form, that is, to satisfy the following relation

$$\frac{3}{\kappa}\tilde{g}^{ab}\partial_a\omega\partial_b\omega = \frac{1}{2}\tilde{g}^{ab}\partial_a\Phi\partial_b\Phi, \tag{3.27}$$

we see that $\omega = \sqrt{\kappa}\Phi/\sqrt{6}$ and by looking at Eq. (3.24) we note that the new scalar field Φ satisfies

$$\Phi := \sqrt{\frac{3}{2\kappa}}\ln F. \tag{3.28}$$

Hence, by choosing the new scalar field as in (3.28) the action in the Einstein frame is

$$S_E = \int d^4x\sqrt{-\tilde{g}}\left[\frac{\tilde{R}}{2\kappa} - \frac{1}{2}\tilde{g}_{ab}\partial_a\Phi\partial_b\Phi - V_{\rm BL}(\Phi)\right] + S_{\rm M}[\Omega^{-2}\tilde{g}_{ab}, \Psi], \tag{3.29}$$

with the potential

$$V_{\rm BL} := \frac{U}{F^2} = \frac{R(\Phi)f_R(\Phi) - f(\Phi)}{2\kappa f_R^2(\Phi)}, \tag{3.30}$$

where we have make use of the fact that the integral $\int d^4x\sqrt{-\tilde{g}}\tilde{\Box}\omega$ in the Eq. (3.26) vanishes on account of the Gauss's theorem. We stress that the conformal factor $\Omega^2 = F = f_R$ is field dependent and is related to R, as $f_R(R) = \exp\sqrt{2\kappa/3}\Phi$, i.e., an implicit function of Φ. It is useful to introduce a coupling function[8] defined by $A(\Phi) := \Omega^{-1}(\Phi) = f_R(R)^{-1/2}$ which further on can

[8]It is rather confusing the introduction of this function in the literature. In most of the derivations of this equivalence, the reduced Planck mass $M_{\rm PL}^2 = \kappa^{-1}$ is used. It is this approach that allows a more direct comparison with the original chameleon theory [86].

be related to a conformal coupling parameter Q as[9]

$$A(\Phi) = \exp Q\sqrt{\kappa}\Phi, \tag{3.31}$$

by setting $Q := -\sqrt{1/6}$. It is, however, extremely important to interpret the quantities in the action (3.29) correctly. Under this formalism it is commonly said that the field Φ is directly coupled to all matter fields with constant Q and is uniquely determined in all $f(R)$ theories. In order to see it more explicitly, by varying the transformed action (3.29), we are left with the subsequent set of equations

$$\tilde{G}_{ab} = k^{-1}\left[\tilde{T}_{ab} + \partial_a\Phi\partial_b\Phi - \frac{1}{2}\tilde{g}_{ab}\partial^c\Phi\partial_c\Phi - \tilde{g}_{ab}V_{\rm BL}\right], \tag{3.32a}$$

$$\tilde{\Box}\Phi = \frac{dV_{\rm BL}}{d\Phi} - \frac{1}{\sqrt{-\tilde{g}}}\frac{\partial\mathcal{L}_{\rm M}}{\partial\Phi}, \tag{3.32b}$$

where $\tilde{\Box} = \tilde{g}^{ab}\tilde{\nabla}_a\tilde{\nabla}_b$ and the covariant derivative $\tilde{\nabla}_a$ obeys $\tilde{\nabla}_a\tilde{g}_{ab} = 0$. $\tilde{T}_{ab}$ is the energy-momentum tensor of matter in the Einstein frame which is given by

$$\tilde{T}_{ab} = -\frac{2}{\sqrt{-\tilde{g}}}\frac{\delta\mathcal{L}_M}{\delta\tilde{g}^{ab}} = \frac{T_{ab}}{F}. \tag{3.33}$$

The derivative of the Lagrangian matter density $\mathcal{L}$ with respect to Φ is

$$\frac{\partial\mathcal{L}_{\rm M}}{\partial\Phi} = \frac{\partial\mathcal{L}_{\rm M}}{\partial g^{ab}}\frac{\partial g^{ab}}{\partial\Phi} = -\sqrt{-\tilde{g}}\frac{1}{2F}\frac{dF}{d\Phi}\tilde{T} \tag{3.34}$$

where the $\tilde{T} = \tilde{T}_{ab}\tilde{g}^{ab}$ is the trace of the transformed energy-momentum tensor. We can proceed by further defining the function $\alpha(\Phi)$ as

$$\alpha(\Phi) := \frac{d\ln A(\Phi)}{d\Phi} = -\frac{1}{2F}\frac{dF}{d\Phi} = Q\sqrt{\kappa}, \tag{3.35}$$

which gives us the strength of the coupling between the scalar field and the matter/energy source since the scalar equation (3.32b) is rewritten as

$$\tilde{\Box}\Phi = \frac{dV_{\rm BL}}{d\Phi} - \alpha(\Phi)\tilde{T}. \tag{3.36}$$

As we will see in the next section, the motivation for this definition starts with the conviction that $f(R)$ gravity is a chameleon theory. There is, of course, one caveat in the Einstein frame formulation. The transformed energy-momentum $\tilde{T}_{ab}$ tensor is not conserved, the contracted Bianchi identities give the following conservation law for the Einstein frame energy-momentum tensor

$$\tilde{\nabla}_a\tilde{T}^a_b = Q\tilde{T}\tilde{\nabla}_b\Phi, \tag{3.37}$$

which tells us that *conformal* matter moves on geodesics of g_{ab} implying that test particles do

[9]The reason for this redefinition can be traced back to equate alternative notations where the Jordan frame metric $g^{\rm J}_{ab}$ and the Einstein frame metric $g^{\rm E}_{ab}$ are related through $g^{\rm J}_{ab} = A^2(\Phi)g^{\rm E}_{ab}$ [12, 23].

not moves on geodesics of $\tilde{g}_{ab}$.[10] It is in the Jordan frame that $\nabla_a T^a_b = 0$ is satisfied. This implies that matter will feel a *fifth* force purely due to the gradients in Φ. A subtle conclusion, is that, when written as a Scalar-Tensor theory, gravity is *essentially* GR with modifications due to the effective contribution of the field Φ.

It is important to point out that there is a longstanding debate on the issue of conformal transformations. From an early stage many questions arised of which frame should be regarded as physical. One of the driving reasons to write $f(R)$ gravity in the Einstein frame was that the equations were much easy to handle. That is strictly speaking not true at all and can lead to confusing statements. The equations are more difficult to threat numerically due to multiple field redefinitions. How can we be sure that $f(R)$ theory and STT in the Einstein Frame are indeed the same theory in a different representation is a question that remains out of the scope of this thesis. The reader is encouraged to follow the discussion in some recent works [63, 115, 130].

The final concept we introduce for the Scalar-Tensor formalism is that of the mass of the scalar field Φ. There are multiple ways to make this precise [62]. Looking at the right-hand side of Eq. (3.36), a possible definition of mass emerges as the second derivative of the potential $\tilde{m}^2(\Phi) := d^2V_{\rm BL}/d\Phi^2\big|_{\Phi_{min}}$ which is true in the absence of matter. Corresponding to this transformation, one can express the derivative of the Einstein frame potential in terms of R, ϕ and Φ by noticing, that

$$\frac{dV_{\rm BL}}{d\Phi} = \frac{dV_{\rm BL}}{dR}\frac{dR}{d\phi}\frac{d\phi}{d\Phi}. \tag{3.38}$$

Let us perform the first and second derivatives of the potential (3.30)

$$\frac{dV_{\rm BL}}{d\Phi} = \sqrt{\frac{2}{3\kappa}}\frac{2f - Rf_R}{2f_R^2}, \qquad \frac{d^2V_{\rm BL}}{d\Phi^2} = \frac{1}{3f_{RR}}\left[1 + \frac{Rf_{RR}}{f_R} - \frac{4ff_{RR}}{f_R^2}\right]. \tag{3.39}$$

The reader who is encountering the apparatus for making the transition from R to Φ may be aghast at the seeming complexity. We have no comfort to offer. Nevertheless, in what follows we will simply forge ahead under the JPS formalism not before explaining the stark differences between both formalisms.

3.1.3 Scalar Tensor vs JPS formulation

A striking issue pointed out by Jaime et al. [78] in the context of static and spherically symmetric spacetimes is that the scalar field potential under the STT approach might be multi-valued. This is true, for example, for the Starobinsky $f(R)$ model proposed to explain the late accelerated expansion [137] (see section 4.1.2). The transformation to the Jordan frame requires $f_{RR}(R) \neq 0$, so, if it vanishes at some point R_0, then the scalar field cannot be inverted and the potential becomes multivalued. As a result, we may need to choose among different sets of solutions of

[10] Indeed, the conservation equation for the stress energy tensor is not conformally invariant. For a symmetric tensor $T^{ab} = T^{ba}$ we have [148],

$$\tilde{\nabla}_a(\Omega^s T^{ab}) = \Omega^s \nabla_a T^{ab} + (s + n + 2)\Omega^{s-1}T^{ab}\nabla_a\Omega - \Omega^{s-1}g^{ba}T\nabla_a\Omega,$$

where s is the conformal weight and n is the dimension of the manifold. In this case $n = 4$ and since $\tilde{T}_{ab} = \Omega^{-2}T_{ab}$, then $\tilde{T}^{ab} = \Omega^{-6}T^{ab}$ and $s = -6$. Thus, it follows that $\tilde{\nabla}_a(\Omega^s T^{ab}) = -\Omega^{-7}Tg^{ba}\nabla_a\Omega = -\Omega^{-5}T\tilde{g}^{ba}\nabla_a\Omega = -\Omega^{-1}\tilde{T}\tilde{\nabla}^b\Omega$. Recall that $\Omega = \exp\left\{-Q\sqrt{\kappa}\Phi\right\}$ thus the conservation law of Eq. (3.37) is recovered.

$R(f_R) = R(\phi)$ which, implies that $R(\phi)$ is not unique [29]. This is a prime requirement for the construction of $V(\phi)$. If there is not a one-to-one relation between ϕ and R, there is no guarantee that the potential has no pathological features. Single valueness is a requirement to construct well-behaved potentials.

These patologies present in the potential might be the route of some curvature singularities reported in [66]. Miranda et al. [96] proposed a $f(R)$ model that is free of such pathologies and is well-behaved during cosmological evolution and the construction of compact (see section 4.1.1).

One of the main advantages of the JPS formalism is that it does not resort on the usual mapping to STT, and therefore, does not deal with this kind pathological behavior.

3.2 Cosmology in $f(R)$ gravity

Although $f(R)$ cosmology is out of scope of this thesis we stress again that many $f(R)$ models have been proposed in the context of cosmic acceleration (see e.g. [131]). Let us recall that the main interest of studying $f(R)$ gravity lies in its potential to explain cosmological observations without the introduction of the dark sector. To be more explicit, the main property of $f(R)$ models is the natural introduction of an effective cosmological constant. When the matter terms are negible or sufficiently small ($T_{ab} \approx 0$), e.g. at the late universe, the JPS equations (3.5) admit the solution $R = R_{\rm dS} = const$ which is a zero of the derivative potential $dV(R)/dR$ (see Eq (3.8)). In this way, Eq. (3.6) reads $G_{ab} = -\Lambda_{\rm eff} g_{ab}$, where

$$\Lambda_{\rm eff} = \frac{R_{\rm dS}}{4} \tag{3.40}$$

which gives rise to the de Sitter type of solutions, where the asymptotic value $R_{\rm dS}$ of the Ricci scalar mimics the role of the cosmological constant. For instance, in the context of the previous section the metric functions behave far away from the star as follows

$$n(r) = m(r)^{-1} = 1 - \Lambda_{\rm eff}\frac{r^2}{3}. \tag{3.41}$$

In turn, it becomes mandatory to ensure the existence of the trivial solution of Eq. (3.5) provided by Eq. (3.40) in various $f(R)$ models, like the ones presented in Chapter 4, in order to produce a late time expansion. The above remarks indicate that a local minimum of the potential (3.9) is in fact the asymptotic value of the Ricci scalar towards the universe will evolve to. Hence, as we will further explain in section 4.1 this local minimum strongly depends on the value of the chosen parameters for each $f(R)$ model. For a more detailed review of $f(R)$ cosmology we refer to the reader to [50, 79, 104].

3.3 Static and spherically symmetric spacetimes

Let us consider the fields equations for stars in static equilibrium in the framework of $f(R)$ models when given an EoS to describe its matter content. So far, static and spherical configurations

in $f(R)$ gravity have been studied in Refs. [2, 48, 49, 56, 67, 73, 83, 99–102, 127, 145, 154]. A more detailed review on this studies is presented in Section 4.3.

Cosmology was usually the prime subject of $f(R)$ gravity, since the first inflationary model $f(R) = R + \alpha R^2$ proposed by Starobinsky [136] and then, as models of accelerated expansion. Many decades after examining modifications of GR have also motivated their confrontation with other experimental tests. Renewed interest in $f(R)$ models was brought because they were once again thought as viable candidates for the weak field gravity in light of the chameleon mechanism [27, 86]. In fact, solar system observations offer a essential laboratory by comparing the parametrized post-Newtonian (PPN) parameters with observations. For that, it is first necessary to obtain the metric outside of a star like the Sun.

Hereafter, we follow the JPS formalism presented in Section 3.1.1. The starting point is to obtain the field equations for a spherically symmetric and static matter distribution. Such an object is given by the line element

$$ds^2 = -n(r)dt^2 + m(r)dr^2 + r^2 d\Omega^2, \tag{3.42}$$

where $d\Omega^2 = d\theta^2 + \sin\theta d\varphi^2$. Plugin the metric (3.42) in Eq. (3.5) yields

$$R'' = \frac{1}{3f_{RR}}\left[m(\kappa T + 2f - Rf_R) - 3f_{RRR}R'^2\right] + \left(\frac{m'}{2m} - \frac{n'}{2n} - \frac{2}{r}\right)R', \tag{3.43}$$

where $' = d/dr$. From the $t-t$, $r-r$ and $\theta-\theta$ components of Eq. (3.6) and using Eq. (3.43) we obtain [78]

$$\begin{aligned}
m' =& \frac{m}{r(2f_R + rR'f_{RR})}\left\{2f_R(1-m) - 2mr^2\kappa T_t^t + \frac{mr^2}{3}(Rf_R + f + 2\kappa T)\right., \qquad (3.44a)\\
&\left. + \frac{rR'f_{RR}}{f_R}\left[\frac{mr^2}{3}(2Rf_R - f + 2\kappa T) - \kappa mr^2(T_t^t + T_r^r) + 2(1-m)f_R + 2rR'f_{RR}\right]\right\},\\
n' =& \frac{n}{r(2f_R + rR'f_{RR})}\left[mr^2(f - Rf_R + 2\kappa T_r^r) + 2f_R(m-1) - 4rR'f_{RR}\right], \qquad (3.44b)\\
n'' =& \frac{2nm}{f_R}\left[\kappa T_\theta^\theta - \frac{1}{6}(Rf_R + f + 2\kappa T) + \frac{R'f_{RR}}{m}\right] + \frac{n}{2r}\left[2\left(\frac{m'}{m} - \frac{n'}{n}\right) + \frac{n'r}{n}\left(\frac{m'}{m} + \frac{n'}{n}\right)\right]. \qquad (3.44c)
\end{aligned}$$

Note that Eqs. (3.44b) and (3.44c) are not independent. One has the freedom to choose any of the two and then use the remaining one to check the solutions. In order to close the system a fluid EoS, $\rho = \rho(p)$ is required. If we set $f(R) = R$ in Eqs. (3.44) they reduce to Eqs. (2.22) which ensure the correct limit to GR. On the other hand, the matter variables are governed by $\nabla_a T^{ab} = 0$. For a perfect fluid $T_{ab} = (\rho + p)u_a u_b + g_{ab}p$ it follows that

$$p' = -(\rho + p)\frac{n'}{2n}, \tag{3.45}$$

where it is important to note that n' is given explicitly by the right-hand side of Eq. (3.44b). Therefor, this is the modified TOV equation of hydrostatic equilibrium for $f(R)$ gravity in the JPS formalism. To solve the system of differential equations, we should impose boundary conditions. We will comeback to these equations later on Chapter 4. For now, let us continue with the general constraints an $f(R)$ theory should satisfy.

3.4 Viability of $f(R)$ gravity

Given the apparent freedom on the form of the $f(R)$ function, it has become evident that, to propose a model consistent with observational data, specific constraints should be imposed. However, so far it is not clear that there exists a single $f(R)$ model capable of passing all available cosmological and astrophysical tests. Below, we consider the observational and theoretical constraints imposed on any metric $f(R)$ gravity in cosmological scale and in the solar system.

In short, despite the primary role that astrophysical and cosmological observations play, not all $f(R)$ models have been able to account for every energy or time scale.

3.4.1 Cosmological Constraints

In order to satisfy the observational tests on cosmological scales, a viable $f(R)$ model should mimic the ΛCDM model, at late times. As pointed out in Eq. (3.40), we need that the value Λ_{eff} is close to the observed cosmological constant Λ. Amendola et al. [5] have derived the conditions regarding the cosmological viability of $f(R)$ models in order to recover the cosmological eras dominated by radiation, then by matter, and finally by acceleration. These conditions are as follows

$$m(r \approx -1) \approx 0 \qquad \frac{dm}{dr}(r \approx -1) > -10 < m \qquad (r \approx -2) \leq 1 \tag{3.46}$$

$$m := \frac{R f_{RR}(R)}{f_R} \qquad r := \frac{R f_R(R)}{f(R)}. \tag{3.47}$$

We urge the reader not to confuse these variables with the metric function $m(r)$ and the radial coordinate r but we have kept the notation used by Amendola et al. [5]. In addition to the aforementioned constraints, a generic $f(R)$ model should be described by monotonically growing and convex functions in order to avoid the presence of ghosts and instabilities,

$$f_R(R) > 0 \qquad f_{RR}(R) > 0. \tag{3.48}$$

Moreover, the condition $0 < f_{RR}(R_{\text{dS}}) < \infty$ is usually imposed to avoid exponentially growing modes when perturbing around the value $R = R_{\text{dS}}$ [29].

3.4.2 Local gravity constraints

It has been shown that many choices of the $f(R)$ function widely agree with cosmological observations. But to make such $f(R)$ satisfy the bounds on the existence of extra scalar degrees of freedom at the same time as describing the dark energy, has been subject of controversy [41, 57, 61].

Since highly accurate solar system tests, including orbital precession, gravitational Doppler effect and light bending, among others, they account for the extraordinary success of GR and so a viable cosmological $f(R)$ theory is expected to pass as well all the current tests that GR has successfully passed. In this regime we can safely assume that the gravitational field is weak and the

velocity of the planets is slow compared with c. Thus, it is natural to consider the PPN formalism to solar system tests. It took some time before a significant consensus regarding the weak-field limit in $f(R)$ gravity was displayed. As mentioned briefly in section 3.1.2, the value $\omega_{BD} = 0$ was used wrongly to conclude that $f(R)$ theories were ruled out since this led to $\gamma = 1/2$ [41] for this PPN parameter as opposed to the value $\gamma = 1$ that it is found by light deflection in the solar system experiments. This wrong conclusion was derived from the assumption that standard BD theory has no scalar field potential. Nevertheless, this γ parameter depends crucially on the presence of such scalar field potential. Studies against the $\gamma \approx 1$ are shown in for example [103, 125]. In particular, careful analysis of solar system tests (at the non-linear level) in $f(R)$ theories are found to be in [36, 41, 42, 51, 64, 68, 94, 103, 155].

For completeness it is enlightening to provide the **incorrect naive perturbative analysis** that was used in the past to claim that $\gamma = 1/2$. We follow [103], in the sense that the scalar degree of freedom is the Ricci scalar as in the JPS formulation instead of the auxiliary redefinition in terms of ϕ. As a first step, let us consider Eq.(3.43) with a Minkoswki background near the Sun, meaning that the metric functions n and m are close to one, this yields

$$R'' + \frac{2R'}{r} = \frac{1}{3f_{RR}}\left(\kappa T + 2f - Rf_R - 3f_{RRR}R'^2\right). \tag{3.49}$$

Eq. (3.49) has a similar structure to that of the original chameleon model [86, 87]. In section 3.5 we give further details. We emphasize that in most treatments [61, 68] Eq. (3.49) is written in terms of ϕ which corresponds to

$$\phi'' + \frac{2\phi'}{r} = \frac{1}{3}\left(\kappa T + 2f - R\phi\right). \tag{3.50}$$

Nevertheless, as Negrelli et al. [103] pointed out the main disadvantage of using Eq. (3.50) is the necessity of inverting all R dependent quantities in terms of ϕ. Considering the metric around the Sun very close to a flat background we define

$$n(r) = 1 - 2\Xi(r), \qquad\qquad m(r) = 1 + 2\psi(r), \tag{3.51}$$

where $|\Xi(r)| \ll 1$ and $|\psi(r)| \ll 1$. If we linearize the Ricci scalar around the minimum value R_0 of the scalar field potential, that is, $R = R_0 + \tilde{R}$, and drop second order terms in $\tilde{R}$, Eq. (3.49) takes the form

$$\tilde{R}'' + \frac{2\tilde{R}}{r} \approx \frac{\kappa T}{3f_{RR_0}} + m^2_{\text{eff},0}\tilde{R}, \tag{3.52}$$

where the effective mass is given as in (3.13), except that is evaluated at the minimum R_0,

$$m^2_{\text{eff},0} = \frac{2f_0 - R_0^2 f_{RR_0}}{3R_0 f_{RR_0}}. \tag{3.53}$$

The quantities with the subscript $_0$ are evaluated at R_0. At this point, let us remind that the minimum is of the order of cosmological density, $R_0 \sim H_0^2$. Thus, $m^2_{\text{eff},0} \ll 1$ in the solar system. Thus, Eq. (3.52) reduces to

$$\tilde{R}'' + \frac{2\tilde{R}'}{r} \approx \frac{\kappa T}{f_{RR_0}}. \tag{3.54}$$

This is the key equation that led to the wrong value $\gamma = 1/2$, since the GR limit cannot be recover from Eq. (3.54) as we will see next. Under the assumption that the interior of the Sun is described by a non-relativistic incompressible fluid $T \approx -\rho_\odot$ the solution of Eq. (3.54) outside the Sun is given by[11]

$$\tilde{R} = \frac{\kappa M_\odot}{12\pi f_{RR_0}} \frac{1}{r}. \tag{3.55}$$

Using the above solution in the linearized versions of Eq. (3.44a) and (4.30d) yields [103]

$$\psi \approx \frac{\kappa M_\odot}{12\pi f_{R_0}} \frac{1}{r} \qquad\qquad \Xi = \frac{\kappa M_\odot}{6\pi f_{R_0}} \frac{1}{r}. \tag{3.56}$$

According to this solution which turns to be independent of a particular $f(R)$ model, the PPN γ parameter is given by

$$\gamma = \psi/\Xi \approx \frac{1}{2}, \tag{3.57}$$

which clearly violates the strict experimental bound on the γ parameter ($|\gamma - 1| \ll 10^{-5}$ [20]). This is, of course, a consequence of the flawed analysis since the assumptions taken from the beginning were incorrect. Similar analyses have been carried out in literature [64, 68]. At the end, as Negrelli et al. [103] conclude, the naive results arise because essentially they do not take into account the screening effects associated with the scalar degree of freedom which emerge due to the non-linearities of the theory.

In light of the discussion presented above, we can now summarize the properties that a viable dark energy $f(R)$ model should satisfy.In summary, for a $f(R)$ model to be viable it must:

- Be free from instabilities and ghosts.
- Be able to generate an accelerated expansion of the Universe (without an explicitly cosmological constant).
- Have a correct weak field limit: pass all the available solar system.

3.5 Chameleon mechanism and $f(R)$ gravity

A construction of a cosmological relevant $f(R)$ theory is expected to have long-range type forces, also known as a fifth force, with an effective mass of $m_{\text{eff}} \lesssim H_0$. Since the dimensionless strength of this additional scalar fifth force is of order unity, it means that matter feels an additional force as strong as gravity itself. Therefore, realistic modifications of gravity must contain a mechanism to suppress scalar interactions at smaller scales, but deviate from GR at one curvature scale. Several screening mechanism have been proposed in the literature [23, 24] since they are relatively a generic prediction in modified gravity theories. Generally, they arise through the non-linear dynamics to effectively decouple cosmological and solar system or large structure

[11] We only write the solution outside the Sun, but in principle a full solution, like the one given in [103] is possible if using the matching conditions at the Sun radius.

scales. Although it is out of the scope of this thesis, a brief review of this class of mechanisms and its relationship with $f(R)$ gravity is worth considering.

The nature and significance of a screening mechanism takes into account the abysmal scale difference of two separate densities. In fact, there are 29 orders of magnitude separating the cosmological and solar densities. Furthermore, at the level of the action two main screening mechanisms classes can be elucidated. The first one is of the *Vainshtein* type [24, 121], whose main function is to suppress the scalar field gradient in the vicinity of the object. The other one is the *Chameleon* type [86], where the scalar field effective mass changes depending on the environment density. It is precisely this variation in the mass that favors the screening in the vicinity of the Sun.

The chameleon type screening mechanism has a standard kinetic term and a non-linear effective potential which depends on the local matter density. In this kind of models the scalar field value minimizing the effective potential depends on the local matter density. Hence, the scalaron mass naturally acquires density dependence. It is important to note that this mechanism was highlighted first under the Scalar-tensor formulation of $f(R)$ since its origin was based on this class of theories [23, 27, 86, 87, 142].

The classical picture of a chameleon field begins by introducing the action for gravity, matter, and the chameleon field ϕ. Then, the equation of motion for the scalar field can be written down in terms of a bare quintessence-type potential V and a contribution of the matter fields. It is precisely this effective potential that gives rise to a local relationship between the mass of the chameleon field and the density of matter [27, 86]. A chameleon theory is essentially a STT in which the potential is constrained to have certain features. Thus, let us come back to Section 3.1.2. The scalar field equation (3.36) can be rewritten as follows:

$$\tilde{\Box}\Phi = \frac{dV_{\rm BL}^{eff}}{d\Phi} := \frac{dV_{\rm BL}}{d\Phi} - \alpha(\Phi)\tilde{T}. \tag{3.58}$$

For non-relativistic matter governed by a perfect fluid energy-momentum tensor, $-\tilde{\rho} \approx \tilde{T}$. Since the two energy-momentum tensors are related through a conformal factor (3.34), then the assumption $T \approx -\rho \approx -\tilde{\rho} \approx \tilde{T}$ holds[12]. Thus, the effective potential in the Einstein frame takes the form

$$V_{\rm BL}^{eff} = V(\Phi) + \rho \ln A(\Phi), \tag{3.59}$$

and thus, depends on the local matter distribution. Let us now consider a spherically symmetric body with radius $\tilde{r}_c$ in the Einstein frame. It follows accordingly that Eq. (3.58) becomes

$$\frac{d^2\Phi}{d\tilde{r}^2} + \frac{2}{\tilde{r}}\frac{d\Phi}{d\tilde{r}} - \frac{dV_{\rm BL}^{eff}}{d\Phi} = 0. \tag{3.60}$$

Then, if we assume two regions that differ in density, that is, the case where inside the object $\rho = \rho_a$ ($\tilde{r} < \tilde{r}_c$) and $\rho = \rho_b$ outside the body ($\tilde{r} > \tilde{r}_c$). Then, the effective potential has two minima at the field values

$$\frac{dV_{\rm BL}(\Phi)}{d\Phi} + \kappa Q \exp\left[Q\sqrt{\kappa}\Phi\right]\rho\Big|_{\rho=\rho_a=\rho_b} = 0, \tag{3.61}$$

[12] The traces in both frames are related by $\tilde{T} = \tilde{g}^{ab}\tilde{T}_{ab} = A^2 g^{ab}\tilde{T}_{ab} = A^4 g^{ab}T_{ab} = A^4 T$.

where we have used $Q = -\sqrt{1/6}$. This indicates that the effective mass of the scalar field Φ changes dramatically from inner to outer density region. In other words, the denser the environment, the more massive is the chameleon field Φ which decreases the range of the fifth force. In this way, the mass field might acquire a sufficiently large value near a massive object (Sun) to hide the local tests. This region is known as the *thin-shell* gap. The field Φ in this region has a characteristic profile interpolating between two equilibrium values Φ_a and Φ_b. Qualitatively, if at $\tilde{r} = 0$ the scalar field value is close to Φ_a, it stays close to Φ_a up until some radius $\tilde{r}_1$. For a spherically symmetric body it is found that, to develop a thin-shell region, the condition

$$\frac{\Delta\tilde{r}_c}{\tilde{r}_c} \sim h\left(\frac{\rho_a}{\rho_b}\right) \ll 1 \tag{3.62}$$

should be satisfied [50, 102, 142], where h is a function that depends on the selected $f(R)$ model and $\Delta\tilde{r}_c = \tilde{r}_c - \tilde{r}_1$. Eq. 3.62 tells us that the thickness $\Delta\tilde{r}_c$ of the region where the field has an interpolating profile, should be very small or, in other words, $\tilde{r}_1$ has to be close to the body radius $\tilde{r}_c$. Moreover, for sufficient massive bodies (such as the Sun), Eq. 3.62 coincides with the thin-shell parameter $\epsilon_{\rm th}$ [86, 87], which, as in the case of the γ parameter, is heavily constrained by experiments. In particular, Equivalence Principle (EP) experiments such torsion-balance measurements [151], place bounds on $\epsilon_{\rm th}$. Using the experimental bound of the Eötvos ratio $\eta_{\rm ET}$ for the difference of two accelerations (free fall accelerations of the Earth and the Moon towards the Sun), $\eta_{\rm ET} < 10^{-13}$ [151], provided that Earth, Sun, and Moon have thin-shells (satisfy condition 3.62), the thin-shell parameter is bounded by [36, 94, 144]

$$\epsilon_{\rm th} = \frac{\Delta\tilde{r}_\oplus}{\tilde{r}_\oplus} < 2.2 \times 10^6, \tag{3.63}$$

where the subscript $_\oplus$ refers to the Earth radius. This bound provides a tight constraint on a $f(R)$ model seeking to satisfy local gravity constraints.

3.6 Discussion

We should point out that the estimations in the last sections were done by doing the transformation of $f(R)$ to STT followed by a series of approximations. However, to study the behaviour of the chameleon mechanism in a more quantitative way, the full non-linear system of equations should be solved. Although the chameleon effect seems to be generic to $f(R)$ theories [23, 36, 64, 103, 142], there are no numerical studies supporting it.

Up to this point we have summarized the general properties of $f(R)$ theories, its theoretical and experimental constraints and its different formulations. We have also outlined the framework for the analysis of static and spherically spacetimes by deriving its field equations in Section 3.3. These are precisely the equations that we are going to solve numerically in the following chapter.

As we emphasized in the sections above, it is advantageous to work in the JPS formalism to avoid the back and forth between the Einstein and Jordan frames. If the chameleon mechanism is independent on the $f(R)$ formulation, it should be noticed at the level of the full non-linear

system. However, as we will see, on the basis of our analysis it is not clear that this effect takes part.

Chapter 4

Stars in $f(R)$ gravity

In the previous chapter we examined the general properties of $f(R)$ gravity and laid down the theoretical framework for the analysis of the hydrostatic equilibrium of stellar structure. We are now in a position to perform such analysis on specific $f(R)$ functions. In this chapter we discuss some cosmologically viable $f(R)$ models and obtain numerical solutions for some equilibrium configurations. We focus only on constant density stars, as we did for the Sun in section 4.1.1, since they represent the most simple scenario to study the behavior of solutions at different scales.[1] It is important to stress that we will use the JPS formalism as opposed to the STT approach (see Appendix A), which has been used extensively in the past because for our purposes it is not only unnecessary but in many cases it turns to be ill-defined in several circumstances (namely when $f_{RR} \geq 0$).

4.1 $f(R)$ models

As explained thoroughly in section 3.4, one of the motivations to study $f(R)$ gravity is that it can account for the late accelerated cosmic expansion. In that section we also mentioned the conditions that $f(R)$ should satisfy in order to obtain a consistent cosmological evolution. In this section we shall review first some of the most successful $f(R)$ models used to mimic dark energy. All these models have the feature that they do not include an explicit cosmological constant ($f(0) = 0$), in contrast to what happens in GR ($f_{GR}(R) = R - 2\Lambda$) where $f_{GR}(0) = -2\Lambda$. In the past, several types of $f(R)$ models have been proposed as dark energy models. However most of them are either not cosmologically viable or, in practice, they cannot be differentiated from ΛCDM. For instance, models of the kind $f(R) = R - \alpha/R^n$ ($\alpha > 0$ $n > 0$), which were one of the first analyzed [4, 39, 57], failed because of the negativity of the second derivative which violates the condition $f_{RR} > 0$ and led to instabilities. Here we focus on models which, in general, can be easily seen as the usual Ricci scalar R term of GR plus some function of R that has a built-in scale $R_* \sim H_0^2$ in order to produce the correct cosmological history. These models

[1] Originally we consider the study of a compressible object such as a polytrope model for the sun, however, as we will see, we were incapable to do so, even for the constant density stars. Therefore the compressible model analysis seemed unnecessary at this point.

have the generic form

$$f(R) = R + R_* F_1\left(\frac{R}{R_*}\right). \tag{4.1}$$

Taking $z = R/R_*$, the derivatives of Eq. (4.1) take the form

$$f_R = 1 + \frac{1}{R_*}\frac{dF_1}{dz}, \qquad f_{RR} = \frac{1}{R_*}\frac{d^2F_1}{dz^2}. \tag{4.2}$$

Some of the $f(R)$ models presented in the following section were supposed to satisfy the solar system experiments, and as we mentioned above, they have the capability to be cosmological successful. However, as we will see in this thesis, it is not obvious that in such models solar system tests can be recovered (at least at the full non-linear level). They have also been extensively studied under different astrophysical scenarios. In particular, such selection of models have been thoroughly analyzed under the JPS formalism (cf. section 3.1.1) by Jaime et al. [79] and Negrelli et al. [103].

4.1.1 MJWQ $f(R)$ model

The $f(R)$ logarithmic model was proposed by Miranda et al. [96]:

$$f(R)^{\mathrm{MJWQ}} = R - \alpha_{\mathrm{M}} R_* \ln\left(1 + \frac{R}{R_*}\right), \tag{4.3}$$

where R_* and α_{M} are free positive parameters. It is straightforward to write the derivatives[2] of $f(R)^{\mathrm{MJWQ}}$ as

$$f_R = 1 - \alpha_{\mathrm{M}}\left(1 + \frac{R}{R_*}\right)^{-1}, \quad f_{RR} = \frac{\alpha_{\mathrm{M}}}{R_*}\left(1 + \frac{R}{R_*}\right)^{-2}, \quad f_{RRR} = -\frac{2\alpha_{\mathrm{M}}}{R_*^2}\left(1 + \frac{R}{R_*}\right)^{-3}. \tag{4.4}$$

In this way, we associate to this $f(R)$ function the following scalar potential

$$V(R)_{\mathrm{MJWQ}} = \frac{R_*^2}{6}\left[\left(1 + \frac{R}{R_*}\right)\left(\frac{R}{R_*} + 6\alpha_{\mathrm{M}} - 1\right) - 2\alpha_{\mathrm{M}}\left(3 + 2\frac{R}{R_*}\right)\ln\left(1 + \frac{R}{R_*}\right)\right]. \tag{4.5}$$

Recall that we remain in the original variables and no transformation to STT whatsoever has been made. Eq. (4.5) is obtained from Eq. (3.8) under the JPS formalism. Figure 4.1 depicts the behavior of the potential (4.5) and its derivative for different values of α_{M}. From that figure, we observe clearly the minimum value (purple stars), which corresponds to $R_1 > 0$, and is the one that should be reached asymptotically (in space, for stellar objects and in time, for cosmology) by a non-trivial solution for R in regions where matter becomes essentially absent and gives rise to the effective cosmological constant $\Lambda_{\mathrm{eff}} = R_1/4$.[3]

Note that Eqs. (4.4) still depend on the parameter α_{M}. We shall consider two values for α_M. For the first choice we follow [79] and set $\alpha_{\mathrm{M}} = 2$ and $R_* = \sigma_* H_0^2$, where H_0^2 is the Hubble constant today and σ_* is a dimensionless parameter which is chosen to be $\sigma_* = 1$. This choice

[2] We omit the superscripts referring to each $f(R)$ model in its derivatives since the notation becomes convoluted.

[3] In the STT this is the only $f(R)$ model where the resulting scalar field potential is single valued, see Appendix A.

of α_M was proved to reproduce correctly the cosmological evolution history [79], however, such a model seems to be inconsistent with the power matter spectrum and with the solar system tests [21, 51, 97, 103]. The second choice is $\alpha_M = 1.2$ and was considered in [78, 96]. Here we used this value in order to check the dependence of this model on the initial parameters, such as the central pressure and density.

In this $f(R)$ model, the condition $f_{RR} > 0$ holds in all the domain where the model is defined ($R/R_* > -1$, see bottom panel of Fig. 4.4), and thus, is free from tachyons and free from ghosts ($f_R > 0$, cf. Section 3.4.1). Using the notation of Eq. (4.2), it follows that $\lim_{R\to\infty} F_1/R = 0$ and $\lim_{R\to\infty} dF_1/dR = 0$, hence GR is recovered at early times.

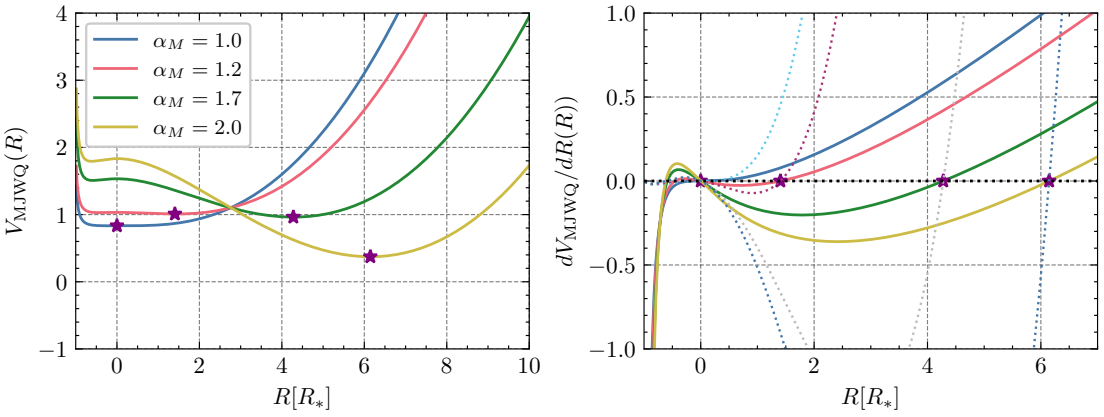

FIGURE 4.1: The scalar potential $V(R)_{\rm MJWQ}$ (left panel) and its derivative (right panel) for the MJWQ model. The purple star represents the local minimum for each choice of the α_M parameter. The dotted line corresponds to dV/dR (cf. Eq.(3.7)).

4.1.2 Starobinsky $f(R)$ model

We now turn our attention to the $f(R)$ model proposed by Starobinsky [137] given by

$$f(R)^{\rm S} = R + \lambda R_S \left[\left(1 + \frac{R^2}{R_S^2}\right)^{-q} - 1\right], \tag{4.6}$$

with q and λ positive parameters and R_S a natural cosmological scale given by $R_S = \sigma_S H_0^2 c^{-2}$, where σ_S is a dimensionless parameter. Computing the derivatives of Eq. (4.6) is straightforward,

$$f_R = 1 - \frac{2R\lambda q\left(\frac{R^2}{R_S^2}\right)^{-q}}{R_S\left(\frac{R^2}{R_S^2}+1\right)}, \qquad f_{RR} = \frac{2R_S\lambda q\left(\frac{R^2+R_S^2}{R_S^2}\right)^{-q}\left(2R^2(q+1) - R^2 - R_S^2\right)}{\left(R^2+R_S^2\right)^2}, \tag{4.7}$$

$$f_{RRR} = \frac{4RR_S\lambda q\left(\frac{R^2+R_S^2}{R_S^2}\right)^{-q}\left(-2R^2\left(q^2+3q+2\right) + 3\left(R^2+R_S^2\right)(q+1)\right)}{\left(R^2+R_S^2\right)^3}. \tag{4.8}$$

The explicit expression of the scalar potential is not very enlightening for an arbitrary value of q, thus we omit it. However, for the case of $q = 2$, the potential simplifies to

$$V(R)_{\rm STBS} = \frac{R_*^2}{3}\left\{\frac{R}{2R_*}\left[\frac{R}{R_*} - 4\lambda - 2\lambda\left(1 + \frac{R}{R_*}\right)\right]^{-1} + 3\lambda \arctan\left(\frac{R}{R_*}\right)\right\}. \tag{4.9}$$

A variety of choices can be made regarding the parameters of the Starobinsky model. Fig. 4.2 depicts the scalar potential and its derivatives for the values of λ, q and σ_s presented in Table 4.1.

For instance, with the values used by Kobayashi and Maeda [88] ($\rm KM_1$ and $\rm KM_2$ from Table 4.1), it is not clear that one can produce a correct cosmological history. Another choice of parameters, that indeed is able to produce an adequate matter epoch prior to the accelerated era, is the one analyzed in Refs. [79, 98] (JM from Table 4.1). Static and spherically symmetric configurations in this model have been studied numerically and non-perturbatively in Refs. [12, 13, 145] using the STT approach; a non-linear approach to stellar configurations is presented in [103].

	λ	q	σ_s
$\rm KM_1$	1.827	2	1
$\rm KM_2$	2.088	1	1
JS	1	2	4.17

TABLE 4.1: Values for the parameters of the Starobinsky $f(R)$ model (Eq. 4.9). The choices $\rm KM_1$ and $\rm KM_2$ are from Refs. [88], whereas the JS is taken from [79].

The properties Starobinksy $f(R)$ model can be summarized as follows. In the high-curvature regime, $|R| \gg R_S$, the model yields $f(R) = R - 2\Lambda(\infty)$ where the high-curvature value of the effective cosmological constant is $\Lambda(\infty) = \lambda R_0/2$. On the other hand, $f_{RR} = 0$ at $R = \pm R_S/\sqrt{2q+1}$, thus, f_{RR} is not positive definite (bottom left panel of Fig. **??**) and leads to ill-defined potentials when transformed to the STT, rising serious doubts when this approach is used (see Appendix A and [29]).

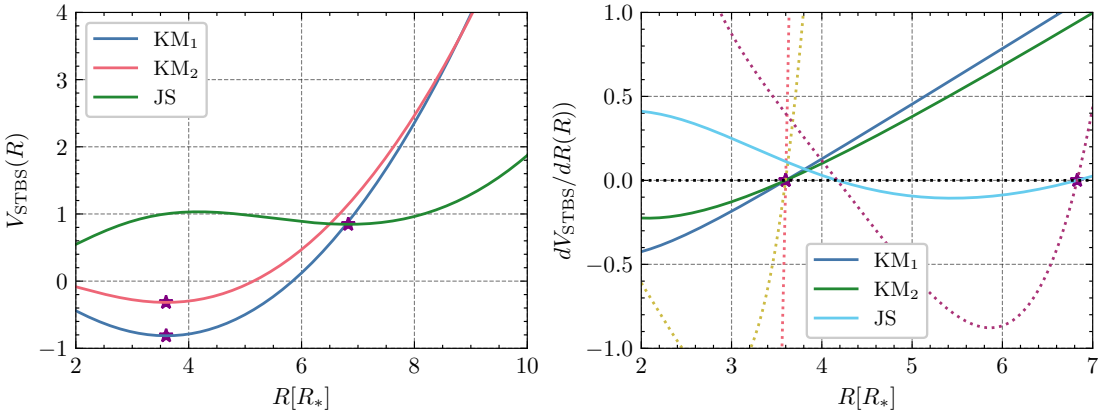

FIGURE 4.2: Same as Fig. 4.1 but for the Starobinksy $f(R)$ model with the parameters listed on Table 4.1.

4.1.3 Hu-Sawicki $f(R)$ model

The Hu- Sawicki [75] model is given by the following $f(R)$ function

$$f(R)^{\rm HS} = R - \frac{c_1 m^2 \left(\frac{R}{m^2}\right)^n}{c_2 \left(\frac{R}{m^2}\right)^n + 1}, \tag{4.10}$$

where m^2, c_1, c_2 and $n > 0$ are its parameters. Following Jaime et al. [78], we assume the parameters $m^2 = 0.24 H_0^2 c^{-2}$, $c_1 = 1.25\times10^{-3}$, $c_2 = 6.56\times10^{-5}$ and $n = 4$, in order to reproduce the observed cosmological constant. The derivatives of Eq. (4.10) are

$$f_R = 1 + \frac{c_1 c_2 m^2 n \left(\frac{R}{m^2}\right)^{2n}}{R\left(c_2 \left(\frac{R}{m^2}\right)^n + 1\right)^2} - \frac{c_1 m^2 n \left(\frac{R}{m^2}\right)^n}{R\left(c_2 \left(\frac{R}{m^2}\right)^n + 1\right)} \tag{4.11a}$$

$$f_{RR} = \frac{c_1 m^2 n \left(\frac{R}{m^2}\right)^n \left(-\frac{2c_2^2 n \left(\frac{R}{m^2}\right)^{2n}}{\left(c_2\left(\frac{R}{m^2}\right)^n+1\right)^2} + \frac{3c_2 n \left(\frac{R}{m^2}\right)^n}{c_2\left(\frac{R}{m^2}\right)^n+1} - \frac{c_2\left(\frac{R}{m^2}\right)^n}{c_2\left(\frac{R}{m^2}\right)^n+1} - n + 1\right)}{R^2\left(c_2 \left(\frac{R}{m^2}\right)^n + 1\right)} \tag{4.11b}$$

$$f_{RRR} = \frac{c_1 m^2 n}{R^3\left(c_2 \left(\frac{R}{m^2}\right)^n + 1\right)} \left(\frac{R}{m^2}\right)^n \left(\frac{6c_2^3 n^2 \left(\frac{R}{m^2}\right)^{3n}}{\left(c_2 \left(\frac{R}{m^2}\right)^n + 1\right)^3} - \frac{12 c_2^2 n^2 \left(\frac{R}{m^2}\right)^{2n}}{\left(c_2 \left(\frac{R}{m^2}\right)^n + 1\right)^2}\right. \tag{4.11c}$$

$$\left. + \frac{6c_2^2 n \left(\frac{R}{m^2}\right)^{2n}}{\left(c_2 \left(\frac{R}{m^2}\right)^n + 1\right)^2} + \frac{7 c_2 n^2 \left(\frac{R}{m^2}\right)^n}{c_2 \left(\frac{R}{m^2}\right)^n + 1} - \frac{9 c_2 n \left(\frac{R}{m^2}\right)^n}{c_2 \left(\frac{R}{m^2}\right)^n + 1} + \frac{2 c_2 \left(\frac{R}{m^2}\right)^n}{c_2 \left(\frac{R}{m^2}\right)^n + 1} - n^2 + 3n - 2\right) \tag{4.11d}$$

The analytical expression for the potential $V(R)$ is rather involved and we do not include it explicitly, but its expression is similar to the Starobinsky scalar potential. Fig. 4.3 shows the scalar potential (left panel) and its derivative (right panel). In this model, the global minimum sits at $R_1 \approx 8.931 R_*$. Thus, $\Lambda_{\rm eff} = R_1/4 \approx 2.23 R_*$. One thing to notice is that the Hu-Sawicki model with $n = 2$ model is equivalent to the Starobinsky model with $q = 2$, modulo a redefinition of their parameters (cf. Section 4.2).

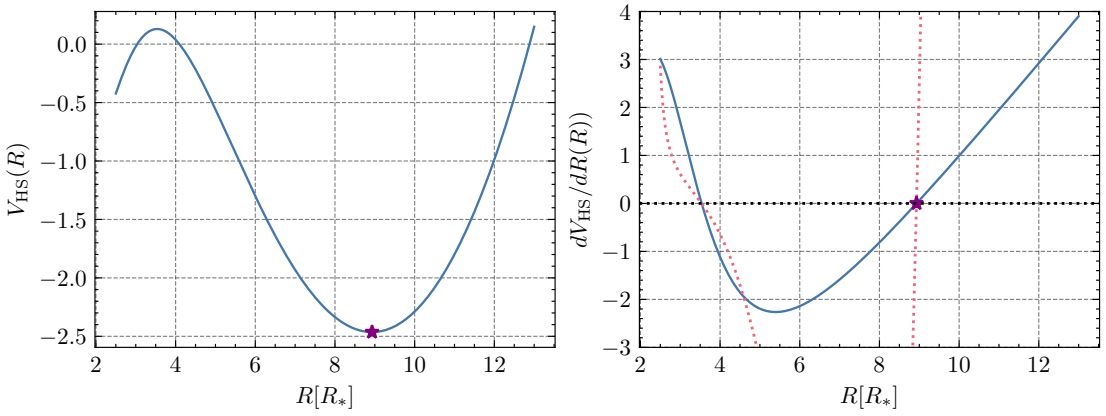

FIGURE 4.3: Same as Fig. 4.1 but for the Hu-Sawicki $f(R)$ model with the cosmological parameters as in [79].

It is important to remark that the Hu-Sawicki model was carefully constructed to pass the solar system tests via the Chameleon mechanism [75]. We will elaborate more about this in Section 4.3. The Hu-Sawicki together with the Starobinsky $f(R)$ model, have been the most analyzed models in the past [36, 53, 103, 143].

Finally, Figure 4.4 depicts the behavior of the $f(R)$ function and its derivatives for all the $f(R)$ models considered in this work. Specifically, in the top left and right panels we plot $f(R)$ and f_R, respectively. We also show $f_{GR}(R) = R - 2\Lambda$ and GR without cosmological constant. The bottom panel shows the second derivative f_{RR} (left), and third derivative f_{RRR} (right). Clearly, $f_{RR} = 0$ near $R \sim 2R_*$ for the Starobinsky and the Hu-Sawicki models. This implies that f_{RR} is not positive definite, and thus, the R equation 3.43 will blow up. We restrict ourselves to the domain where $f_{RR} > 0$ to avoid such calamities. As it turns out, in the limit where $R \gg R_*$, $f_R \to 1$, whereas $f_{RRR}, f_{RR} \to 0$, in the same limit. This behavior already introduces a numerical difficulty since, for an $f(R)$ theory to not deviate from GR in the regime where $R \sim \kappa\rho$, the second and third derivative will be close to zero and both quantities appear explicitly in the field equations (3.44).

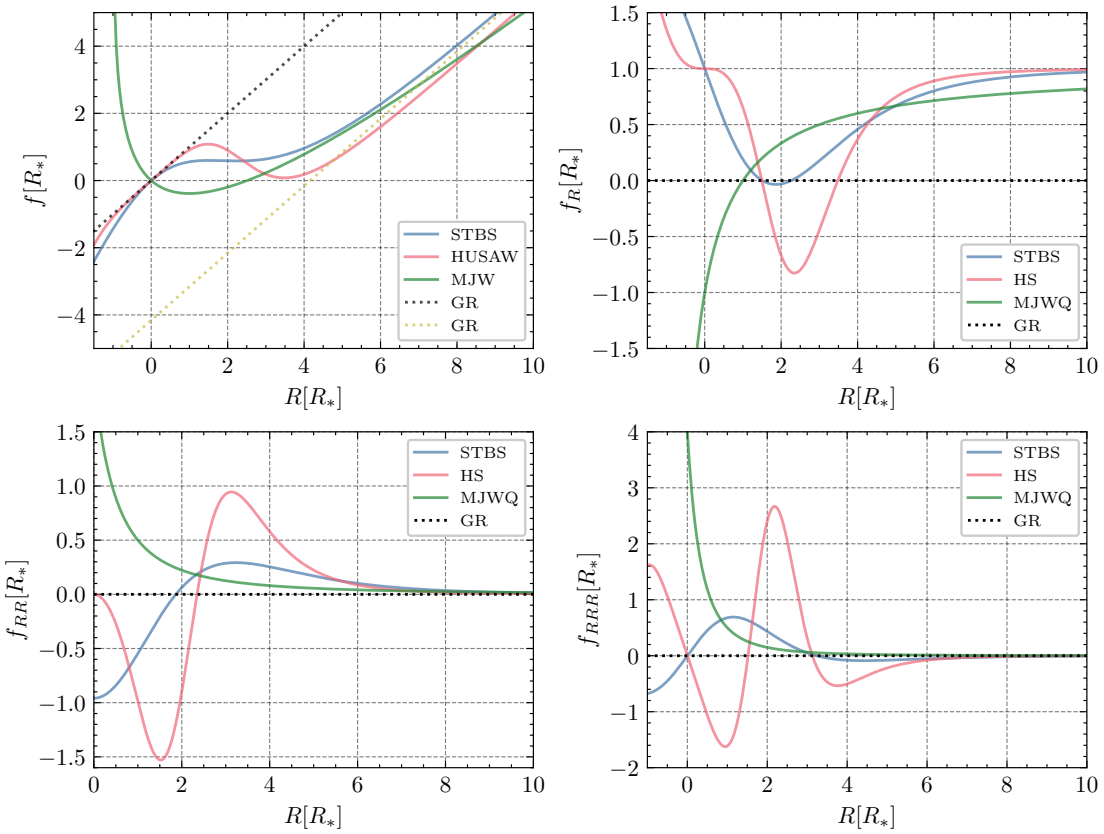

FIGURE 4.4: *Top panels*: $f(R)$ function for all models considered (left panel). Specifically, the JM values (cf. Table 4.1) for the Starobinsky model and $\alpha_M = 2$ for the MJWQ model. For reference, the GR case ($f(R)_{GR} = R$) and GR + Λ are depicted. Note that, as R/R_* increases, all the $f(R)$ models tend to the form $f(R) \sim R \approx 2\Lambda_{\text{eff}}$. The first derivative $f_R(R)$ for the same three $f(R)$ models is shown in right panel. *Bottom panel*: Second derivative f_{RR} (left panel) and third derivative f_{RRR} (right panel). R is in units of R_*. Notice that f_{RR} is not positive definite for the Starobinsky and Hu-Sawicki functions. We restrict the solutions space to $R > 0$.

4.2 Curvature regimes

The discussion in previous chapters has been limited to an arbitrary $f(R)$ function. In this section we focus, for concreteness, in the $f(R)$ models introduced in previous section. Within the context of equilibrium stars like the Sun, roughly two *curvature* regions can be identified. First we name the *high-curvature* regime as the region where a non-trivial solution $R(r)$ satisfies $R \gg R_*$ (see Eq. (3.43)). Second, a *low-curvature* region is such that $R \sim R_*$. This will, in general be true provided that the high-curvature regime happens inside the object where the curvature is of the order of the central density ($R \sim \kappa\rho_c$) and is much higher than the cosmological value R_*. On the other hand, the low-curvature region will generally happen outside the stellar object.

Given these two regions, we can consider for each $f(R)$ function a separation of the following manner

$$f(R) = R + \Delta, \qquad f_R = 1 + \Delta_R, \qquad f_{RR} = \Delta_{RR}, \qquad f_{RRR} = \Delta_{RRR}, \tag{4.12}$$

which isolates the *correction* to the linear term R. We observe that $\Delta = R_* F(z)$ from Eq. (4.1). For instance, in the Starobinsky model these functions read

$$\Delta^{\rm S} \approx \lambda R_S \left[\left(\frac{R}{R_S}\right)^{-2q} - 1\right], \qquad \Delta^{\rm S}_R = -\frac{2R\lambda q\left(\frac{R^2}{R_S^2}\right)^{-q}}{R_S\left(\frac{R^2}{R_S^2}+1\right)} \approx -2\lambda q\left(\frac{R_S}{R}\right)^{2q+1}, \tag{4.13}$$

$$\Delta^{\rm S}_{RR} \simeq \frac{2\lambda q(2q+1)}{R_S}\left(\frac{R}{R_S}\right)^{-2q-2}, \tag{4.14}$$

where R_S/κ is of the same order of magnitude as the cosmological density ($\rho_\Lambda \sim 10^{-29}\text{g/cm}^3$). Thus, we observe that $\Delta^S \ll R$ and $\Delta^S_R \ll 1$, when $R \gg R_S$.

On the other hand, for the Hu-Sawicki model, something similar happens. If we redefine its parameters (see Eq. (4.10)) as $\lambda = c_1/c_2$, $R_S = m^2$ and $n = 2q$, the Hu-Sawicki function (4.10) becomes

$$f(R)^{\rm HS} = R - \lambda R_c \frac{(R/R_c)^{2q}}{(R/R_c)^{2q}+1}, \tag{4.15}$$

where

$$\Delta^{\rm HS} \approx \lambda R_S \left[\left(\frac{R}{R_S}\right)^{-2q} - 1\right], \tag{4.16}$$

$$\Delta^{\rm HS}_R = +\frac{2\lambda q\,(R/R_S)^{2q-1}}{\left[(R/R_S)^{2q}+1\right]^2} \approx -2\lambda q\left(\frac{R_S}{R}\right)^{2q+1}, \tag{4.17}$$

$$\Delta^{\rm HS}_{RR} = 2q\lambda R_S\left(\frac{R}{R_S}\right)^{2q}\left[\frac{(R/R_S)^{2q}+2q\left[(R/R_S)^{2q}-1\right]+1}{R^2\left[(R/R_S)^{2q}+1\right]^3}\right] \simeq \frac{2\lambda q(2q+1)}{R_S}\left(\frac{R}{R_S}\right)^{-2q-2}, \tag{4.18}$$

which proves that, in the high-curvature regime, the Hu-Sawicki behaves similarly, if not identically, to the Starobisnky model or viceversa. This is not surprising since both models can be

traced back to a function of the form [96, 143]

$$\Delta^G = \lambda\beta R_S \left[\left(1+\left(\frac{R}{R_S}\right)^n\right)^{-1/\beta} - 1\right]. \tag{4.19}$$

In this way, if we choose $\beta = 1$ and $n = 2q$, we obtain the Hu-Sawicki function (4.15). On the other hand, the choice $n = 2$ and $0 < \beta \leq 1$ corresponds to the Starobinsky parametrization of Eq. (4.6). Moreover, in the case of $\beta \to \infty$ and $n = 1$, the MJW (4.3) is recovered.[4] Notice that in the high-curvature regime Eq. (4.19) takes the form

$$\Delta^G \approx \lambda\beta R_S \left[\left(\frac{R}{R_S}\right)^{-n/\beta} - 1\right] \qquad \Delta^G_R \approx -\lambda n \left(\frac{R}{R_S}\right)^{-(n/\beta+1)}. \tag{4.20}$$

where it follows that $\Delta^G_R \ll 1$ when $R \gg R_S$. We are now in a position to be more specific about how the local constraints and the chameleon mechanism play a role.

Recall that the scalar potential in the JPS formalism $V_{JPS}(R)$ is given by Eq. (3.9). Using (4.20) in the potential we obtain the high-curvature regime approximation

$$V_{JPS}(R) = -\frac{1}{3}(R^2 + R\Delta^G) + \int^R x + \Delta^G(x)dx \approx R_S^3\left(\frac{R}{R_S}\right)^{n/\beta+4}, \tag{4.21}$$

We stress that the introduction of this potential is useful to identify the critical points and it is not used in the main numerical computations.

At the minima R_{min} inside the object, where is expected that $R \sim \kappa\rho_c$, the effective chameleon mass m^2_{eff}, defined in Eq. (3.13) as the second derivative of $V_{JPS}(R)$ evaluated at R_{min}, can be approximated as

$$m^2_{\text{eff}} = \frac{1}{3}\left[\frac{f_R}{f_{RR}} - R\right]\Big|_{R_{min}} = \frac{1}{3}\left[\frac{1}{\Delta^G_{RR}} + \frac{\Delta^G_R}{\Delta^G_{RR}} - R\right]\Big|_{R_{min}} \approx \frac{1}{3\Delta^G_{RR}}\Big|_{R_{min}} = \frac{R_S}{3n/\beta\lambda+1}\left(\frac{R}{R_S}\right)^{n/\beta+2}\Big|_{R_{min}}. \tag{4.22}$$

On the other hand, the extremum of the effective potential $V^{\text{eff}}_{\text{JPS}}(R,T)$ (cf. Eq. (3.12)) is

$$2f - Rf_R\Big|_{R_{min}} \approx R_{min} = -\kappa T. \tag{4.23}$$

Assuming $T = \kappa(3p_c - \rho_c)$, where p_c and ρ_c are the central density and pressure respectively of a stellar object, the mass in the high-curvature regime (4.22) is of the order of

$$m_{\text{eff}} \approx \left(\frac{R_S}{3n/\beta\lambda+1}\right)^{1/2}\left(\frac{-\kappa(3p_c-\rho_c)}{R_S}\right)^{n/2\beta+1}, \tag{4.24}$$

where $R_S \sim \kappa\rho_\Lambda$. It should be noticed that in general, the Ricci scalar can vary in distance scales of its Compton wavelength $\lambda_R := m^{-1}_{eff}$. As we will discuss below, this wavelength turns to be very small compared to the radius of the object in the high-density regime. Thus, it becomes crucial to calculate the ratio between the curvature length scale (i.e. the radius of the star r_*) and the scalar field Compton wavelength r_*/λ_R, which will be proportional to the number of

[4] Also, if we let $\beta = -1$, which violates the cosmological viability conditions of Eq. (3.46), the model $f(R) = R - \lambda R_S(R/R_S)^n$ is recovered [39].

integration steps in a brute force implementation. For that, recall from GR that $r_*^2 = 12p_c/(\kappa\rho_c^2)$, and using the non-relativistic approximation $\rho_c \gg p_c$ in (4.24), we obtain

$$r_*/\lambda_R \sim \left(\frac{\rho_c}{\rho_\Lambda}\right)^{n/2\beta+1}, \tag{4.25}$$

Thus, the size of r_*/λ_R depends on the density contrast, which happens to be absurdly large for the actual densities of stellar objects, meaning that the number of steps needed for the integration in the stellar interior is extremely large. As we will see in the next section this stark fact has been the main difficulty so far to obtain numerical solutions for the stellar equilibrium in $f(R)$ theories.

4.3 Review of stellar configurations in $f(R)$ gravity

Before proceeding to perform any calculation, it is worth considering the numerical status of star-like object in this class of theories. As stressed in Chapter 3, in vacuum, cosmologically viable $f(R)$ naturally produce a de Sitter spacetime rather than the usual Minkwoski solution of GR. This means that, to find a unique exterior solution for the stellar object, the interior solution is matched to a de Sitter metric with an effective cosmological constant. In other words, a complete solution of the field equations of $f(R)$ gravity involves *a fortiori* two completely different densities (or curvature scales). Indeed, as reflected in Section 4.1 each $f(R)$ model is characterized by a curvature scale $R_* := H_0^2/c^2$ which can be used to introduce an associated density

$$\rho_* := \frac{c^4}{8\pi G_0}\frac{R_*}{c^2} \approx 3.008 \times 10^{-27}\text{kgm}^{-3}. \tag{4.26}$$

If we take the density of the Sun as $\rho_\odot = 1408\text{kg/m}^3$, or worst of a neutron star density $\rho_{\text{NS}} \backsimeq 10^{17}\text{kg m}^{-3}$, then the density contrast between both scales becomes huge. This contrast is shown in Table 4.2, the ratio between the solar density $\rho_\odot$ and the characteristic cosmological density ρ_* is of the order of $\rho_\odot/\rho_* \sim 10^{29}$ and only becomes worse when neutrons stars are considered ($\rho_{\text{NS}}/\rho_* \sim 10^{44}$). This ratio appears naturally in the field equations as seen from their dimensionless form (4.30) and the dimensionless parameters (4.31), and it is also intrinsically responsible for the chameleon effect to take part (see Eq. (4.25)). This large disparity in density scales has been a technical issue that one faces when integrating stellar objects embedded in a realistic de Sitter background.

	$\rho[\text{ kg/m}^3]$	$\rho/\rho_\odot$	ρ/ρ_*
$\rho_\odot$	1408	1	4.6808×10^{29}
ρ_*	3.008×10^{-27}	2.1363×10^{-30}	1
ρ_{NS}	10^{17}	$\sim 10^{14}$	$\sim 10^{44}$

TABLE 4.2: Density contrast depicted as the ratio between the involved characteristic densities.

So far, this technical problem has been present in all of the studies regarding stellar objects and, in order to circumvent it, the majority of authors have considered objects far from representing

real stars embedded in a realistic cosmological background. It is one of the main objectives of this work to try to obtain numerical solutions for realistic objects.

In these studies there are basically two points of view. In one, the authors are not worried at all of taking $f(R)$ as a dark energy model, but simply, they use this class of theories as a proof of concept for stellar configurations. This viewpoint encompasses studies of relativistic stars in models such as $f(R) = R + \alpha R^2$ (analyzed briefly in the last chapter) [8, 10, 11, 37, 45, 67, 109, 153] $f(R) = R + \alpha R^2 + \beta \ln(R/\mu^2)$ [2, 6], or other even more complex $f(R)$ functions [7, 10, 28, 73, 83, 85, 124]. This $f(R)$ models are not cosmologically motivated and they are often treated only in the strong field regime of gravity. In fact, from a perspective of curvature scales, one can further see that the characteristic scales appearing in this models satisfy $\alpha, \beta \cdots \gg R_*$.

The other point of view, which is the one we are considering in this work, is to take the $f(R)$ theories as a universal model of nature that should be valid at all scales. Thus, we are essentially dealing with viable dark energy $f(R)$ models and trying to prove its validity in other gravity sectors such as their stellar counterpart. Following this trend, stable star configurations have been found in [6, 12, 13, 78, 88, 96]. In particular, the Newtonian limit of $f(R)$ theories provides further understanding of these models [28, 33, 34, 99, 100], together with solar systems tests [36, 42, 61, 68, 94, 103]. Treating $f(R)$ gravity as a chameleon theory also falls in this category [23, 25, 48].

From these distinct points of view we can draw some preliminary conclusions about the status of stars in $f(R)$. It is immediately apparent that the choice of the parameters of the $f(R)$ model far from the characteristic cosmological scales permits to consider realistic central densities at the sake of keeping a cosmological non-viable $f(R)$ model. On the other hand, assuming $f(R)$ as a real alternative to the current ΛCDM paradigm, and as serious alternative theory of gravity, leads to the technical difficulties presented at the beginning of this section. Let us highlight some studies within this viewpoint.

Not so long after Frolov [66] pointed out that $f(R)$ models generically suffer from the problem of curvature singularities (later proved to be as a consequence of using the STT approach by Jaime et al. [78]), Kobayashi and Maeda [88] considered the study of relativistic stars using incompressible objects with relatively low central densities ($\rho_c \sim 10^6 \rho_\Lambda$) under the STT formalism in the JF, and concluded that such objects cannot exist in the $f(R)$ Starobinsky model due to the same singularity encountered by Frolov [66]. They solved numerically the TOV equations presented in Appendix A. Given these circumstances multiple authors embarked on addressing the existence of compact objects in cosmological viable $f(R)$ models. Babichev and Langlois [12, 13] found numerical solutions corresponding to static star configurations with a strong gravitational potential ($U_c := GM_*/r_* \lesssim 0.3$) in the Starobinsky model. They used the STT conformal transformation in the EF both for constant energy-density configurations and also for a polytropic equation of state. Then in a different study again Kobayashi and Maeda [89] proceeded to add a high-curvature correction $\sim R^m/\mu^{2m-1}$ to remedy the nonexistence controversy. It seems that such controversy was settled down by Upadhye and Hu [145] where, again, numerical solutions were found but this time using the JF variables for constant density stars under wide range of central pressures but keeping a extremely low central density $\rho_c = 100\rho_\Lambda$. One of the main conclusions reached by Upadhye and Hu [145] was that such singularities encountered before were due to numerical instabilities. Indeed, as we will see in the following sections, the scalar

field (R in the JPS approach rather than ϕ or Φ in the STT approach) value inside a compact object can be very close to the value where the derivative of effective scalar potential becomes very large. Another important remark made by Upadhye and Hu [145] was that the chameleon screening effect is unrelated to strong gravitational field and thus can appear in non-relativistic stars (like our sun $U_\odot \sim 10^{-6}$). At roughly the same time, Miranda et al. [96] also made an analysis on relativistic stars considering low central densities using their proposed model (cf section 4.1.1) that was specifically designed to circumvent the divergences also mentioned in [88]. Jaime et al. [78] also made a brief numerical analysis of practically the same kind of stellar models alluded above but this time using the JPS formalism (cf. section 3.1.1).

For our purposes, it is important to acknowledged some works regarding solar system tests in $f(R)$ gravity. The analysis done by Guo [68] provides some solutions that might suggests that the MJWQ is ruled out. As the works mentioned above, the author uses the JF as well and solve numerically an approximated form of the equation for the scalar field $\phi = f_R$ (specifically Eq. (3.50)) for the Hu-Sawicki and the MJWQ $f(R)$ models using a non-homogeneous density model for the sun. According to the author, the chameleon screening effects can alleviate the theoretical and the observed value of the PPN γ parameter. However, Guo does not use the cosmological values for the model parameters. Even if one were to choose another set of parameters, it is not clear that Guo's numerical solutions (for the approximated version of the equation for f_R) can be used as an argument against the models themselves. In this way, Guo's analysis is fairly inconclusive since the author do not specify a clear relation between γ parameter and the solutions that are reported.

Another worth mentioning analysis was given by Negrelli et al. [103]. Contrary to the aforementioned works, they perform a novel non-standard linear perturbation approach in the JPS formalism using the Ricci scalar itself as the fundamental variable. They manage to obtain solutions for both the metric and the Ricci scalar for the same models considered in this work[5] and conclude that the MJWQ was incompatible with $\gamma = 1$ leaving the Starobinsky and the Hu-Sawicki $f(R)$ models as the only ones that satisfy the experimental bounds on γ. They consider the solar system as a model of three constant density layers (the sun, its corona and the interstellar medium). In this way, they effectively manage to work with realistic densities for the Sun an its surrounding medium. An important aspect arising from their solutions, is that the Ricci scalar profile *follows* the density function as the field changes in the radial coordinate r.

Closing this section we comment on the paper by Hu and Sawicki [75] where they introduced their model (cf. section 4.1.3) and confront it with the available solar system constraints. They consider an inhomogeneous model for the Sun and claimed to solve numerically (the perturbed) the field equations written in the ST way in the JF.[6] We must point out that their work appears to be the only one in the literature that presents a specific profile of the Ricci scalar for the case of the Sun as a result of solving numerical the TOV modified equations in $f(R)$ gravity. However, it is unclear how they managed to circumvent the density problem that we discuss before.

In summary, numerical solutions of stellar objects in viable $f(R)$ models are plagued with contradictory and controversial claims. How to understand the status and significance of real physical solutions clearly presents serious challenge that we will explore in the following sections.

[5] They consider an additional $f(R)$ model: the exponential model given by $f(R) = R - \beta R_*(1 - \exp -R/R_*)$ [44].
[6] According to our notation of Eq. (4.12) $\Delta(R) = f_{HS}(R)$ where $f_{HS}(R)$ is the function that they used.

4.4 Numerical strategy

The numerical method chosen to solve the modified TOV equations in $f(R)$ gravity is based in a higher-order adaptive size Runge-Kutta method that implements a shooting technique (cf. Section 4.4.2). This is a widely used tecnhique to solve boundary value problems for differential equations, which we discuss in more detail below. In order to implement that method, the first step is to write the set of differential equations of Section 3.3 in a suitable way. For this purpose we introduce the following rescaled dimensionless variables

$$r = \hat{r} r_\star, \qquad R = \hat{R} R_\star, \qquad \rho = \hat{\rho}\rho_\star, \qquad p = \hat{p} p_\star, \qquad \hat{f}_{R_l} = R_\star^{l-1} f_{R_l}, \tag{4.27}$$

where the index l indicates the order of the derivative respect R. From Eq. (4.1), we observe that the $f(R)$ function intrinsically contains the numerical contrast η,

$$\hat{f}(\hat{R}) := \frac{f(\hat{R})}{R_\star} = \hat{R} + \eta F_1\left(\frac{\hat{R}}{\eta}\right), \tag{4.28}$$

where $\eta := R_*/R_\star$ is the ratio between the cosmological scale R_* and the units chosen to measure R. Since we are considering a perfect fluid, it follows from Eq. (4.27) that the dimensionless trace of the energy-momentum tensor is given by

$$\hat{T} = \frac{T}{p_\star} = \left(-\frac{\hat{\rho}}{b} + 3\hat{p}\right), \tag{4.29}$$

where, as in GR, $b = p_\star/\rho_\star c^2$. Note that, if we choose to measure the pressure in density units, then $b = 1$. Therefore, using the above rescaling (4.27) we write the set of equations (3.43)-(3.44) in dimensionless form:

$$\hat{R}'' = \frac{1}{3\hat{f}_{RR}}\left[m(\alpha\hat{T} + \beta(2\hat{f} - \hat{R}\hat{f}_R)) - 3\hat{f}_{RRR}\hat{R}'^2\right] + \left(\frac{m'}{2m} - \frac{n'}{2n} - \frac{2}{\hat{r}}\right)\hat{R}' \tag{4.30a}$$

$$m' = \frac{m}{\hat{r}(2\hat{f}_R + rR'\hat{f}_{RR})}\left\{2\hat{f}_R(1-m) - 2\alpha m\hat{r}^2\hat{T}^t_t + \frac{m\hat{r}^2}{3}\left[\beta(R\hat{f}_R + \hat{f}) + 2\alpha\hat{T}\right]\right. \tag{4.30b}$$
$$\left. + \frac{\hat{r}R'\hat{f}_{RR}}{\hat{f}_R}\left[\frac{mr^2}{3}[\beta(2R\hat{f}_R - \hat{f}) + \alpha\hat{T}] - \alpha m\hat{r}^2(T^t_t + T^r_r) + 2(1-m)\hat{f}_R + 2\hat{r}R'\hat{f}_{RR}\right]\right\}$$

$$n' = \frac{n}{\hat{r}(2\hat{f}_R + \hat{r}R'\hat{f}_{RR})}\left[m\hat{r}^2[\beta(\hat{f} - \hat{R}\hat{f}_R) + 2\alpha\hat{T}^r_r] + 2\hat{f}_R(m-1) - 4\hat{r}R'\hat{f}_{RR}\right] \tag{4.30c}$$

$$n'' = \frac{2nm}{\hat{f}_R}\left[\alpha T^\theta_\theta - \frac{1}{6}[\beta(\hat{R}\hat{f}_R + \hat{f}) + 2\alpha T] + \frac{R'\hat{f}_{RR}}{m}\right] + \frac{n}{2\hat{r}}\left[2\left(\frac{m'}{m} - \frac{n'}{n}\right) + \frac{n'r}{n}\left(\frac{m'}{m} + \frac{n'}{n}\right)\right] \tag{4.30d}$$

The two dimensionless parameters, α and β, that appear in the above equations have been defined as:

$$\alpha = \frac{8\pi G}{c^4} r_\star^2 p_\star, \qquad \beta = R_\star r_\star^2, \tag{4.31}$$

which together with b and η encode the chosen units. Hereafter, we choose to measure the pressure in density units ($p_\star = \rho_\star c^2$), thus $b = 1$. Given these considerations, we could, in principle, select a set of units to deal in the best possible manner the numerical contrast

discussed in previous sections. We can consider three different but equivalent approaches to reach gradually the density of the Sun $\rho_\odot \approx 10^{29}\rho_*$.

For instance, we consider the case where the Ricci scalar is measured in units of the cosmological scale $R_\star = R_*$, implying that $\eta = 1$, and the radial coordinate in units of $r_\star = (R_*)^{-1/2}$, thus $\beta = 1$. Furthermore, if we set the units of the density as that of the cosmological value $\rho_\star = \rho_*$, we obtain

$$\alpha = 1, \qquad \beta = 1, \qquad \eta = 1. \tag{4.32}$$

Then, we gradually increase the density of the object until the value $\rho_\odot$ is approached. For instance, we could start with an non-realistic object characterized by a constant density $\rho_c = 10^2\rho_*$, that is 27 orders of magnitude away from the Sun's density. Another choice is to keep the Ricci scalar and the radial coordinate measured in terms of R_* (thus $\beta = \eta = 1$) but to measure the density in terms of the central density of the object, $\rho_\star = \rho_c$. Then,

$$\alpha = \frac{R_c}{R_*}, \qquad \beta = 1, \qquad \eta = 1, \tag{4.33}$$

where $R_c := 8\pi G/c^2\rho_c$. In this case, α acts as a parameter that measures the ratio between the cosmological density and the central density of the object (which, in this units, is set always to 1). Eventually, when $R_c = R_\odot$, α will become extremely large ($\alpha \sim 10^{29}$). Finally, another possibility is to measure both the Ricci scalar and the radial coordinate in terms of the stellar curvature R_c (implying $\beta = 1$) and the density in units of ρ_c (meaning $\alpha = 1$). The set of dimensionless parameters becomes

$$\alpha = 1, \qquad \beta = 1, \qquad \eta = \frac{R_*}{R_c}. \tag{4.34}$$

In this case, we observe that as the density of the star ρ_c increases gradually up to the Sun's density $\rho_\odot$, we will eventually have to deal with the scale $R_*/R_\odot \sim 10^{-30}$ inside the $f(R)$ function, encoded in the η parameter (see Eq. (4.28)).

In view of the above discussion, we conclude that there is not a simple set of units that allows us to avoid the numerical contrast at the level of the equations. The numerical contrast will be present in on one way or another. We have tested each of the three strategies without finding an apparent numerical advantages in any of them.

In addition to the dimensionless implementation, we write the system (4.30) as a system of first order differential equations. By the substitution $R' = Q$ Eq. (4.30a), transforms in two first order differential equations, in this way the full set of equations (4.30) can be expressed as the following system

$$\hat{R}' = F_1(\hat{r}, \hat{R}, Q, m, n, \hat{p}) \tag{4.35a}$$
$$Q' = F_2(\hat{r}, \hat{R}, Q, m, n, \hat{p}) \tag{4.35b}$$
$$m' = F_3(\hat{r}, \hat{R}, Q, m, n, \hat{p}) \tag{4.35c}$$
$$n' = F_4(\hat{r}, \hat{R}, Q, m, n, \hat{p}) \tag{4.35d}$$
$$\hat{p}' = F_5(\hat{r}, \hat{R}, Q, m, n, \hat{p}). \tag{4.35e}$$

In order to close the system, an EoS for the matter inside the star is needed, which as we state before, it is given by an incompressible fluid. Finally, to obtain numerical solutions for the system (4.35) we need to supply boundary conditions that we discuss below.

4.4.1 Boundary and regularity conditions

The requirement of asymptotic de Sitter implies that $\hat{R} \to \hat{R}_{\rm dS}$ as $\hat{r} \to \infty$. The boundary value problem (BVP) can be tackled as an initial value problem (IVP) by imposing the conditions at the center of the star ($\hat{r} = 0$), with aid of a shooting procedure in such a way that the correct asymptotic behavior is obtained.

Near the center of the object, the regularity condition (smoothness) implies the following expansion $\theta(0) = \theta_0 + \theta_1 r^2/2 + O(r^4)$ where θ stands for R, m, n. This implies $\hat{R}' = m' = n' = 0$ at $\hat{r} = 0$. We set $m(0) = 1$ (local flatness condition) and $n(0) = 1$. At the end of the integration $n(r)$ is re-escalated *a posteriori* by dividing it with its maximum value. The coefficients θ_0 and θ_1 are related to each other. For the pressure, the condition is simply $\hat{p}(0) = \hat{p}_c$. Since we are considering a constant density object, $\hat{p}_c$ is fixed by hand to some value, because we are not imposing an EoS.

A crucial aspect to obtain numerical solutions with the desired asymptotic behavior concerns the value of the Ricci scalar at the center $\hat{R}_0 := \hat{R}(0)$. In the classical version of the shooting method the boundaries are fixed, and thus, a root searching algorithm can be used to find the correct *initial* condition at the center. However, in our case one boundary remains strictly at infinity, thus, for some initial guess of $\hat{R}_0$ slightly smaller or slightly larger than the right one, the function $\hat{R}(\hat{r})$ at some distance $\hat{r} > \hat{r}_{\rm crit}$ will eventually go to $-\infty$ or $+\infty$, respectively, leading to unphysical solutions. We thus determine the correct value of $\hat{R}_0$ up to some distance $\hat{r}_{\rm crit}$ limited the numerical accuracy such that R approaches $R_{\rm dS}$ are r goes to infinity.

One important feature that needs to be clarified is that the numerical integration proceeds in two stages. Given a density $\hat{\rho}_c$ and the central values of the pressure $\hat{p}_c$ and the Ricci scalar $\hat{R}_0$, we integrate the system (4.35) numerically from the center $\hat{r}$ to the surface of the star $\hat{r}_\diamond$, defined through the pressure as $\hat{p}(\hat{r}_\diamond) = 0$. Then, imposing continuity for all the functions at the stellar surface, we integrate outwards the same system (4.35) but we set $\hat{\rho} = \hat{p} = 0$ up to $\hat{r}_{\rm crit}$.

4.4.2 High-precision arithmetic

Given the high numerical contrast present in the field equations the standard 64-bit IEEE floating point is not sufficient for the demanded resolution. Therefore, we need to implement high precision floating-point arithmetic. All our algorithms were implemented in JULIA using the BigFloat package library for arbitrary-precision floating-point arithmetic based on GMPY2, which supports integer and rational arithmetic via the GMP library and real and complex arithmetic by the MPFR and MPC libraries Bailey et al. [16].

In general, the number of decimal digits from a given number of bits b is:

$$d = \log_{10}(2^b) \tag{4.36}$$

For a quadruple precision binary-floating point the significant precision is 113 bits which give roughly $d \approx 34$ [16]. Therefore, we will have up until 34 decimal places of precision. We generally set the precision above the quadruple precision.

Given the high accuracy needed for the numerical solutions, the well known classic Runge-Kutta (RK) of order 4 is not recommended. Thus, a more suitable integrator is needed. A good start up is the DOP853 method [71], which is a high-order RK embedded method. To illustrate briefly how these class methods works, lets take the notation of Eq. 4.35. Thus, a solution for the system $y'^i = F^i(r, y^i)$, is given by y_i. Numerically, at each time step n, two approximations to the solution, y^i_n and $\tilde{y}^i_n$, are made and compared. Usually, different order RK methods are used for each approximation to obtain a more accurate solution. An estimate of the error in this class of methods is controlled by

$$|y^i_n - \tilde{y}^i_n| < Rtol + \max(y^i_0, y^i_1)Atol, \tag{4.37}$$

where *Rtol* and *Atol* are known as the relative and absolute tolerance, respectively. This values are prescribed by us and we choose them as $Rtol \approx 10^{-26}$ and $Atol \approx 10^{-34}$ (we refer the reader to [71, 76, 128, 147] to know more about this class of methods). We use the **DiffEq** Julia package [116], which provides a handful of high-order RK embedded methods with variable time step.

4.5 Numerical results

We present now the main numerical results of this work. In Section 4.5.1, we consider constant density stars with the same central pressure and density that have been used in the works alluded in Section 4.3. We focus on the MJWQ and Starobinksy $f(R)$, where the parameters of each $f(R)$ model slightly differ from the ones that successfully give rise to the cosmological evolution history. Our aim is to provide further analysis on those configurations and, in the meantime, calibrate our numerical code after reproducing their results. Meanwhile, in Section 4.5.2 we obtain solutions for the Starobinksy $f(R)$ model with cosmological parameters, whereas in Section 4.5.3 we do the same but for the Hu-Sawicki $f(R)$ model.

It is important to stress again that we are solving the system of differential equations (4.35). The central pressure p_c and density are *a priori* fixed. Then, we perform a shooting procedure to find the Ricci scalar at the center $R_c := R(0)$. Hereafter, the units are chosen so that R is measured in units of R_*, thus the coefficients from Eq. (4.31), are $\alpha = \beta = \eta = 1$.

4.5.1 Non-realistic compact object solutions

The configurations that follows are non-realistic in the sense that their mass and density do not correspond to an actual star. For the MJWQ $f(R)$ model we take the central parameters introduced in Miranda et al. [97], whereas for the Starobisnky $f(R)$ model, the configurations analyzed in [78, 88].

MJWQ

The first configuration is, as given in [78, 96], a constant density star with

$$\rho_0 = 5 \times 10^7 R_1 c^2/G \approx 5.3 \times 10^{-18}\text{kgm}^{-3} \approx 1.76 \times 10^9 \rho_*, \tag{4.38a}$$

$$p_c = 0.3\rho_0 c^2 \approx 4.6 \times 10^{25}\text{Nm}^{-2}, \tag{4.38b}$$

where R_1 is the asymptotic de Sitter value for the Ricci scalar which, as discussed in Section 3.1.1, corresponds to a non-trivial algebraic solution of $dV_{JPS}/dR = 0$. In this case, we set $\alpha_{\text{M}} = 1.2$. To find R_1, we solve $dV_{JPS}/dR = 0$ for the scalar potential (4.5). The value is found numerically,

$$R_1 = 1.40538297 R_*. \tag{4.39}$$

We show in Fig. 4.5 all the solutions. In particular, the top left panel depicts the solution for the Ricci scalar as function of the radial coordinate r. Note that the solution smoothly interpolates from the central value $R_c \approx 1.93 R_*$ to the cosmological value $R_1 \approx 1.4 R_*$. The location of the star radius (red star) is confined to a region where the largest gradients $R(r)$ occur. However, we see that the central value R_c is of the same order as R_1. Such value is extremely far from the GR value $R_{GR} \sim \kappa\rho_0 \gg R_c$. This can be understood as low-curvature solution (cf. Section 4.2), i.e., where the Ricci scalar remains at the order of magnitude of the cosmological value $R(r) \sim R_*$ through the radial evolution inside the star. Finally, notice that the Ricci scalar is a differentiable function, even though the density is not. In GR, the Ricci scalar is a constant, reminiscence of behavior of the density function. In $f(R)$ gravity, the Ricci scalar is not zero immediately outside the star, but asymptotically tends to R_1 at a sufficient distance from the surface of the star.

The top right panel of Fig. 4.5 shows the metric functions (bold lines) and its product (dashed lines). Contrary to GR (cf. Section 2.2.1), immediately outside the star, the product $m(r)n(r)$ is not equal to one. This can be explained by the contribution that the Ricci scalar makes to the exterior region. Notice also that after reaching a flat region, where the product is one, the metric functions change its behavior; m grows as r^2, while n decreases and tends to the cosmological horizon ($n = 0$). Eventually, if we continue the integration up to infinity, $n \to 0$ and $m \to \infty$. Finally, we see the non-differentiable character of the $m(r)$ function. This is due to the discontinuity of the density function in the same way as in GR.

Let us now look at the bottom panel of Fig. 4.5. The right panel shows the pressure function $p(r)$. In particular, we observe how the surface of the star is reached exactly where the pressure vanishes. The left panel shows the mass function $\mu(r)$. We clearly observe that we are dealing with a non-realistic star. Indeed, the asymptotic mass (just before blows up to infinity due to $m \to \infty$), settles at $\mu_0 \sim 0.4 \times 10^{18} M_\odot$, while the radius of the star $\sim 3.01742 \times 10^{21}$ km, extremely close to the cosmological horizon $R_*^{-1/2} \sim 10^{26}$ km. Furthermore, if we compute its compactness, we obtain $C \sim 0.208$. This implies that the object we are dealing with, has nothing to do with a star like the Sun and is far from resemble GR.

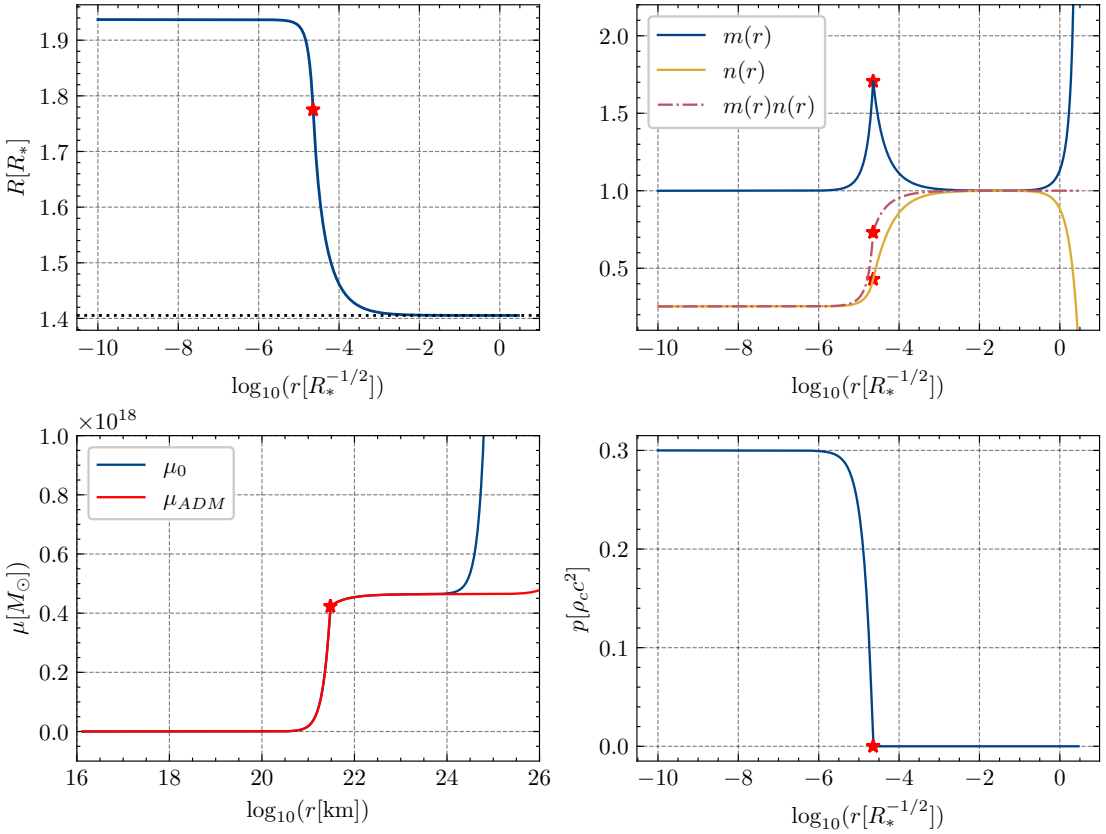

FIGURE 4.5: *Top panels:* Ricci scalar profile with $R_c = 1.93704R_*$ (left panel). Metric functions $m(r)$, $n(r)$ and its product $m(r)n(r)$ (right panel). *Bottom panels:* Mass functions in units of $M_\odot$ (left panel). Pressure profile in units of $\rho_0 c^2$ (right panel). The red stars indicate the surface of object. Except for the mass plot, the radial coordinate is measured in units of $r[R_*]^{-1/2}$. For comparison we plot μ_{ADM} which is defined as $\mu_{ADM} = \frac{rc^2}{2G}\left(1 - m^{-1} - R_1 r^2/12\right)$, where R_1 is the de Sitter value of the $f(R)$ function [29]. The extra term r^2 ensures the non-divergence which happens in μ_0.

To investigate how more generally the Ricci scalar depends on the density and central pressure value, we subsequently performed a set of runs with a set of values spanning several orders of magnitude. First we consider how the Ricci scalar at the center and the metric potentials depend on the central pressure, but keeping the central density fixed as in (4.38a).

The left panel of Fig. 4.6 depicts the radial profiles for the Ricci scalar for increasing central pressures. As the central pressure increases, a characteristic pattern emerges: $R(r)$ becomes stepper with higher central pressures. We also notice on the right panel of Fig. 4.6, how the Ricci scalar at the origin, R_c, increases until some value close to $p_c = 0.3\rho_0$, and then decreases. However, despite this increase in R_c, is very far from the GR value $R_{GR} \sim \kappa\rho_0$.

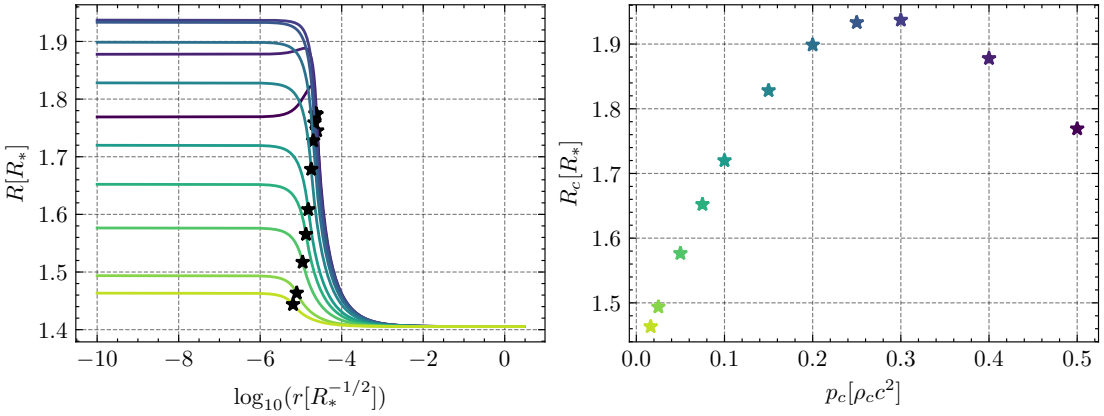

FIGURE 4.6: Radial profiles for the Ricci scalar (left panel). Ricci scalar at the center as function of the central pressure (right panel). Colors from green to violet indicate increasing central pressures. The solutions belong to the MJWQ model with $\alpha = 1.2$ and fixed density $\rho_0 = 10^7 R_1 c^2/G$

Next we check the dependence of the MJWQ model on the value of the density. Left panel of Fig 4.7 shows multiple R radial profiles with increasing density ($\rho_0/(5R_1c^2/G) = 10^4 - 10^{10}$), whereas the right panel depicts the central value R_c as a function of the density. We notice a change in the star radius as the density increases but the R_c stays almost at the same value on all the configurations. Thus, we can conclude

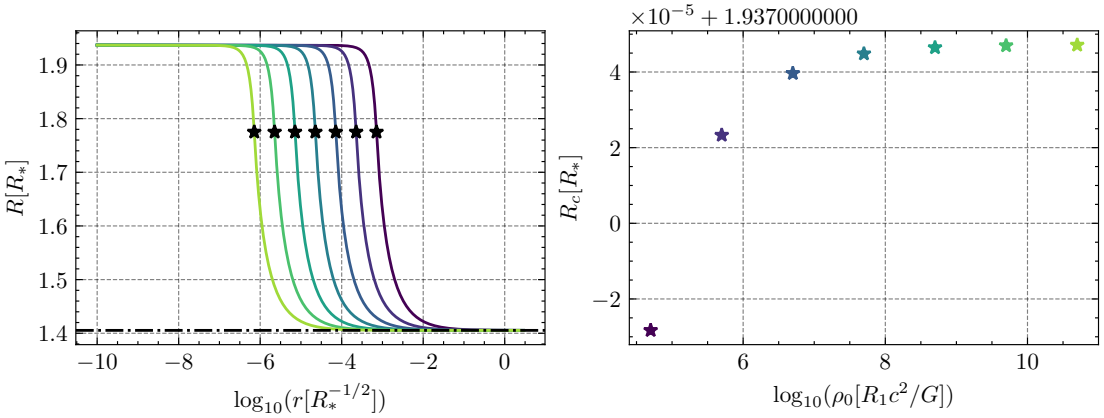

FIGURE 4.7: Radial profiles for the Ricci scalar (left panel). Ricci scalar at the center as function of the density (right panel). Colors from green to violet indicate increasing densities. The solutions belong to the MJWQ model with $\alpha = 1.2$ and fixed central pressure $p_c = 0.3\rho_0$.

The same aforementioned features can be said about the solutions presented from Fig. 4.8 to Fig. 4.16, where we have carried out numerical calculations varying the value of the parameter $\alpha_{\rm M}$ keeping fixed the density and central pressure of Eq. (4.38a). We display in Table 4.3 the central values R_c that give rise to a desired asymptotic behavior R_1 and the respective value of $\alpha_{\rm M}$. Figure 4.17 shows how these values are related. We observe a slight increase of the central value as $\alpha_{\rm M}$ reaches the values 2. Neither of these values is sufficient to obtain a high-curvature solution.

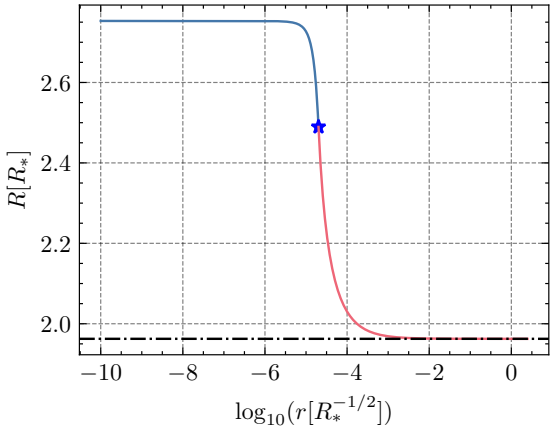

FIGURE 4.8: Ricci scalar ($\alpha_{\mathrm{M}} = 1.3$).

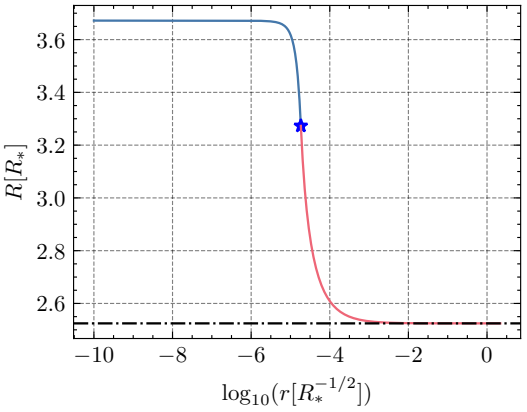

FIGURE 4.9: Ricci scalar ($\alpha_{\mathrm{M}} = 1.4$).

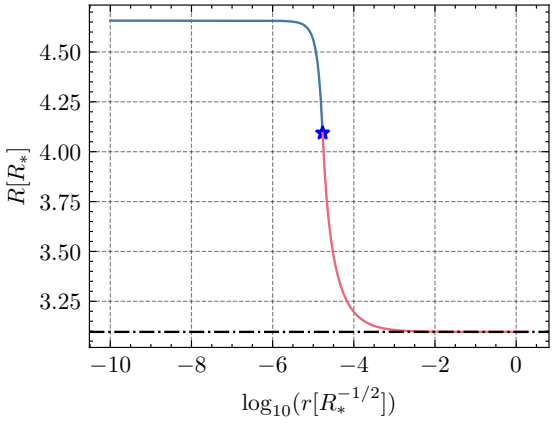

FIGURE 4.10: Ricci scalar ($\alpha_{\mathrm{M}} = 1.5$).

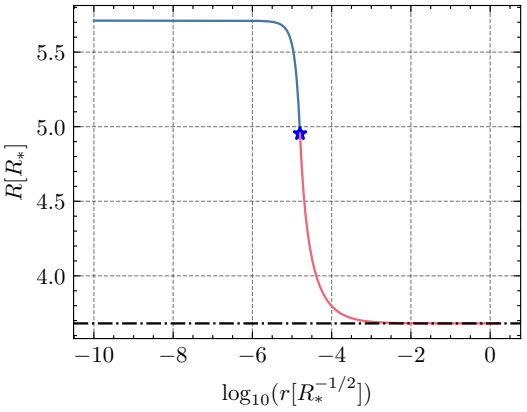

FIGURE 4.11: Ricci scalar ($\alpha_{\mathrm{M}} = 1.6$).

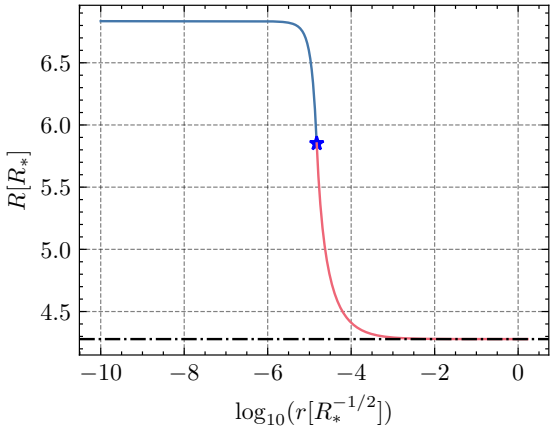

FIGURE 4.12: Ricci scalar ($\alpha_{\mathrm{M}} = 1.7$).

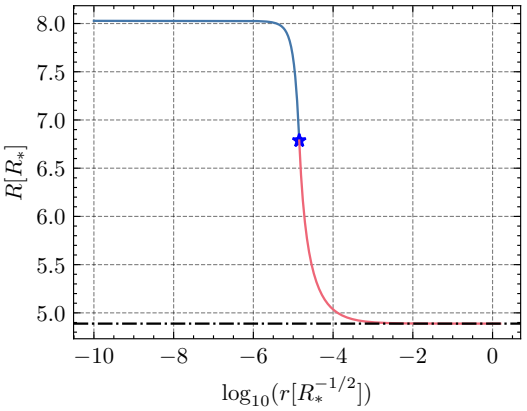

FIGURE 4.13: Ricci scalar ($\alpha_{\mathrm{M}} = 1.8$).

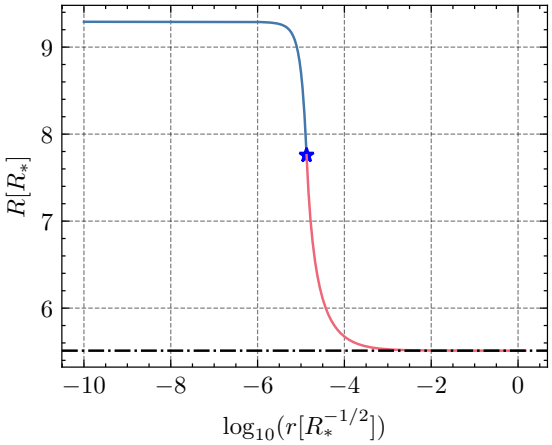

FIGURE 4.14: Ricci scalar ($\alpha_{\mathrm{M}} = 1.9$).

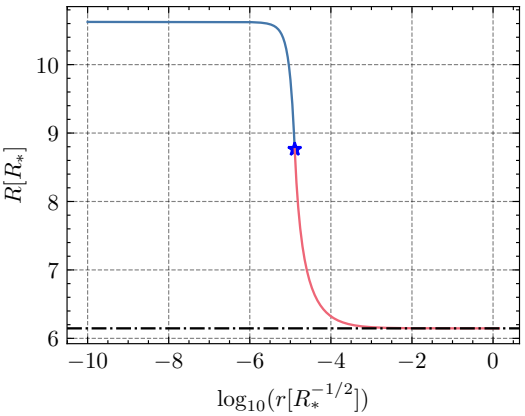

FIGURE 4.15: Ricci scalar ($\alpha_{\mathrm{M}} = 2.0$).

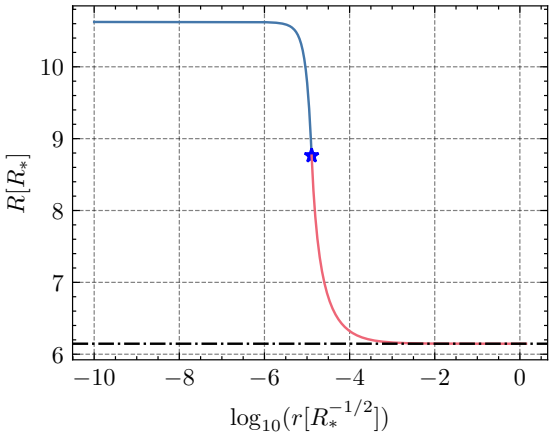

FIGURE 4.16: Ricci scalar ($\alpha_{\mathrm{M}} = 2$).

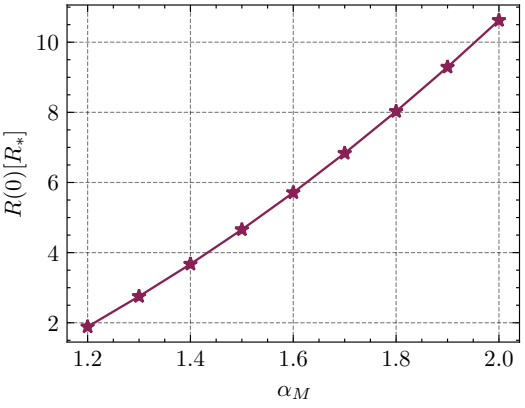

FIGURE 4.17: Central values of the Ricci scalar as function of (α_{M}).

α_{M}	$R(0)[R_*]$
1.2	1.88617354
1.3	2.75303442
1.4	3.67199171
1.5	4.6571184
1.6	5.71093358
1.7	6.83439925
1.8	8.02778131
1.9	9.29100258
2.	10.62380923

TABLE 4.3: Ricci scalar values at the center for the MJWQ model found using the shooting technique. These values are computed with 128 bit precision but for the sake brevity we only display 8 figures .

Kobayashi-Maeda

As we thoroughly discussed in Section 4.3 the numerical analysis presented by Kobayashi and Maeda [88] about their solutions is flawed. To be more specific, they solved the field equations (in the form of Appendix A) but their solutions for the scalar field never reach the desired cosmological value and seem to blow up. We follow the choice of the Starobinsky model (4.6) and consider the configurations presented below [88]. First, setting $\lambda = 2.088$, $q = 1$ (KM_2 of Table 4.1) and the values of density and pressure as

$$\rho_0 = 10^6 c^2 R_1 (16\pi G)^{-1} \approx 5.4138 \times 10^{-21} [\text{ kg/m}^3] \approx 1.7994 \times 10^6 \rho_* \tag{4.40a}$$

$$p(0) := p_1 = 0.05\rho_0 c^2 \approx 2.4328 \times 10^{-5} \text{Nm}^{-2} \tag{4.40b}$$

$$p(0) := p_2 = 10^{-4}\rho_0 c^2, \tag{4.40c}$$

respectively. Contrary to the claim of KM [88], we find that stellar solutions exist. We obtain the profile for the Ricci scalar R that is shown in Figs. 4.18 (p_2) and 4.19 (p_1). We notice that for both choices of pressure, a non-zero value for R asymptotically is obtained as a result of the shooting method. This value coincides with the cosmological minimum R_1 of the scalar potential $V(R)_{\text{JPS}}$ (Eq. (3.9)) given the choice of parameters λ and q. We also notice that these two solutions can be classified as low-curvature solutions ($R_c \ll \kappa\rho$) since the resulting value of the Ricci scalar at the center of the star is in fact very close to R_1. It should be noted that this behaviour is against the natural expected solutions which would *track* the density profile. That is, the value at the center of the star should be of the order of $R \sim \kappa\rho_0$, which happens to be the minimum of the effective potential specified in Eq. (4.23), and then interpolate to the value R_1 in the absence of matter.

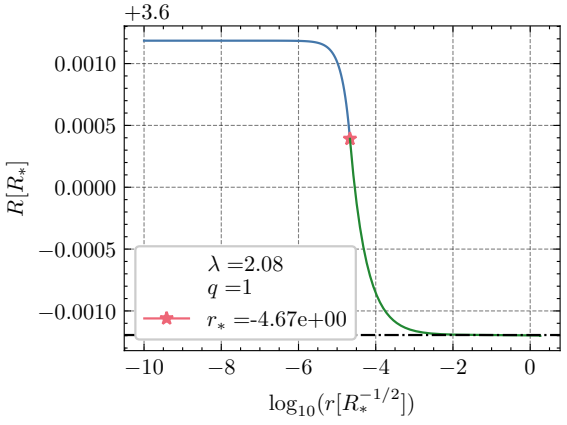

FIGURE 4.18: Ricci scalar taking $\lambda = 2.088$ and $q = 1$ with $\rho_0 = 10^6 c^2 R_1 (16\pi G^{-1}$ and $p(0) = 10^{-4}\rho_0 c^2$ with $R_1/R_* \approx 3.59880517$. The value at the center is tunned to be $R_c = 3.602 R_*$.

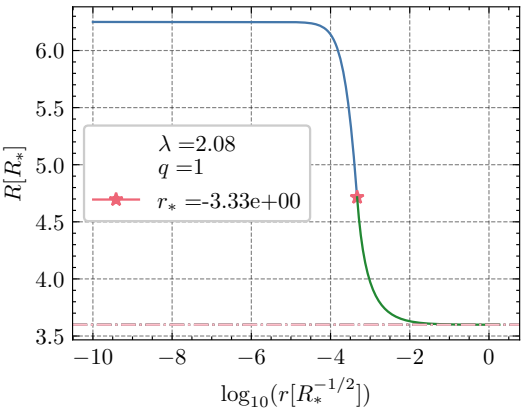

FIGURE 4.19: Ricci scalar taking $\lambda = 2.088$ and $q = 1$ with $\rho_0 = 10^6 c^2 R_1 (16\pi G^{-1}$ and $p(0) = 0.05\rho_0 c^2$ with $R_1/R_* \approx 3.59880517$, The value at the center is tunned to be $R_c = 6.2502 R_*$.

For comparison purposes, we have also considered computations for the parameter choice $\lambda = 1.827$, $q = 2$ (KM_1 of Table 4.1) with the following density and central pressures

$$\rho_0 = 10^6 c^2 R_1 (16\pi G)^{-1} \approx 5.4138 \times 10^{-21} [\text{ kg/m}^3] \approx 1.7994 \times 10^6 \rho_* \tag{4.41a}$$

$$p(0) := p_3 = 5 \times 10^{-4} \rho_0 c^2 \approx 2.4339e \times 10^{-7} \text{Nm}^{-2} \tag{4.41b}$$

$$p(0) := p_4 = 10^{-2} \rho_0 c^2. \tag{4.41c}$$

Figs. 4.20 and 4.21 show the numerical solution which is asymptotically de Sitter. As one can see, the choice p_3 results in a low-curvature solution, but p_4 gives an interesting high-curvature solution which, indeed, interpolates between the two minima. This property is somehow remarkable as it provides us with insight on how to obtain the desired solution in the STBS model. Thus, in one way or another the pressure at the center is required to be of the order of the average density of the star in order to obtain the desired high-curvature solution.

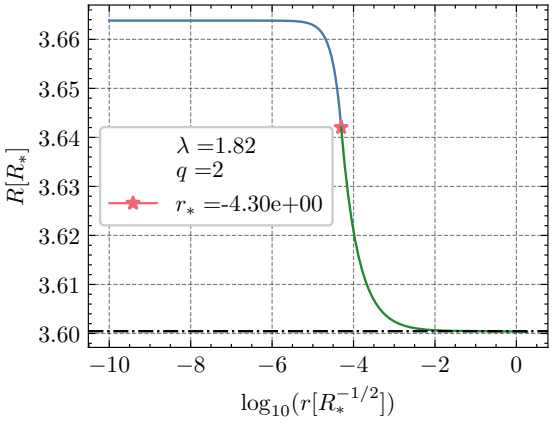

FIGURE 4.20: Ricci scalar taking $\lambda = 1.827$ and $q = 2$ with $\rho_0 = 10^6 c^2 R_1 (16\pi G)^{-1}$ and $p(0) = 5 \times 10^{-4} \rho_0 c^2$ with $R_1/R_* \approx 3.60118507$. The value at the center is tunned to be $R_c = 3.602 R_*$.

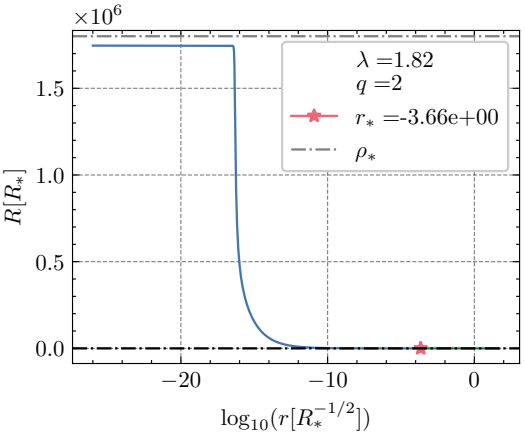

FIGURE 4.21: Ricci scalar taking $\lambda = 1.827$ and $q = 2$ with $\rho_0 = 10^6 c^2 R_1 (16\pi G)^{-1}$ and $p(0) = 10^{-2} \rho_0 c^2$ with $R_1/R_* \approx 1.746227 \times 10^6$, The value at the center is tunned to be $R_c = 6.2502 R_*$.

4.5.2 Starobinsky solutions with cosmological parameters

In this section we set the parameters for the Starobinsky model that fits the cosmological scenario [79]. These are $q = 2$, $\lambda = 1$ and $R_S = 4.17$. We then proceed to gradually increase the density to see the behavior of the solutions.

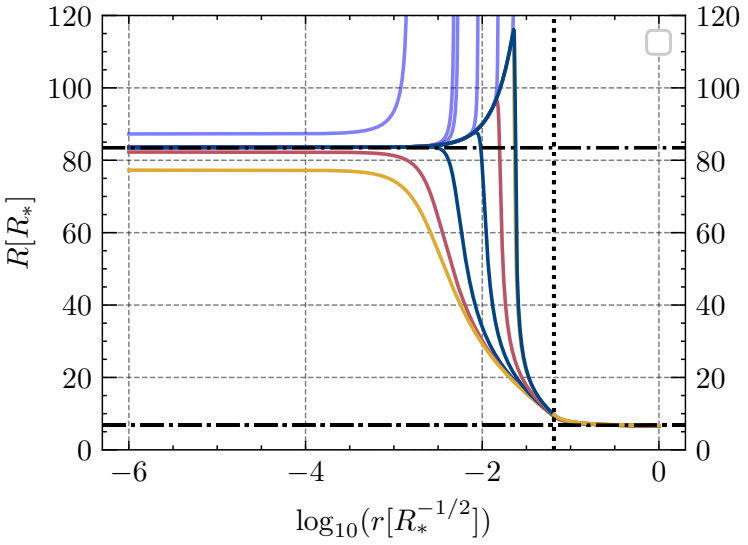

FIGURE 4.22: Shooting procedure for the Ricci scalar taking $\lambda = 1$ and $q = 2$ and $R_S = 4.17$ with $\rho_0 = 10^2 c^2 R_1 (16\pi G)^{-1}$ and $p(0) = 0.26\rho_0 c^2$ with $R_1/R_* \approx 6.82795191$. The value at the center is tunned to be $R_c \sim R_{\min}$. The vertical dotted line indicates the star radius.

Fig. 4.22 depicts how the shooting procedure takes place. The colored solutions are either undershoot or overshoot solutions depending on their divergence towards the end of the integration. In this case, the choice of the central density and the central pressure are $\rho_c = 10^2 c^2 R_1 (16\pi G)^{-1}$, $p(0) = 0.26\rho_0 c^2$, respectively. In this regime, the obtained interior solution appears to be of the order of $R_c \sim -\kappa T$. In Fig. 4.22, the minimum of the effective potential is $R_{min} = 83.44 R_*$, which is the upper dashed black horizontal line. We observe clearly the so called *screneed* solutions first described by [145]. These solutions have the characteristic of having an interval of a small width respect to the star radius for which the Ricci scalar will increase and then turn around.

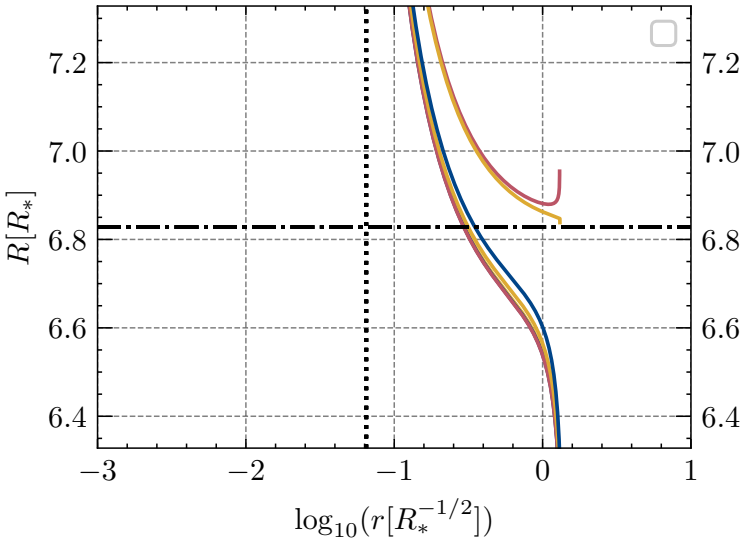

FIGURE 4.23: Zoom for shooting procedure for the Ricci scalar taking $\lambda = 1$ and $q = 2$ and $R_S = 4.17$ with $\rho_0 = 10^2 c^2 R_1 (16\pi G)^{-1}$ and $p(0) = 0.26\rho_0 c^2$ with $R_1/R_* \approx 6.82795191$. The value at the center is tunned to be $R_c \sim R_{\min}$.

Fig. 4.23 shows multiple undershoot and overshoot solutions. We can safely conclude that a solution with the desired boundary conditions exists.

Next, we check the dependence of the solutions on the choice of central pressure. As we see in Fig. 4.24, keeping the same central value R_c, a change in the central pressure reduces the star radius (indicated by the dotted vertical line), which is expected since the pressure itself takes less time[7] to vanish.

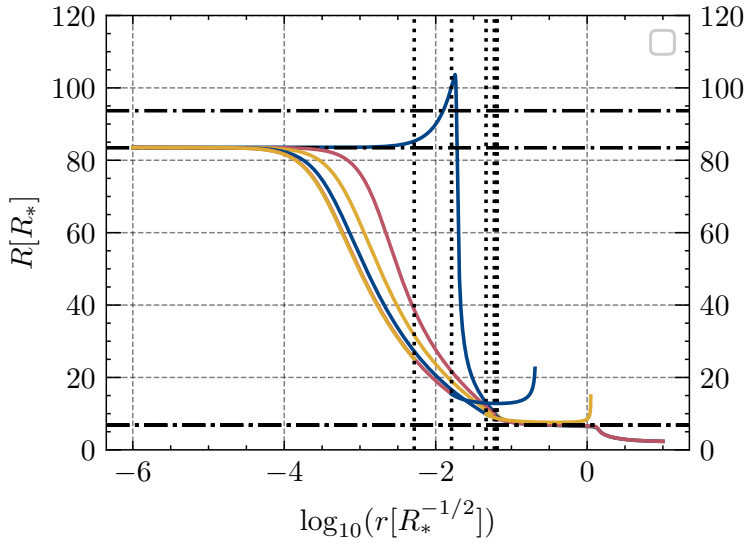

FIGURE 4.24: Lowering the pressure for $\lambda = 1$, $q = 2$ and $R_S = 4.17$ with $\rho_0 = 10^2 c^2 R_1 (16\pi G)^{-1}$ and $p(0)/\rho_0 c^2 = (0.26, 0.25, 0.2, 0.1, 0.01, 0.001)$, with $R_1/R_* \approx 6.82795191$. The value of the Ricci at the center is fixed to $R_c/R_* \approx 83.532263123$.

On the other hand, if we perform the shooting procedure to find the correct R_c value for each central pressure, we obtain the three corresponding configurations of Fig. 4.25. It should be noticed that a change in the pressure implies immediately a change of the value of the minimum of the effective scalar potential.

[7] If we make a crude analogy of the radial coordinate r as a *time* coordinate.

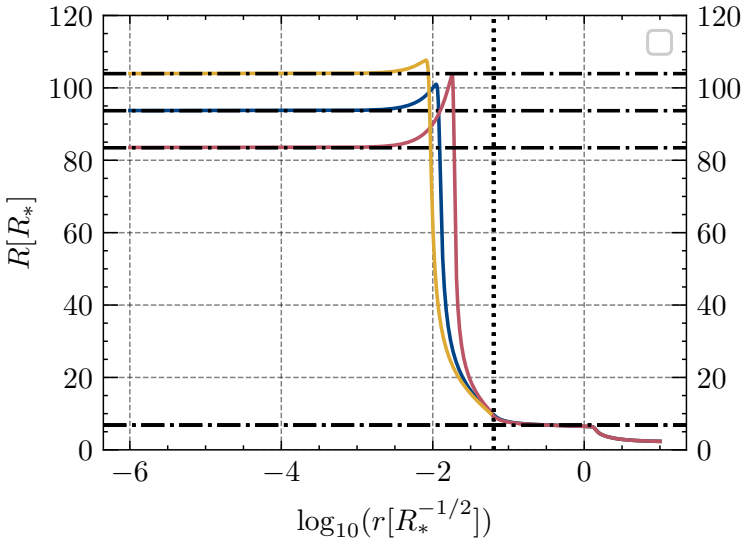

FIGURE 4.25: Undershoot solutions for $\lambda = 1$, $q = 2$ and $R_S = 4.17$ with $\rho_0 = 10^2 c^2 R_1 (16\pi G)^{-1}$ and $p(0)/\rho_0 c^2 = (0.26, 0.25, 0.24)$ with $R_1/R_* \approx 6.82795191$. As expected, R_c changes for each choice of central pressure.

Fig. 4.26 shows the numerical solution for a central density of $\rho_0 = 2 \times 10^2 c^2 R_1 (16\pi G)^{-1}$, whereas Fig. 4.27 shows the case for $\rho_0 = 5 \times 10^2 c^2 R_1 (16\pi G)^{-1}$. We observe that as the density increases, it becomes more and more difficult to find a set of overshoot and undershoot solutions.

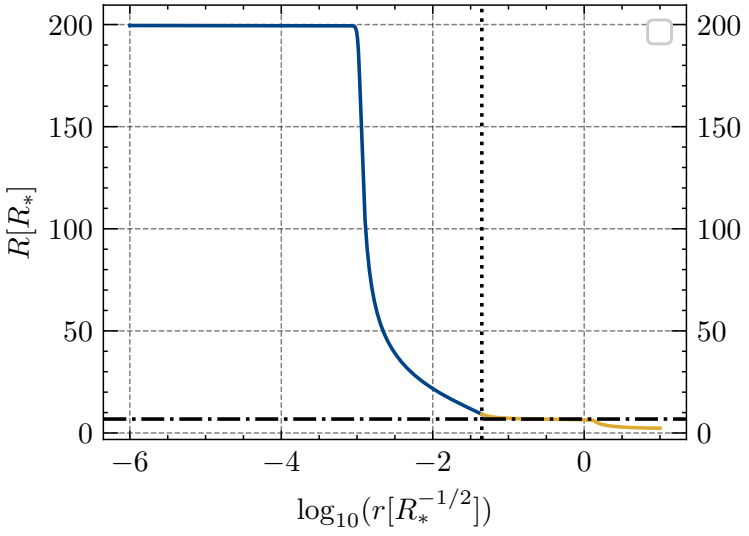

FIGURE 4.26: Undershoot solutions for $\lambda = 1$, $q = 2$ and $R_S = 4.17$ with $\rho_0 = 2 \times 10^2 c^2 R_1 (16\pi G)^{-1}$ and $p(0)/\rho_0 c^2 = 0.24$ with $R_1/R_* \approx 6.82795191$.

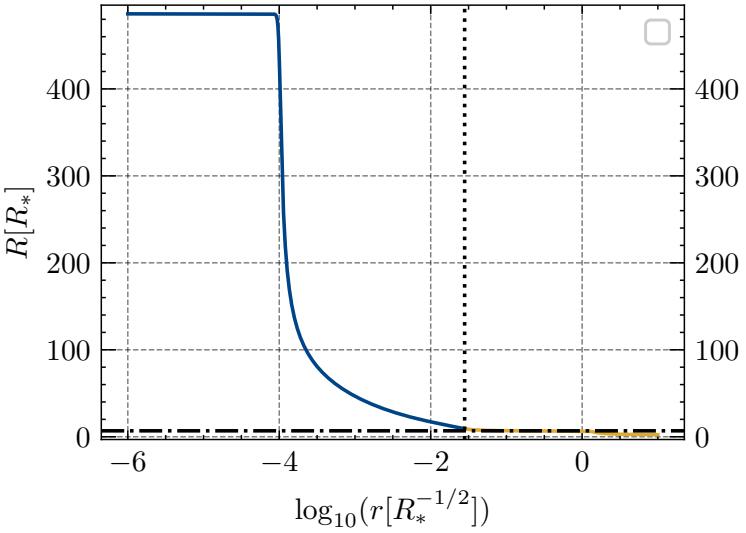

FIGURE 4.27: Undershoot solutions for $\lambda = 1$, $q = 2$ and $R_S = 4.17$ with $\rho_0 = 5 \times 10^2 c^2 R_1 (16\pi G)^{-1}$ and $p(0)/\rho_0 c^2 = 0.24$ with $R_1/R_* \approx 6.82795191$.

In Fig. 4.28, we slightly decrease the pressure but keep the same parameters of the above configurations. We observe, by the aid of the zoom of Fig. 4.29 for the same configuration, that both an overshoot and undershoot solution exist.

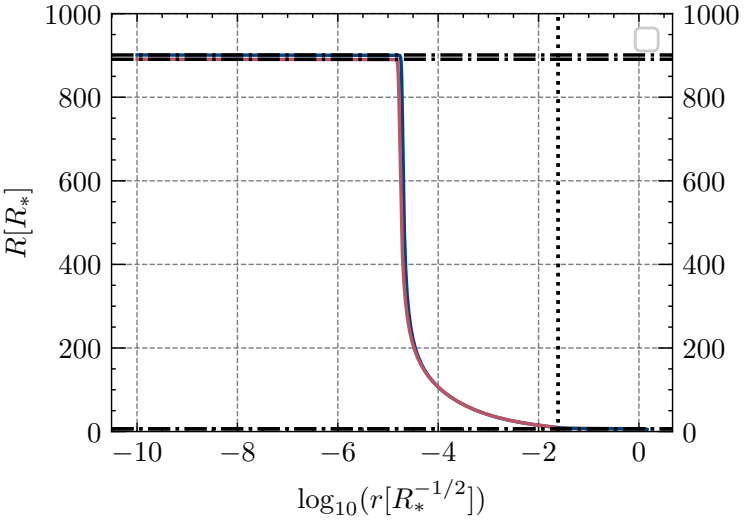

FIGURE 4.28: Undershoot and overshoot solutions for $\lambda = 1$, $q = 2$ and $R_S = 4.17$ with $\rho_0 = 5 \times 10^2 c^2 R_1 (16\pi G)^{-1}$ for two central pressures $p(0)/\rho_0 c^2$, $(0.159, 0.161)$ with $R_1/R_* \approx 6.82795191$.

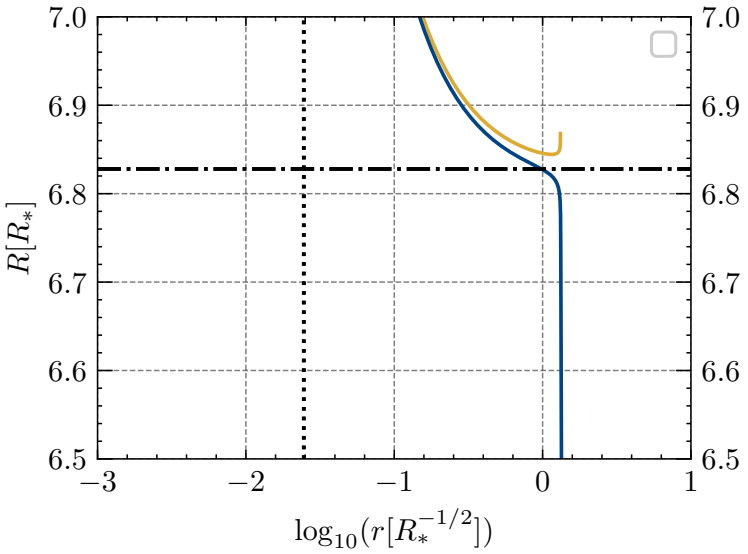

FIGURE 4.29: Zoom for undershoot and overshoot solutions for the same configuration of Figure 4.28.

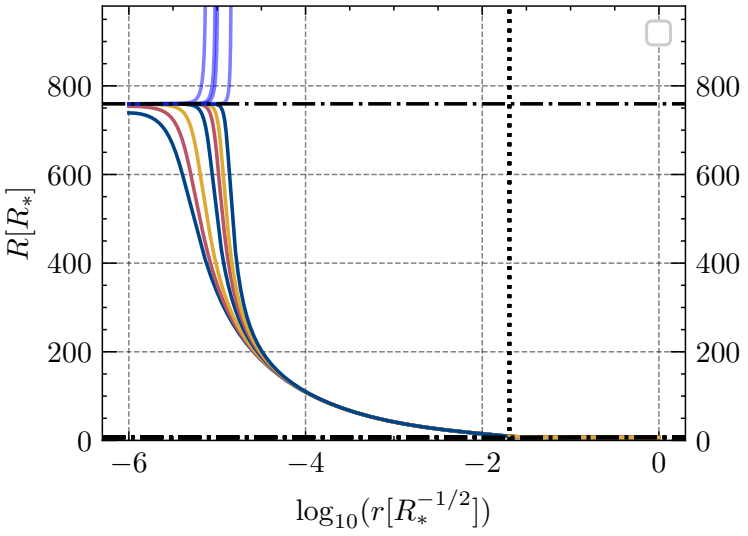

FIGURE 4.30: Shooting procedure for the Ricci scalar taking $\lambda = 1$ and $q = 2$ and $R_S = 4.17$ with $\rho_0 = 10^3 c^2 R_1 (16\pi G)^{-1}$ and $p(0) = 0.26\rho_0 c^2$ with $R_1/R_* \approx 6.82795191$. The value at the center is tunned to be $R_c \sim R_{\min}$.

Fig. 4.30 shows undershoot and overshoot solutions for the central density $\rho_0 = 10^3 c^2 R_1 (16\pi G)^{-1}$, whereas Fig. 4.31 depicts the same but for $\rho_0 = 10^4 c^2 R_1 (16\pi G)^{-1}$. At this order of magnitude of the density, overshoot solutions cannot be found.

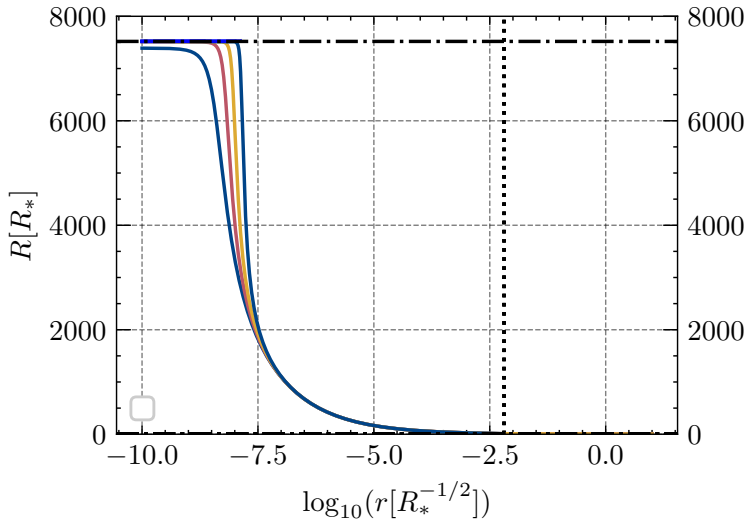

FIGURE 4.31: Shooting procedure for the Ricci scalar taking $\lambda = 1$ and $q = 2$ and $R_S = 4.17$ with $\rho_0 = 10^4 c^2 R_1 (16\pi G)^{-1}$ and $p(0) = 0.26\rho_0 c^2$ with $R_1/R_* \approx 6.82795191$. The value at the center is tunned to be $R_c \sim R_{\min}$.

Although we have managed to find the desired high-curvature solution for low densities, it was at the cost of keeping high central pressures. We can conclude from the aforementioned figures that for the Starobinsky $f(R)$ model apparently is not possible to increase the density in such a way that a solution which interpolates between the effective minimum $R_{\min}$ and the vacuum R_1 exist. We recall that such high-curvature solution is what one would expect from a theory that closely resembles GR.

4.5.3 Hu- Sawicki solutions

In this section we explore the solution space of the Hu-Sawicki model following the same procedure as in the Starobinksy model. We start by considering relative low densities. Fig. 4.32 depicts the solution for the Ricci scalar for a start of density $\rho_0 = 10^2 c^2 R_1 (16\pi G)^{-1}$ but changing the pressure slightly. We clearly observe how little variations in the central pressure imply bigger changes on the Ricci scalar at the center.

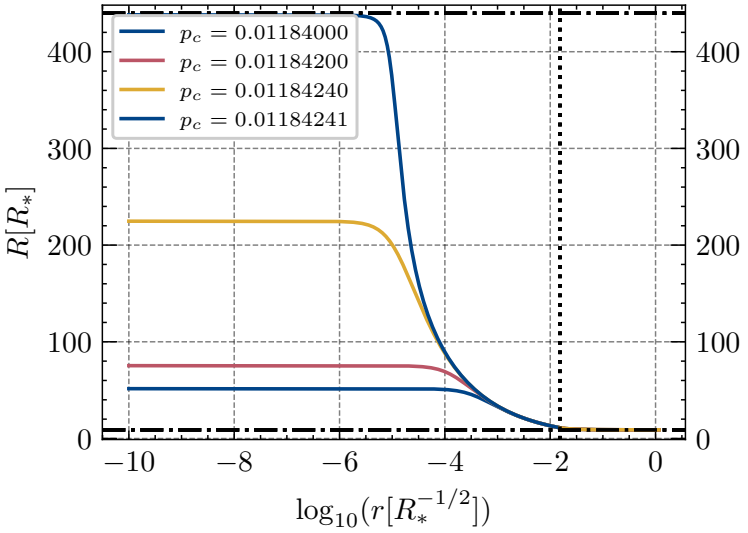

FIGURE 4.32: Ricci scalar for the Hu-Sawicki model keeping a fixed central density $\rho_0 = 10^2 c^2 R_1 (16\pi G)^{-1}$ an varying the pressure with $R_1/R_* \approx 8.931080$. Little changes in the pressure reflects enormous changes in the Ricci at the center.

Then, if we keep the pressure fixed. Fig. 4.33 shows both the undershoot and overshoot solution, as well as a third solution between both. As in the case of the Starobinsky model, we observe a screened behavior. Hereafter, we will gradually increase the density and look for high-curvature solutions. Recall that the average density of the Sun in this units is $\rho_\odot \approx 10^{29} c^2 R_1 (16\pi G)^{-1}$. And, therefore, we are still very far from this realistic values.

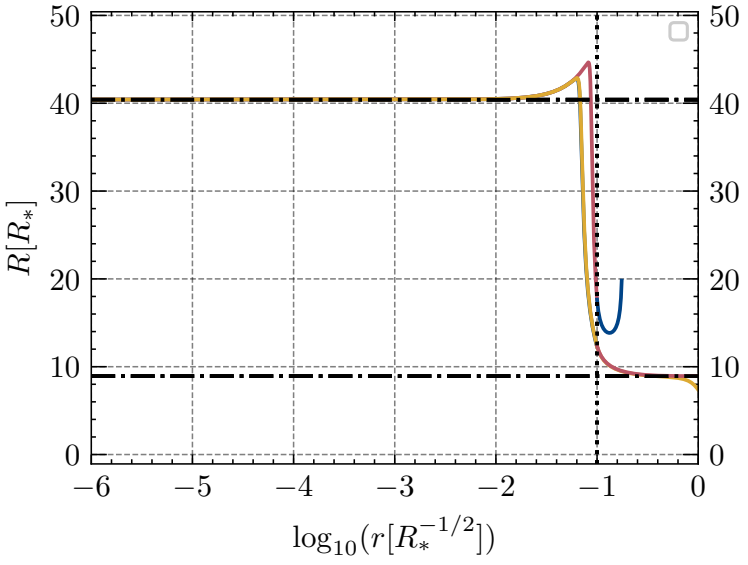

FIGURE 4.33: Undershoot and overshoot solutions of scalar for the Hu-Sawicki model keeping a fixed central density $\rho_0 = 10 c^2 R_1 (16\pi G)^{-1}$ an keeping a pressure of $p(0) = 0.1\rho_0 c^2$ with $R_1/R_* \approx 8.931080$.

In Fig. 4.34 we observe an undershoot solution for the Hu-Sawicki model with the central density $\rho_0 = 10^2 c^2 R_1 (16\pi G)^{-1}$. The pressure is set to $p(0) = 0.1\rho_0 c^2$, which is far from representing a non-relativistic object such as the Sun. Fig. 4.34 also shows a decreasing behavior in

the region where the Ricci scalar remains close to the value $\kappa\rho_0$. As we will see in the following figures, this regions shrinks as the density increases.

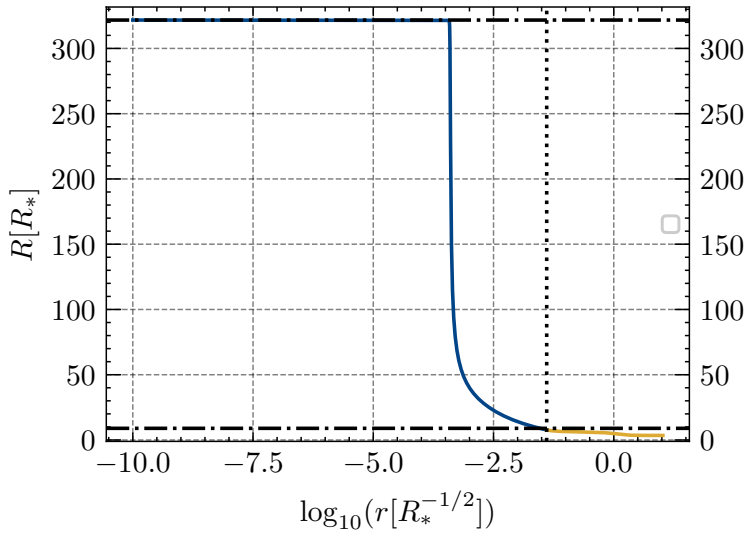

FIGURE 4.34: Undershoot solutions of scalar for the Hu-Sawicki model keeping a fixed central density $\rho_0 = 10^2 c^2 R_1 (16\pi G)^{-1}$ an keeping a pressure of $p(0) = 0.1\rho_0 c^2$ with $R_1/R_* \approx 8.931080$.

Figs. 4.34, 4.35, 4.36 show solutions for different central densities varying from 10^2 to 10^4 in $\rho_0(16\pi G)/(c^2 R_1)$ units. Note that, as the central density increases, we keep the central pressure fixed in order to obtain the desirable solutions. We point out that Fig. 4.36 represents the last values of the density for which we could obtain a numerical solution.

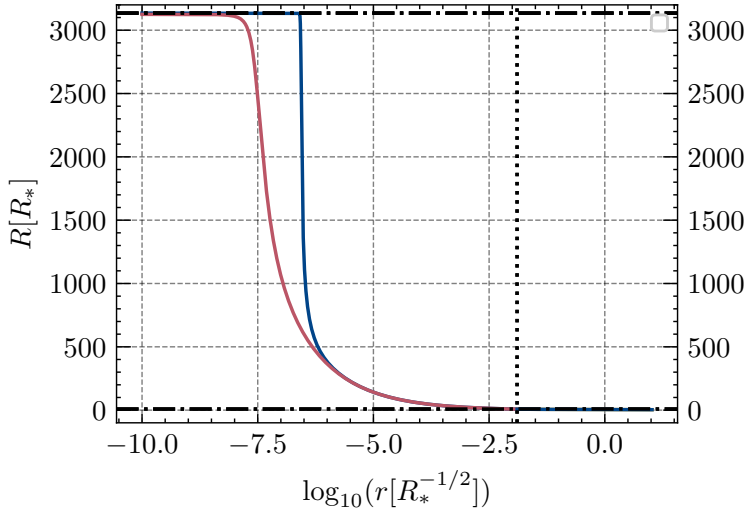

FIGURE 4.35: Undershoot solutions of scalar for the Hu-Sawicki model keeping a fixed central density $\rho_0 = 10^3 c^2 R_1 (16\pi G)^{-1}$ an keeping a pressure of $p(0) = 0.1\rho_0 c^2$ with $R_1/R_* \approx 8.931080$.

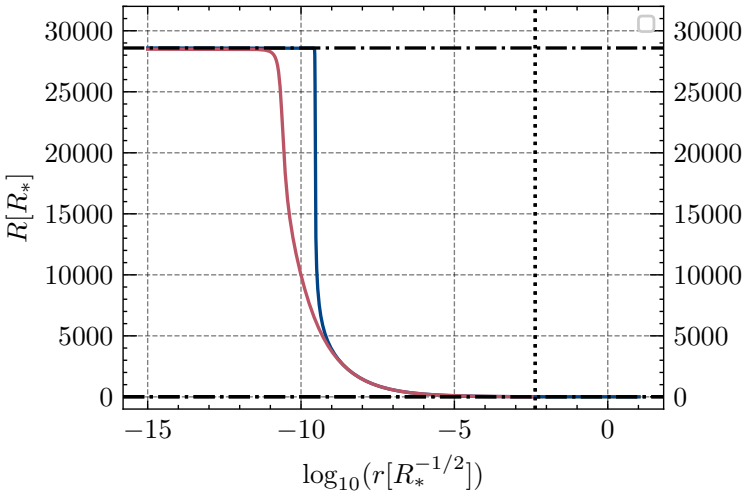

FIGURE 4.36: Undershoot solutions of scalar for the Hu-Sawicki model keeping a fixed central density $\rho_0 = 10^4 c^2 R_1 (16\pi G)^{-1}$ an keeping a pressure of $p(0) = 0.12\rho_0 c^2$ with $R_1/R_* \approx 8.931080$.

We thus conclude that in the Hu-Sawicki $f(R)$ model the desired density of the Sun cannot be achieved within our framework. As in the case of the Starobinky $f(R)$ model to obtain a high-curvature solution a high pressure is necessary. Moreover, even if the pressure remained large we could not find solution for higher densities than $\rho_0 = 10^4 c^2 R_1 (16\pi G)^{-1}$.

4.6 Simplified approach

Since, in the previous section we saw that we were unable to solve the full system for the actual parameters of the Sun, here we try to simplify the problem to find the potential technical problems that are responsible of inability to obtain the desired solutions. In order to do so, we provide further insight on the differential equation for the Ricci scalar alone for the Hu-Sawicki $f(R)$ model. We opt to solve only the Ricci scalar equation in the high-curvature limit where the condition $2f(R) - Rf_R \approx R$ holds (cf. Section 4.2). This extremely simplified version can be specified by the following system

$$R'' = \begin{cases} \frac{1}{3f_{RR}}(-\kappa\rho + R) - \frac{2}{r}R' & \text{if } r < r_\star \\ \frac{1}{3f_{RR}}(-R_{HS} + R) - \frac{2}{r}R' & \text{if } r > r_\star \end{cases} \tag{4.42}$$

where $R_{HS} \approx 6.8279$ is the de Sitter minimum and $r_\star$ is the radius of the star. Considering a density of $\rho_0 = 20c^2 R_1 (16\pi G)^{-1}$ first, the Ricci scalar at the center must be fixed and then, a shooting is performed to find the star radius which matches the asymptotic conditions, since the differential equation for the pressure is not present at all in this simplified approach. Fig. 4.37 depicts the behavior of some solutions keeping the above considerations. We observe that as R_c approaches to the value $R_{\min} = \kappa\rho_0$, the stepper the solution becomes.

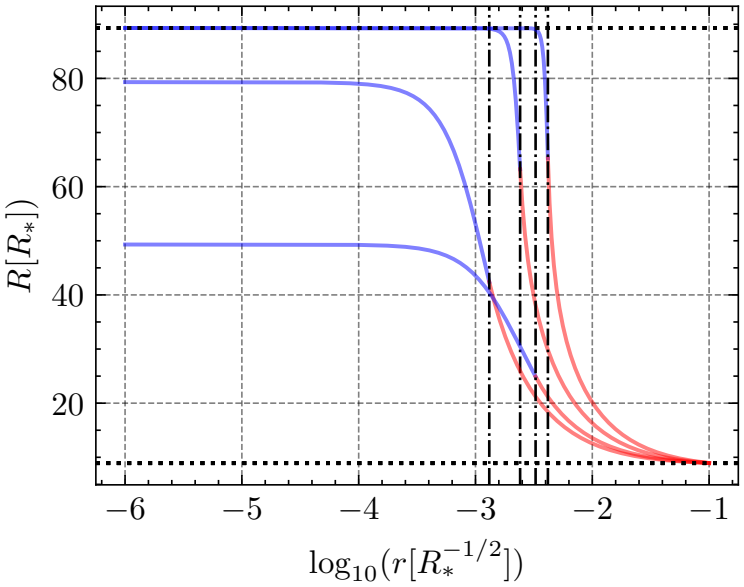

FIGURE 4.37: Multiple Ricci scalar profiles for $\rho_0 = 2\times10^1 c^2 R_1 (16\pi G)^{-1}$. The shooting parameter is the star radius (vertical black dashed lines). The upper dotted horizontal line represents the value $R_{\min} = \kappa\rho_0$ and the inferior dotted horizontal line is the value R_{HS}.

Furthermore, we found more solutions than that depicted in Fig. 4.37. As we see in Fig. 4.38, the star radius decreases as we increment the curvature at the center of the star. Each one of the configurations derives from a shooting procedure with the radius as the shooting parameter.

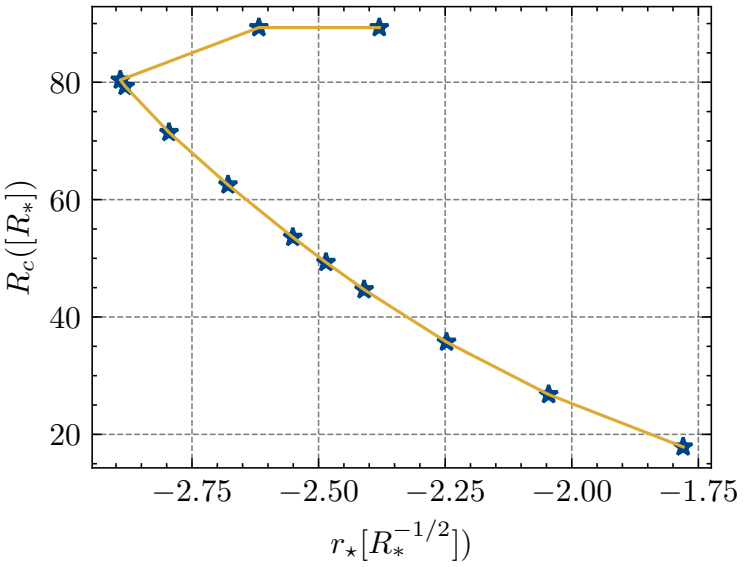

FIGURE 4.38: Ricci scalar at the center as function of the star radius for multiple configurations (blue stars) keeping the density fixed as $\rho_0 = 2\times10^1 c^2 R_1 (16\pi G)^{-1}$.

Fig. 4.39 show the same approximation for $\rho_0 = 50c^2 R_1 (16\pi G)^{-1}$ and Fig. 4.40 shows the same but for a higher density $\rho_0 = 100c^2 R_1 (16\pi G)^{-1}$. From both figures we observe the same behavior. One stark difference of the approximation (4.42), relative to the full system explored

before, is that for values of R_c closer to $R_{\min}$ the radius of the star is confined to a thin region. This resembles the thin-shell solution from the original chameleon model [41].

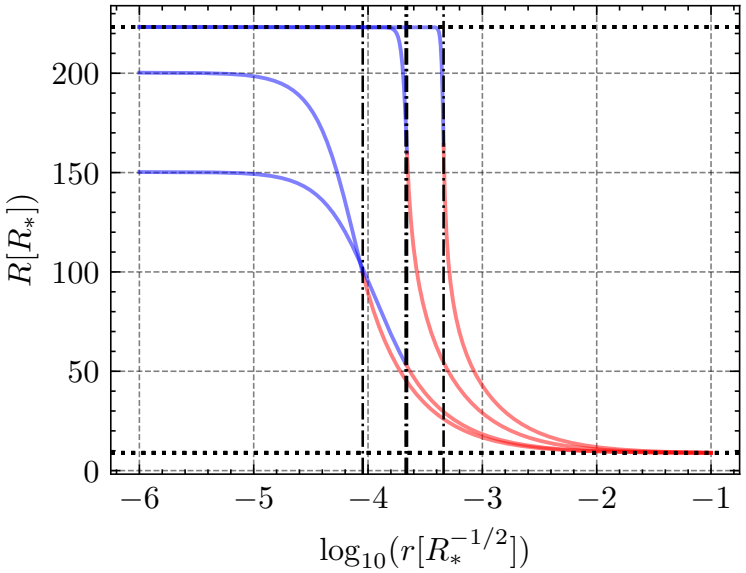

FIGURE 4.39: Similar as Fig. 4.37 using $\rho_0 = 5 \times 10^1 c^2 R_1 (16\pi G)^{-1}$.

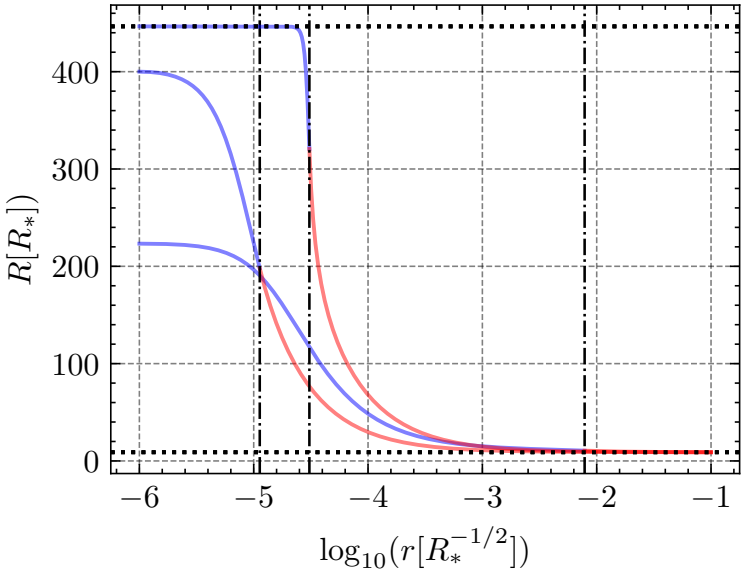

FIGURE 4.40: Multiple solutions for $\rho_0 = 100 c^2 R_1 (16\pi G)^{-1}$ and making a shooting method varying the star radius.

The main drawback of the system (4.42) is that is only valid in the high-curvature regime. As we will see in the following examples, this shortcoming reflects itself as objects of higher density are considered. For this regard, we can explore several better approximations by including more terms in order to see its effects appearing in the full R equation. These further approximations are:

$$R'' = \begin{cases} \frac{1}{3f_{RR}}(-\kappa\rho + (2f - f_R R)) - \frac{2}{r}R' & \text{if } r < r_\star \\ \frac{1}{3f_{RR}}(-\kappa\rho + (2f - f_R R) - 3f_{RRR}R'^2) - \frac{2}{r}R' & \text{if } r < r_\star \end{cases} \tag{4.43}$$

where, in the region $r > r_\star$, the minimum of the approximated derivative of the scalar potential sets the asymptotic value, contrary to Eq. (4.42), where was supplied by hand. In the following we discuss the solutions for the Ricci scalar under the three aforementioned approximations for a different range of densities. We pay particular attention on the impact of different values of ρ_0 have on the solutions were the Ricci scalar at the center is close to $\kappa\rho_0$.

In the left panels of Figs. 4.41, 4.42, 4.43 we observe solutions under three different approximations for the decoupled Ricci differential equation. Given a fixed Ricci at the center, a shooting method is performed to find the radius that matches the de Sitter solution in vacuum. The three figures correspond roughly to three different curvature regimes in respect to the de Sitter minimum R_*. As Fig. 4.41 shows, in the regime where $R_c \lesssim R_*$, the three approximations are virtually indistinguishable. The same cannot be said for the medium-cuvature regime (Fig 4.42) and the high-curvature regime (Fig 4.43). The former and the latter show stark differences between the three approximations.

On the other hand, the right panels of the same figures depict the behavior of the derivative of the Ricci scalar. The appearance of a smooth peak indicates the change of sign of the second derivative itself. Within the low-curvature solution (right panel of Fig. 4.41), we note that the radius of the star coincides where the first derivative is maximal. However, for the medium and high-curvature solutions (right panels of Figures 4.42 and 4.43), the radius does not coincide at the same value.

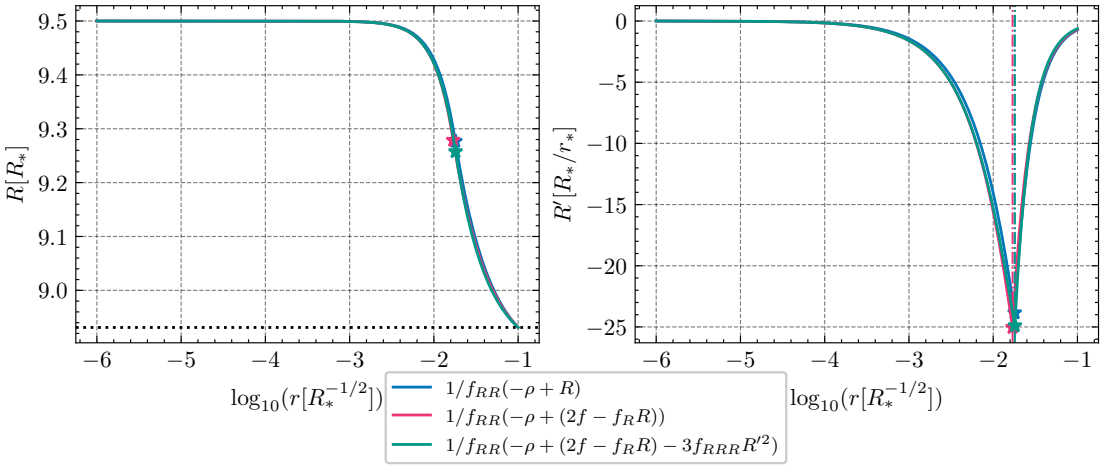

FIGURE 4.41: Ricci scalar a low-curvature solution $\rho_0 = 20c^2R_1(16\pi G)^{-1}$ fixing the Ricci at the center at $R_c/R_* \approx 9.5$. The colored stars represent the star surface.

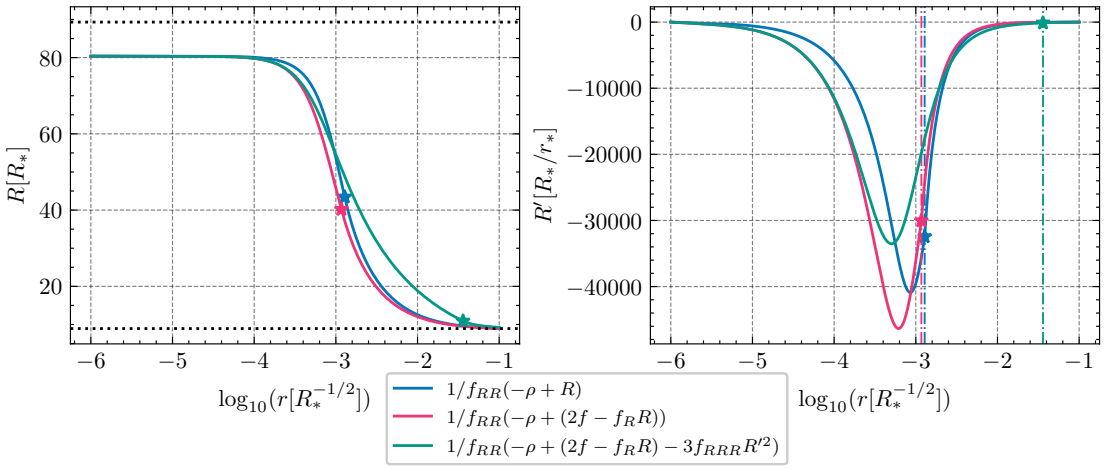

FIGURE 4.42: Solutions for a low-curvature solution $\rho_0 = 20c^2R_1(16\pi G)^{-1}$ fixing the Ricci at the center at $R_c/R_* \approx 80.3797223$. The colored stars represent the star surface.

It is observed for the third approximation (second part of Eq. (4.43)) that, as we transitioned to a high-curvature solution (see right panels of Figures 4.42 and 4.43), the radius of the star dramatically changes to a value where the Ricci scalar is close to the cosmological value R_1. This can be interpreted as the necessity of choice of high central pressure, if it was considered. In other words, the term $-f_{RRR}/f_{RR}R'^2$ introduces this property in the solutions. A term that is usually dropped in the linear approaches (cf. Section 3.5).

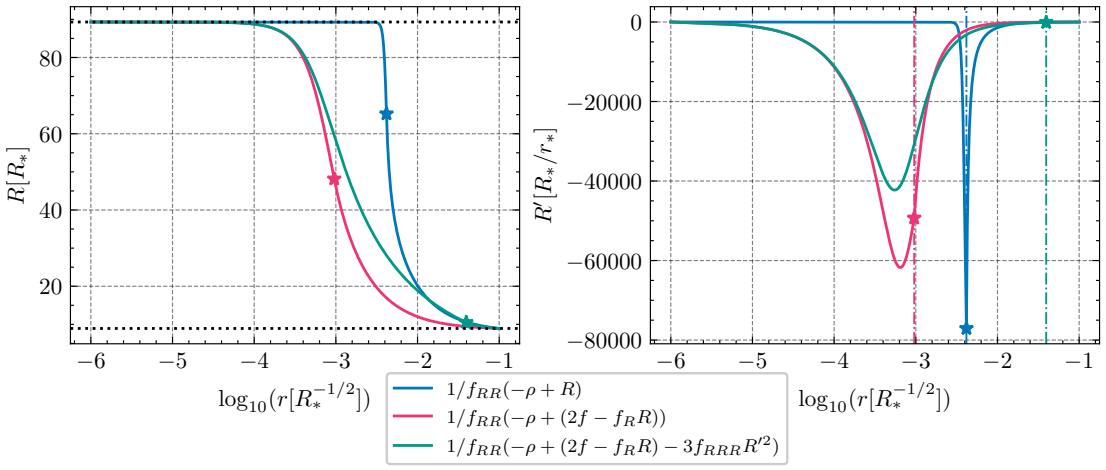

FIGURE 4.43: Solutions for a low-curvature solution $\rho_0 = 20c^2R_1(16\pi G)^{-1}$ fixing the Ricci at the center at $R_c/R_* \approx 89.31080262$. The colored stars represents the star surface.

Through Fig. 4.44 to Fig.4.49, high-curvature solutions that have a gradually increased density are shown. As discussed before, the three approximations considered differ partially. From Figure 4.47, which display the solution for $\rho_0 = 5 \times 10^3 c^2 R_1(16\pi G)^{-1}$, notice that the three solutions are stepper; this fact can be related to the increase of density. As we further increase the density ρ_0, we reach the larger achievable density $\rho_0 = 7.3 \times 10^3 c^2 R_1(16\pi G)^{-1}$ in Fig. 4.48. Solutions of Fig. 4.49 start to blow up.

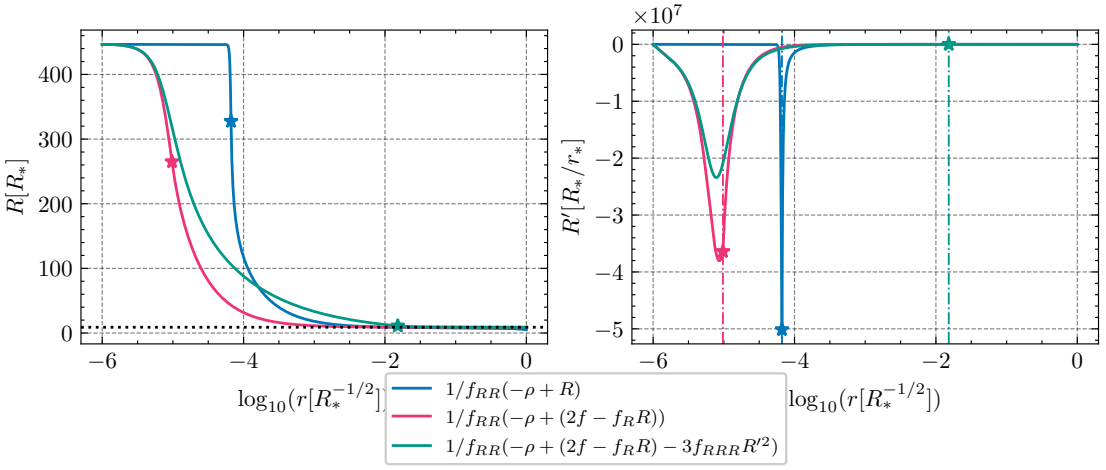

FIGURE 4.44: Solutions for a low-curvature solution $\rho_0 = 1 \times 10^2 c^2 R_1 (16\pi G)^{-1}$ fixing the Ricci at the center at $R_c/R_* = 446.55401323660863118$. The colored stars represents the star surface.

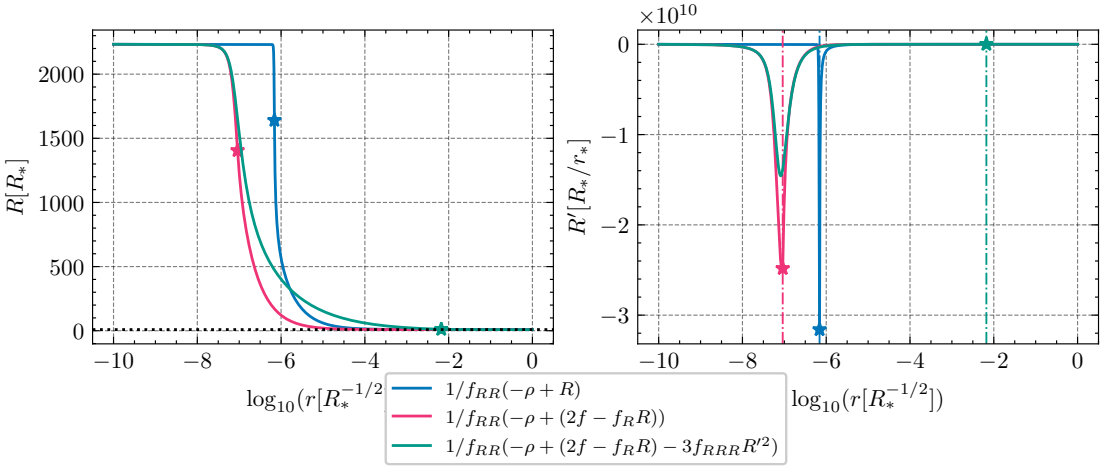

FIGURE 4.45: Solutions for a low-curvature solution $\rho_0 = 5 \times 10^2 c^2 R_1 (16\pi G)^{-1}$ fixing the Ricci at the center at $R_c/R_* = 2232.77006618304315592142416$. The colored stars represents the star surface.

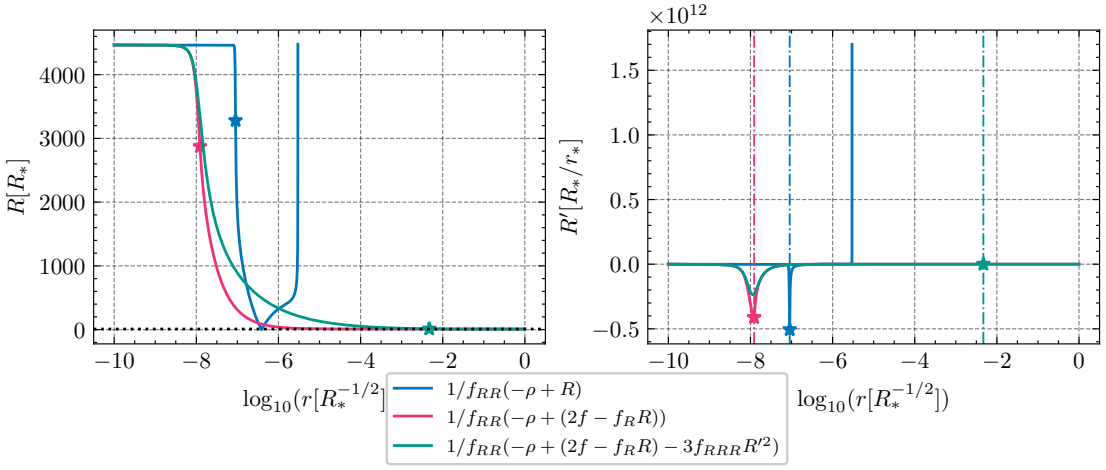

FIGURE 4.46: Solutions for a low-curvature solution $\rho_0 = 1 \times 10^3 c^2 R_1 (16\pi G)^{-1}$ fixing the Ricci at the center at $R_c/R_* = 4465.5401323660086311842848330$. The colored stars represents the star surface.

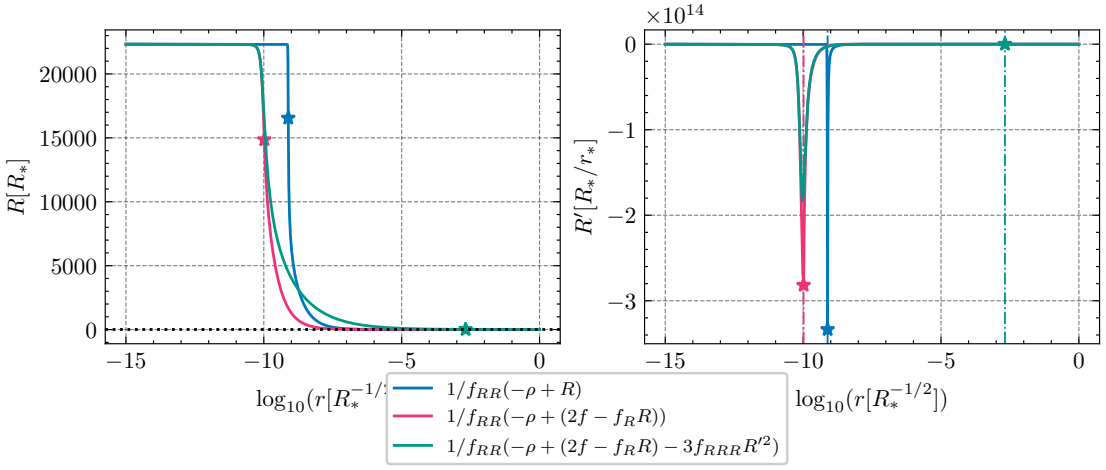

FIGURE 4.47: Solutions for a low-curvature solution $\rho_0 = 5{\times}10^3 c^2 R_1 (16\pi G)^{-1}$ fixing the Ricci at the center at $R_c/R_* = 22327.700661830431559214241653696 62$. The colored stars represents the star surface.

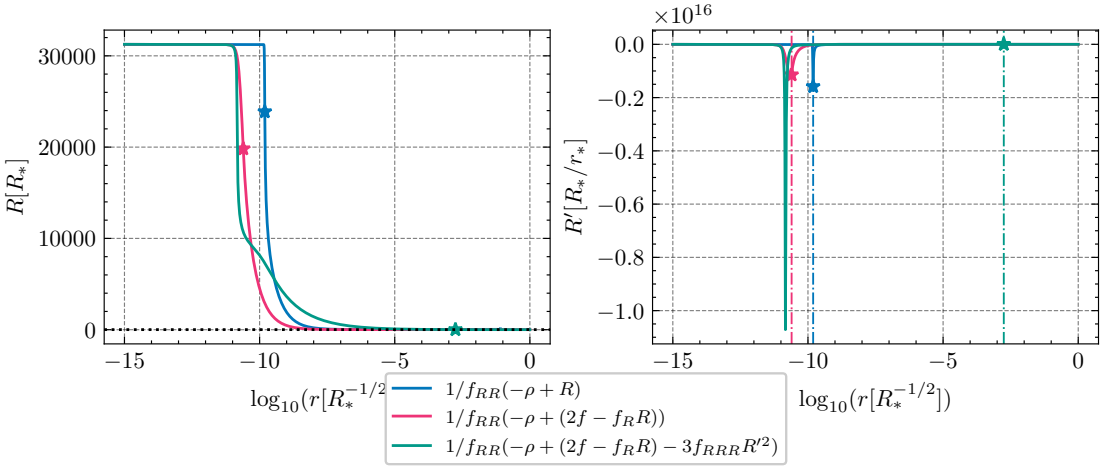

FIGURE 4.48: Solutions for a low-curvature solution $\rho_0 = 7 \times 10^3 c^2 R_1 (16\pi G)^{-1}$ fixing the Ricci at the center at $R_c/R_* = 31258.780926562604182899938315175278$. The colored stars represents the star surface.

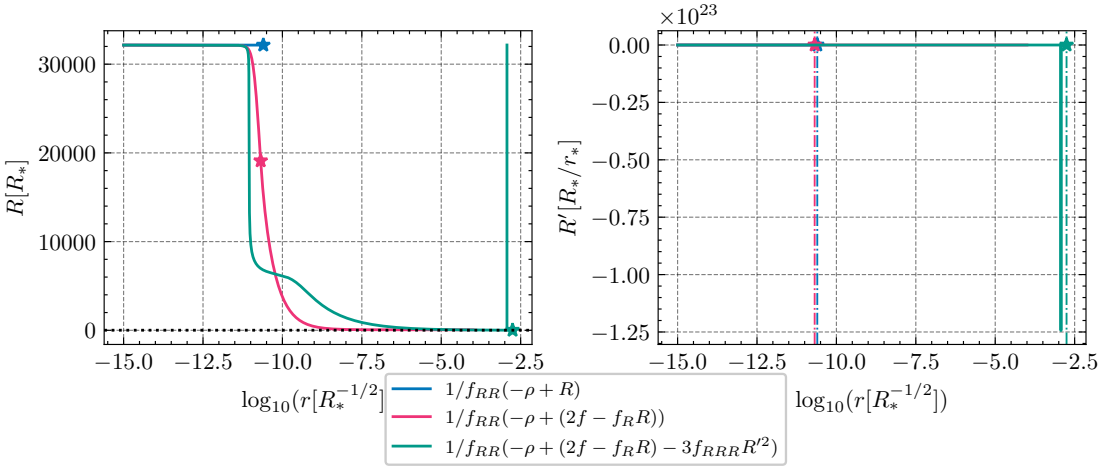

FIGURE 4.49: Solutions for a low-curvature solution $\rho_0 = 7.2 \times 10^3 c^2 R_1 (16\pi G)^{-1}$ fixing the Ricci at the center at $R_c/R_* = 32151.888953035821445268507981323143 23$. The colored stars represents the star surface.

4.7 Discussion

Throughout this chapter we have shown that objects that resemble constant density stars can be constructed numerically within the JPS formalism. Two main conclusions can be drawn from our results regarding the Starobinsky and Hu-Sawicki $f(R)$ models.

First, the objects that we found are far from representing a star like the Sun, namely these are low density objects with relative large central pressures. Moreover, in order to obtain solutions within the shooting technique, the central pressure must be supplied. As we have said, the differential equation system forces us to increase the central pressure in order to obtain the expected high-curvature solutions, which are the ones that closely resemble GR. This means that, solutions for R depend strongly on the central pressure choice. This is, at first sight, a

seemingly contradictory conclusion since, from looking at the $f(R)$ field equations, the pressure function appears to have a somewhat irrelevant role. So, although we tried to find solutions resorting to multiple strategies, we could not find a suitable solution where the Ricci scalar tracks the density for any of the $f(R)$ models. For instance, in the work by Hu and Sawicki [75] the role of the pressure was overlooked and was deprecated. In the work by Negrelli et al. [103], the radius was fixed by hand, so in that study, the role of the pressure is not clear.

Another point is that we believe that all these problems and difficulties are not merely due to numerical systematics. We performed numerous tests for the code using a variety of integrators and the inability to found a desired solution persisted. It is a fact that using arbitrary precision arithmetic opened the door to manage large numbers, present in the numerical contrast regarding the difference of curvature scales, and therefore we manage to reach better results from the shooting procedure. However, at this point we are not sure how further increasing the precision could alleviate the encountered difficulties.

These analysis show up to what extent it is difficult to treat a theory with a cosmological scale embedded in its action. As we will see in the last chapter, this is not the case if we take an unmotivated cosmological $f(R)$ theory, where the numerical contrast problem is absent.

Chapter 5

Neutron stars in non-cosmological motivated $f(R)$ models

In this chapter we review some numerical solutions for Neutron Stars (NS) in the $f(R) = R + \alpha R^2$ model. The main purpose of this chapter is to show that the main difficulty to obtain solutions to the $f(R)$ modified TOV equations, lies precisely in the numerical contrast between the characteristic curvature scales. We also present an argument against studies about neutrons stars in such $f(R)$ model.

5.1 Starobinsky R-squared model

Contrary to the $f(R)$ models presented in Chapter 4, the R-squared $f(R)$ Starobinsky model was first proposed as a model of inflation for the early universe in order to obtain a quasi-de Sitter solution [136]. It is given by

$$f(R) = R + aR^2, \tag{5.1}$$

where $a > 0$. This model is part of a wider class of $f(R)$ models where $f(R) = R + \alpha R^n$ ($a > 0$ and $n > 0$) [50]. Additionally, other similar higher order models such as $f(R) = R + \alpha R^2 + \beta R^3$ or $f(R) = R + \alpha R^2(1 + \gamma \ln R)$ can also be encompassed as a subclass. Although these models emerged to achieve inflation, many authors have related them to the presence of strong gravitational fields, which are naturally found in NS, hoping that deviations from GR in this regime can be used obtain constraints for the model parameters [8, 11, 37, 45]. In this way, the dimensionful parameters contained in the $f(R)$ function on these models determine not a cosmological scale, but typical scale for a compact stellar object. For instance, the R-squared model Eq. (5.1) introduces a new scale through the value of the parameter a which have dimensions of km^{-2}, in order to observe its effects in strong gravitational fields. This scale already reveals a stark difference in respect to the characteristic curvature scale R_* of viable dark energy $f(R)$ models analyzed in the previous chapter, since $R_* \ll a$.

It has been shown that such $f(R)$ models, with quadratic and cubic terms, can give rise to NS with larger maximum masses with respect to GR considering the same equations of state (EoS) [6, 10, 11, 37, 45, 85, 153]. Thus, the main goal of works regarding the R-squared and other

similar models lies on the possible signatures in NS which are reflected in the mass-radius relation given an EoS.

So again, the argument of considering R-squared models as a higher-order is to use NS as a natural laboratory where high curvature phenomena is expected to happen. Let us now compute the derivative of the R-squared model (5.1). It is straightforward to show that

$$f_R = 1 + 2aR, \qquad f_{RR} = 2a, \qquad f_{RRR} = 0. \tag{5.2}$$

Following the previous chapters, we consider the JPS formalism and analyze the properties for this model. Substituting the above expression in the derivative potential (3.8), gives us $dV(R)_{\rm JPS}/dR = R/3$. Furthermore, let us take a look at the equation for the Ricci scalar from (3.43) in this model. Using Eqs. 5.2 we obtain

$$R'' = \frac{1}{6a}\left[m(\kappa T + R)\right] + \left(\frac{m'}{2m} - \frac{n'}{2n} - \frac{2}{r}\right)R'. \tag{5.3}$$

As we observe, for the R-squared model the Ricci scalar equation reduces to one of the approximations presented in the previous chapter. In contrast to the previous $f(R)$ models considered, it is clear there is only one global minimum at $R = 0$ and consequently, the late cosmological expansion cosmological era could not be recovered. Given such minima of the scalar potential $V(R)_{\rm JPS}$ this implies that an interior solution for the Ricci scalar must interpolate to the asymptotic flat value $R = 0$.

5.1.1 Neutron stars in R-squared gravity

We now consider in more detail NS in the R-squared $f(R)$ model. Roughly the analysis of such objects has been divided into two approaches, the first one being a perturbative method and the other one considers the solution of the complete set of differential equations of $f(R)$ gravity.

Cooney et al. [45] showed the existence of NS in the R-squared model by means of a perturbative approach. Arapoglu et al. [8] and Orellana et al. [109] have also employed the same method to obtain mass-radius curves to constraint the value of a for a sample of various EoS. One of the obvious limitations of perturbative solutions lies precisely on the inability of comparing them with the unknown exact solutions. This indicate that possible effects deviating from GR are the dominant and the GR limit cannot be considered as the leading contribution to the pertubative solutions as one expects. Thus, this considerations motivated the need to solve the exact high-order differential equations.

Yazadjiev et al. [153] followed a non-perturbative method by resorting to the usual STT transformation of $f(R)$ gravity in order solve numerically the conformally transformed set of differential equations for four realistic EoS. They argued about the inconsistency of the perturbative approach. Similarly, Kase and Tsujikawa [85] presented numerical solutions using the STT in the JF. More specifically they report the SLy [59] and FPS EoS mass-radius curves. Other relevant studies of NS in R-squared gravity that use the STT transformation are [58, 138].

On the other hand, Capozziello et al. [37] obtained the mass-radius relationship by solving directly the full modified field equations, without resorting to the usual STT transformation in a

similar philosophy to the JPS formalism. They considered, aside from the R-squared model, the $f(R) = R + \alpha R^2(1 + \gamma R)$ and $f(R) = R^{1+\epsilon}$ models. They used the analytical representations of the so called BSkX EoS [110, 113] and the Sly EoS. Within this approach other studies explored the possibility of other EoS [10, 11, 65].

One of the main features is the consideration of **realistic** EoS, which are motivated by microphysics and differ from one parameter polytropic EoS. Due to the existence of stable higher mass configurations of NS in the R-squared model, some EoS, which are in principle ruled out by observational constraints in GR, can lead to interesting solutions and eventually reconcile with NS observations of higher masses $O(2.2M_\odot)$.

5.2 Numerical Results

In this model the scale is given by the parameter a. We choose units such that (see Section 4.4)

$$r_\star = r_g \qquad \rho_\star = M_\odot/r_g^3 \qquad p_\star = M_\odot c^2/r_g^3 \qquad R_\star = r_g^{-2}, \tag{5.4}$$

where we set $r_g = GM_\odot/c^2 \approx 1.47473$ km, that is the Sun's half Schwarzschild radius. Thus, the coefficients (4.31) are set to be $\alpha = 8\pi$ and $\beta = 1$. Moreover, the parameter a is given in units of $r_\star^{-2}$. In this way, the field equations (4.30) for the R-squared model (5.2) are solved numerically using the same procedure described in Section 4.4 following the JPS formalism. The boundary conditions at spatial infinity are met by the requirement to obtain an exterior asymptotically flat solution. Thus as $r \to \infty$,

$$R \to 0, \qquad n, m \to 1. \tag{5.5}$$

We define the ADM mass of the star as the asymptotic limit of the mass function $\mu(r)$,

$$\mathcal{M} := \lim_{r\to\infty} \mu(r) = \frac{rc^2}{2G}\left(1 - \frac{1}{m}\right) \tag{5.6}$$

and again, the star radius r_s is determined by the condition $p(r_s) = 0$. To this regard, Sbisà et al. [126] addressed the issue of nonequivalent definitions of gravitational mass in R-squared gravity since one can, in principle, identify diverse quantities as the mass in the context of R-squared gravity. In particular, one can distinguish between the mass inside the star surface ($M_s = \mu(r_s)$) and the gravitational mass measured by a distant observer given by Eq. (5.6). Contrary to GR, for which the two masses coincides, in R-squared gravity they differ partially, due to the contribution of R outside the star.

5.2.1 Mass-radius relations

We choose the Sly EoS presented in Chapter 2, which is a Piecewise Polytropic Parametric (PPP) EoS. We generate the mass-radius relations and also the density-mass relation for different values of the paramater a/r_g^2 between 0 and 100. Results are depicted in Figures 5.1 and 5.2.

As seen from Fig. 5.1, which presents the results for the EoS SLy, the smaller the value a the smaller is the difference with respect to GR. This is often interpreted a the GR limit, however we must stress that if we enforce smaller values for a the system then suffer from the same density scale contrast problems encountered in the cosmological motivated $f(R)$ models studied in previous sections.

Each point of Fig. 5.1 represents a NS configuration, which has been computed by means of a shooting technique to obtain the correct asymptotic behavior.

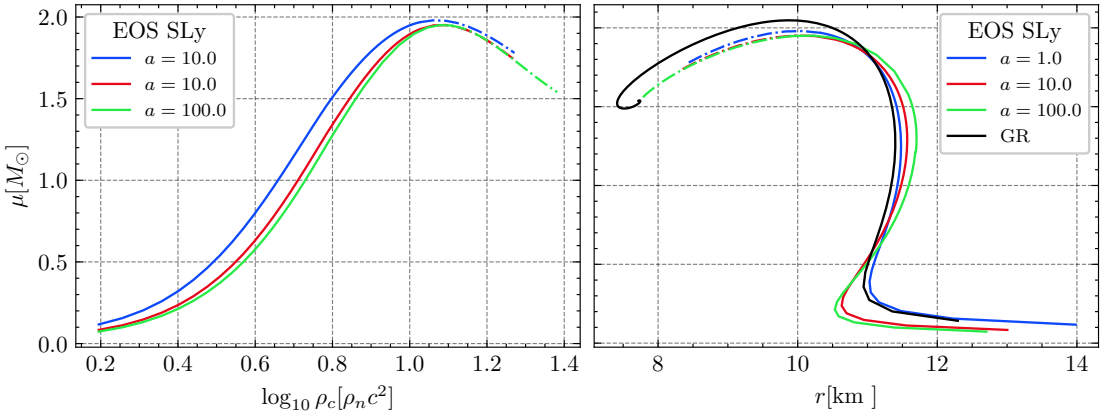

FIGURE 5.1: The density-radius relation for EOS SLy (left panel) and its mass-radius curve(right panel) for the R-squared model. For comparison the prediction from GR is shown in solid black. The dotted lines are configurations where $T < 0$, meaning the adjusted Ricci scalar at the center is $R(0) < 0$.

The central density increases monotonically along the mass-radius curves. Figure 5.2 shows the radial profile for the Ricci scalar and the metric functions after performing the shooting method for multiple central densities. The color code tells us that for lower densities (violet colors) the Ricci profile appears flatter and thus *unscreened*, in the sense that a screened solution will go up and down in a narrow radial region. Most interestingly is the emergence of solutions with negative curvature at the center of the NS.

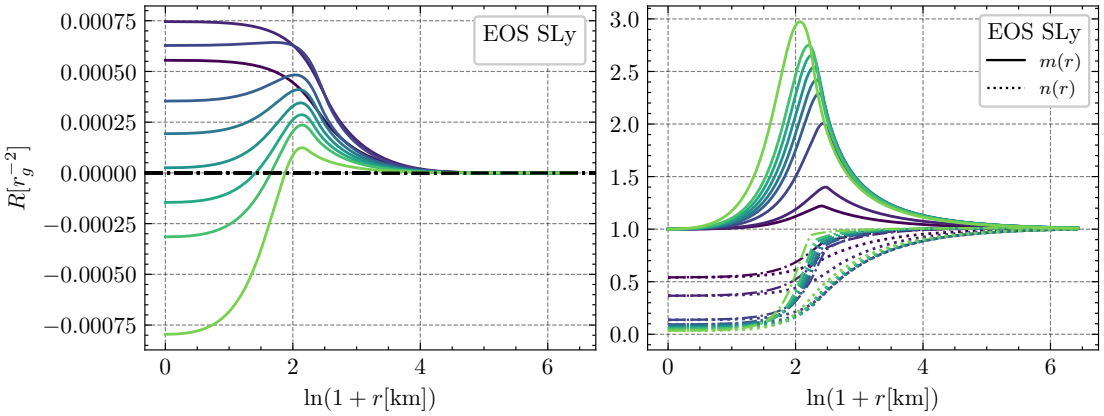

FIGURE 5.2: Ricci scalar versus the radial coordinate (left panel) and the metric components as functions of the radial coordinate (right panel) for the R-squared model with $a/r_g^{-2} = 100$. Colors from violet to green indicate increasing central densities. For comparison the prediction from GR is shown in solid black.

As far as we know the solutions presented above are novel in the sense that we are solving the exact high-order $f(R)$ equations without resorting to the usual STT using instead the JPS formalism. The difference with the results from Capozziello et al. [37] and ours, is that they consider other EoS and deprecated the region where $R < 0$.

5.2.2 Incompressible fluid

We can ask now what happens when an incompressible object is considered in this class of $f(R)$ theories. Let us keep the units of (5.4), but now consider an incompressible fluid with constant density and central pressure. Left panel of Fig. 5.3 depicts multiple solutions with decreasing central pressure (colors violet to green). The right panel of the same figure displays the Ricci scalar at the center of the object as a function of the central pressure. The three peak black marker represents the value of the trace of the energy-momentum tensor that belongs to the exact value in GR ($R = \kappa T$). We observe how for large central pressure choices, both values remain roughly of the same order. As the central pressure decreases, they dramatically star to differ.

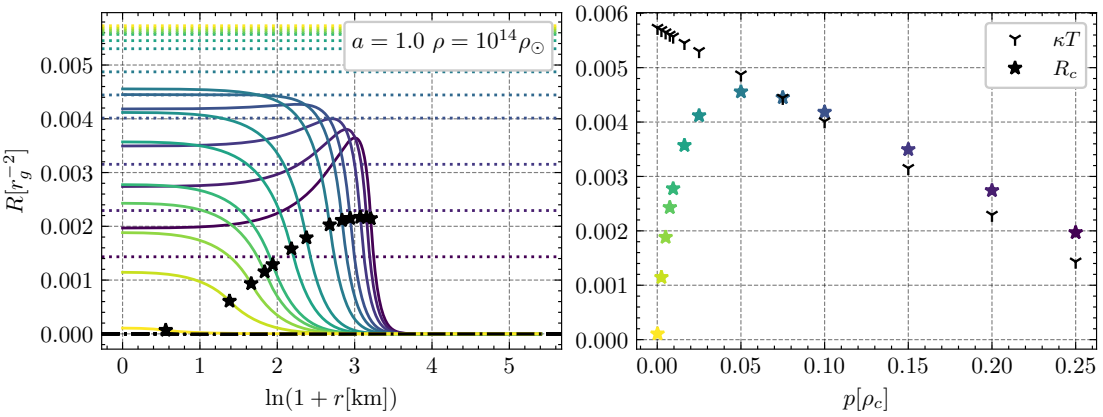

FIGURE 5.3: The value of the Ricci scalar versus the radial coordinate (left panel) and the Ricci scalar at the center as a function of the central pressure (right panel) for the R-squared model with $a = 1$. Colors from violet to green indicate decreasing central pressures. The dotted horizontal lines (left panel) indicate the values κT_c where T_c is the value of the trace of the energy momentum tensor at the center.

Fig. 5.4 (left panel) shows the mass function for the same configurations displayed in Fig. 5.3. The right panel depicts how the mass at the surface relates to variations in pressure. We observe almost a linear relation between both quantities.

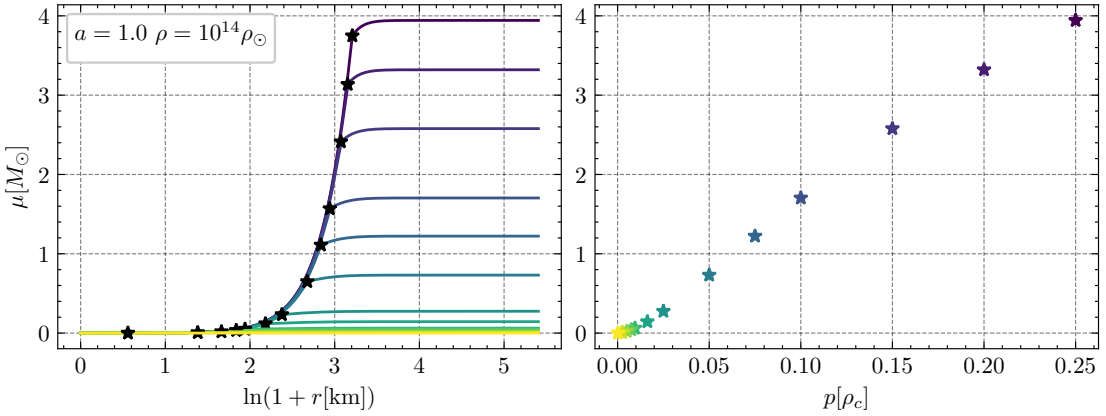

FIGURE 5.4: The value of the mass as a function of the radial coordinate (left panel) and the asymptotic mass as a function of the central pressure (right panel) for the R-squared model with $a = 1$. Colors from violet to green indicate decreasing central pressures. The dotted horizontal lines (left panel) indicate the values κT_c where T_c is the value of the trace of the energy-momentum tensor at the center.

Finally, we present results obtained by setting a lower central pressure for a constant density object of $\rho = 10^{14}\rho_\odot$. The units are the same of the previous plots. In Fig. 5.5 we observe the value scalar curvature R for this configuration. The choice of the scale of R indicates that it is seven order of magnitude below the value $\kappa\rho$. So again, this seems to be same phenomenon encountered in the cosmological viable $f(R)$ models. But the situation is actually a bit more subtle here. It is true that scalar R at the center is near the vacuum minimum value $R = 0$, however the object is smaller and the metric functions (right panel) do not depict a cosmological horizon.

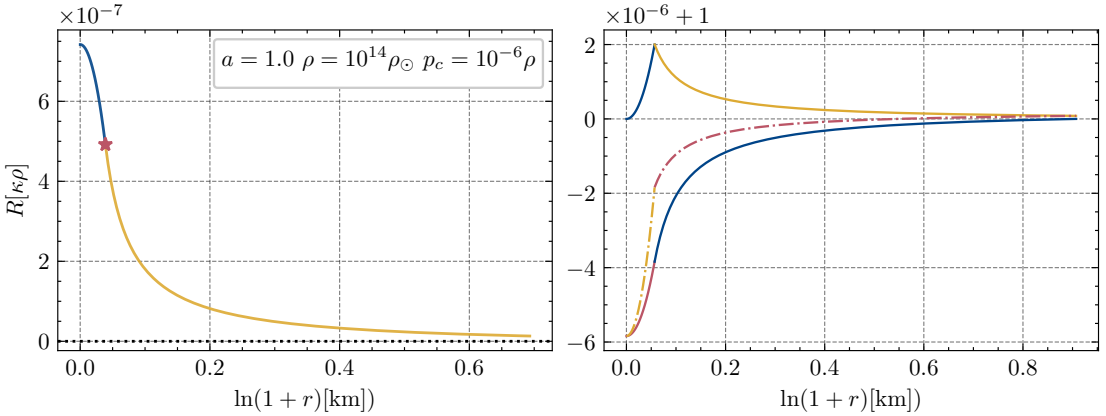

FIGURE 5.5: Solutions for constant density object with $\rho = 10^{14}\rho_\odot$ $p_c = 10^{-6}\rho_c$. The left panel depicts the Ricci scalar. The right panel shows the metric functions.

Figure 5.6 (left panel) shows that the object, although is extremely dense, has a small mass. Just for the sake of completeness we can ask what happens to the γ parameter in this scenario, although the object is far from representing a star like the Sun where the bounds of γ are given.

We set

$$\gamma_{neg} = \left|\frac{1-m}{1-n}\right|, \qquad \gamma_{HM} = \left|\frac{mn-m}{1-m}\right|. \tag{5.7}$$

In the right panel of Fig. 5.6 we observe how neither of these two equivalent definitions of the γ manage to give the correct value one.

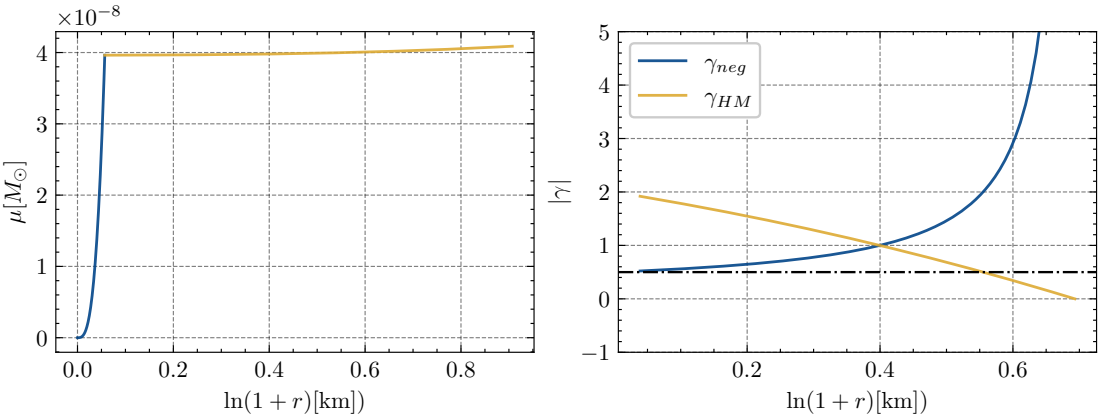

FIGURE 5.6: Solutions for constant density object with $\rho = 10^{14}\rho_\odot$ $p_c = 10^{-6}\rho_c$. The left panel depicts the mass function. The right panel shows the gamma parameters as defined in Eqs. 5.7.The horizontal dashed black line corresponds to $\gamma = 1/2$.

5.3 An argument against stars in R-squared gravity

In this chapter we have shown, that it is possible to obtain numerical solutions using the JPS formalism for static and spherically symmetric configurations such as NS in the context of R-squared gravity. The numerical difficulties mentioned along Chapter 4 do not appear here since the characteristic curvature scales are manageable.

As mentioned in the introduction of this chapter, several models of the same nature have been proposed. We stress that such $f(R)$ models, in particular the R-squared model, seem to not pass the solar system tests at the level of the action because the quadratic or even cubic terms, will naturally appear at the Solar System Scale deviating immediately from the expected GR value for the Ricci scalar ($R \sim \kappa\rho_\odot$). A preliminary analysis, not included in this thesis, shows that it is not possible to reach the solar densities with that scale of a. Many authors try to argue about this flaw by saying that at solar system scales a is very small and conclude naively that a is unconstrained by such tests but, at the same time, they consider values of a of the order of the Schwarzschild of the Sun $r_s^\odot \sim 3$ km, $a \sim (r_s^\odot)^{-2}$ (see for e.g. [6, 37] for such an argument). Others authors, go so far as to assume that the R-squared function (5.1) is an approximation from a more general $f(R)$ in the strong gravitational regime such as inside NS. But those authors argue that such an approximation is not valid in the weak field limit [124]. It is not clear why the R-squared gravity models can be taken as effective corrections to GR which only appear in curvature scales characteristic of NS.

However, if one chooses to consider solar system constraints on the parameter a, it results that a should bounded by $a < 10^{-17}$ km^{-2} (see section V of [67]). Thus, from this point of view, the values of a considered so far in the literature are unrealistic.

After reviewing a large amount of NS literature in $f(R)$ gravity, all that we can do now is maintain a clear statement in what we oppose. Beneath the surfaces of aesthetic mass-radius plots, the use of non cosmological viable $f(R)$ models, continues produce a series of works that do not contribute to any significant arguments for ruling out $f(R)$ models. It is common to read the use of up-to-date nuclear equations of state as a justification to obtain mass-radius plots keeping always unrealistic values of the parameters contained in the $f(R)$ function. Note that our analysis has kept the values of these parameters (specifically a) in order to reproduce their results using the JPS formalism. Although the immediate conclusion can be understood as the existence of NS with larger masses than that of their Einsteinian (GR) counterparts, it can only be said that the R-squared $f(R)$ theory, in fact, deviates from GR and that its differences are considerable. However, even though the deviations are large there is intrinsic uncertainty by the realistic EoS used which needs to be confronted with observations before the R-squared model itself [153]. Thus, the goal of constraining the parameter a of the R-squared in the aforementioned studies lacks support.

We emphasize that if one is to take any $f(R)$ model seriously, meaning, to take in consideration that $f(R)$ gravity can be used as an alternative to GR in all gravity regimes, then any realistic astrophysical scenario should be part of the domain of applicability of the $f(R)$ model in question. Hence, the solar system tests are needed to be taken in to consideration.

Chapter 6

Conclusions

Solar system tests have a main role in any gravity theory for several reasons. They represent our most tested gravitational environment for which GR passes all its constraints. Also, they place strong bounds on any alternative theory of gravity. Although $f(R)$ gravity has been extensively studied to explain the late accelerating expansion of the universe, in this thesis, we have investigated its effects at the solar systems scale.

Even if our aim was to find numeric solutions for stars in $f(R)$ that properly entail realistic densities, we found that in $f(R)$ gravity, the system of differential equations of stellar structure is more involved than in GR, and thus, we were forced to implement more robust numerical methods to obtain solutions. Contrary to other works in the literature we did not resort to the usual STT conformal transformation to obtain our results.

After giving a brief review on stars in GR on Chapter 2 and on the general properties of $f(R)$ theories in Chapter 3, we have analyzed in detail a handful of cosmological viable $f(R)$ models through Chapter 4. It turns out that the JPS approach to solve the equations derived from $f(R)$ gravity gave us solutions equivalent to those previously encountered by some authors within different contexts.

Concerning the local solar system tests, we could not reach the desired density due to the numerical difficulties, even after we resorted to arbitrary numerical precision. However, one of our key findings is that, in order to obtain the desired numerical solutions where the Ricci Scalar, $R(r)$, follows the density of the star as r changes (similar to what happens in GR) in some $f(R)$ models, is to enforce a high central pressure. This is clearly in contrast to GR, where in the case for non-relativistic stars like the Sun, modeled as constant density objects, the central pressure is negligible and yet $R \sim \kappa\rho_{\odot}$ inside the body.

As concerning the chameleon mechanism not so much can be said. It is well known that this effect has been invoked along the literature to justify the success of the solar system tests in some cosmological motivated $f(R)$ theories. However, the results obtained show that is not completely clear where this effect leaves its signatures at the full non-linear level.

The review done on literature shows that almost in all numerical studies of $f(R)$ gravity, approximations have been made to try to argue that solar system bounds are satisfied. However, one

cannot rule out yet this pertubative studies. As our study shows, taking into account the complete set of non-linear differential equations, it appears that it is technically difficult to reproduce the successes of the pertubative case. One may hope to start seeing some effects of the at some high density scale, but the results does not support this behavior. To this end, it turns out to be rather paradoxical that the chameleon mechanism, which is defined and thought as a result of the non-linear dynamics of the extra scalar degree of freedom, has to be assumed a priori in the pertubative case, but fails to be isolated from the numerical analysis.

In addition, in Chapter 5 we obtained some mass-radius relations for the R-squared $f(R)$ gravity model which is not cosmological motivated. This confirms that the JPS formalism can be used to obtain solutions within the aforementioned context. As we manifestly declared, these kind of $f(R)$ models are not physically motivated since the characteristic curvature scale differs abysmally from that of a cosmological viable $f(R)$ model, not to mention that they might not be pass successfully the solar system tests.

Regarding work for the future, introducing for example a more detailed model for the Sun and its environments might alleviate the technical difficulties that we discussed in Chapter 4. However, it is not clear that such amendments will solve those drawbacks since in GR one does not have to resort to complex solar models to obtain its observed mass and radius.

As a final comment let us mention that, from the plethora of alternative theories of gravity, not even one has managed to correctly describe all gravity regimes that GR successfully entails without resorting to gimmicky ways to suppress some unwanted effects which emerge in these theories when they are confronted with tests such as the ones given by the solar system. The underlying idea of replacing the cosmological constant by an alternative theory seems unfeasible unless a robust observational motivation to discard the ΛCDM paradigm appears. This means that models, as the cosmological viable $f(R)$ functions, presented through the first part of this thesis, which are built in an engineering way as trial and error, might not have particular relevance at all. The forthcoming dark energy experiments, like DESI [92], might reveal if the cosmological constant is dynamic or not. If the outcome is positive, these types of alternatives theories might have the chance to be taken more seriously.

In conclusion, what emerges from this analysis, is that to reconcile an alternative gravity theory with the stringent constraints placed by observations, without having any good physical motivation is perhaps, not the most efficient way to discover new physics. We need to look for new physical principles or thought experiments, like the ones that gave rise to GR at the beginning of the 20th century, to be able to enhance our understanding of the universe.

Appendix A

STT equations for spherical static symmetry

It is possible to transform the Eqs. (3.44) to the Scalar-Tensor formulation. In fact, we can use the same line element from Eq. (3.42) and substitute it in Eq.(3.21) to obtain

$$\phi'' = \frac{1}{3}\left[m(\kappa T + 2f - \phi R)\right] + \left(\frac{m'}{2m} - \frac{n'}{2n} - \frac{2}{r}\right)\phi' \tag{A.1a}$$

$$n' = \frac{n}{r(2\phi + r\phi')}\left[mr^2(f - R\phi + 2\kappa T_r^r) + 2\phi(m-1) - 4r\phi'\right] \tag{A.1b}$$

$$m' = \frac{m}{r(2\phi + r\phi')}\left[-mr^2(f - \phi R + 2\kappa T_t^t) + 2\phi(1-m) + 4mr\phi' + 2r^2\phi''\right] \tag{A.1c}$$

Notice that eq. (A.1c) can be rewritten in a more suitable way as

$$\begin{aligned} m' =& \frac{m}{r(2\phi + r\phi')}\Bigg\{2\phi(1-m) - 2mr^2\kappa T_t^t + \frac{mr^2}{3}(R\phi + f + 2\kappa T) \\ &+ \frac{r\phi'}{\phi}\left[\frac{mr^2}{3}(2R\phi - f + \kappa T) - \kappa mr^2(T_t^t + T_r^r) + 2\phi(1-m)\right]\Bigg\}, \end{aligned} \tag{A.2}$$

where $R(\phi)$ and $f(R(\phi))$, i.e., explicit functions of ϕ. Eq. (A.2) resembles that of Eq. (3.44a) from the JPS formalism. We further point out that Eqs. (A.1) can be shown to be derived from (3.44) by noting that

$$\phi' = f_{RR}R' \qquad\qquad \phi'' = f_{RRR}R'^2 + f_{RR}R'' \tag{A.3}$$

Under this mapping the Ricci scalar behaves as $R \sim 1/(\phi - \phi_0)$. For instance, for the Starobinsky model [137] we obtain the scalar field ϕ in the JF as

$$\phi(R) = 1 - \frac{2R\lambda q\left(\frac{R^2}{R_S^2} + 1\right)^{-q}}{R_S\left(\frac{R^2}{R_S^2} + 1\right)} \tag{A.4}$$

which is not possible to be inverted analytically.

A.1 High-curvature regime in STT

In this regime assuming the high-cruvature regime $R \gg R_*$ it is possible to invert the relation between the scalar field ϕ and R to obtain an explicit formula expressing R as a function of ϕ. Thus, we have

$$R(\phi) \approx R_S \left(\frac{2\lambda q}{1-\phi}\right)^{1/(2q+1)} \tag{A.5}$$

One sees as $\phi \to 1$ then $R \to \infty$. With relation (A.5) then $f(R)$ can be written in terms of ϕ as

$$f(R(\phi))^{\mathrm{S}} \approx R(\phi) + \lambda R_S \left[\left(\frac{2\lambda q}{1-\phi}^{-2q/(2q+1)}\right) - 1\right] \tag{A.6}$$

It remains to link the notion of the high-curvature regime in the JPS formalism detailed above with the STT formalism. According to the definitions introduced in section 3.1.2, in the high curvature regime we have the following relations

$$\phi = \exp 2\sqrt{\kappa/6}\Phi = 1 - \Delta_R^G \approx 1 - \lambda n \left(\frac{R}{R_S}\right)^{-(n/\beta+1)}, \tag{A.7}$$

With the aid of this relation the conformally transformed scalar potential in the EF defined by Eq. (3.30) can be expressed in the high curvature regime as

$$V_{\mathrm{BL}}(\Phi) \approx \frac{\lambda R_S}{2\sqrt{\kappa}\phi^2}\left[1 - (n/\beta+1)\left(\frac{1-\phi}{n/\beta\lambda}\right)^{\frac{n/\beta}{n/\beta+1}}\right], \tag{A.8}$$

where one should keep in mind that $\phi = \phi(\Phi)$. From the relation (A.7), we observe that small values for Φ imply high curvature ($R \gg R_S$). Thus, in this regime we have $\Phi \ll 1$ which allows us obtain the expansion $\phi \approx 1 + 2\sqrt{\kappa/6}\Phi$, meaning $1 - \phi \approx -2\sqrt{\kappa/6}\Phi$. Using this fact in Eq. (A.8), leads to

$$V_{\mathrm{BL}}(\Phi) \approx \frac{\lambda R_S}{2\sqrt{\kappa}} e^{-4\sqrt{\kappa/6}\Phi}\left[1 - (n/\beta+1)\left(\frac{-2\sqrt{\kappa}\Phi}{\sqrt{6}n/\beta\lambda}\right)^{\frac{n/\beta}{n/\beta+1}}\right]. \tag{A.9}$$

In the limit that $R \to \infty$ we have $\phi \to 1$ and $\Phi \to 0$ implying a constant potential $V_{\mathrm{BL}}(\Phi) \to \frac{\lambda R_S}{2\sqrt{\kappa}}$ which corresponds to a singularity since $dV_{\mathrm{BL}}(\Phi)/d\Phi \to \infty$ as highlighted by Frolov [66]. [1]

Recall that the expression for the field Φ is given by Eq. (3.28), which implies the following

$$\Phi = \sqrt{\frac{3}{2\kappa}}\ln(1+\Delta_R) \approx \sqrt{\frac{3}{2\kappa}}\Delta_R, \tag{A.10}$$

with aid of Eq. (3.61) the minimum of the effective potential can be estimated as

$$\frac{dV_{\mathrm{BL}}^{eff}(\Phi)}{d\Phi} = \sqrt{\frac{2}{3\kappa}}\frac{R(1-\Delta_R)+2\Delta}{2(1+\Delta_R)^2} + \sqrt{\kappa}Q\exp\left[Q\sqrt{\kappa}\Phi\right]\rho_c = 0. \tag{A.11}$$

[1] One can check that Eq. (A.8) is the same as Eq. 5.20 from [50] with a slightly different notation.

Notice that if we assume the approximation $\Delta_R \ll 1$ and $\Delta \ll R$ the first term of Eq. (A.11) approximates to $-QR/\sqrt{\kappa}$. An thus, taking into account Eq. (A.9) the minimum of the effective potential in the EF has a value of

$$\Phi_{min} = -\sqrt{6/\kappa}n/(2\beta)\lambda\left(\frac{R_S}{\kappa\rho_c}\right)^{n/\beta+1}. \tag{A.12}$$

Thus, the effective mass about the minimum of the effective potential is of the order

$$m_{eff}(\Phi_{min}) \sim \left(\frac{k\rho_c}{R_S}\right)^{n/2\beta+1} \tag{A.13}$$

which coincides with the mass obtained in the JPS picture of Eq. (4.24).

Bibliography

[1] Akmal, A. et al. "Equation of State of Nucleon Matter and Neutron Star Structure". *Physical Review C*, **58**, (1998), 1804–1828. [DOI] (cit. on p. 15).

[2] Alavirad, H. and Weller, J. M. "Modified Gravity with Logarithmic Curvature Corrections and the Structure of Relativistic Stars". *Physical Review D*, **88**, (2013), 124034. [DOI] (cit. on pp. 35, 52).

[3] Amanullah, R. et al. "Spectra and Light Curves of Six Type Ia Supernovae at 0.511 < z < 1.12 and the Union2 Compilation". *The Astrophysical Journal*, **716**, (2010), 712–738. [DOI]. [arXiv:1004.1711] (cit. on p. 1).

[4] Amendola, L. et al. "Are $f(R)$ Dark Energy Models Cosmologically Viable ?" (2006). [DOI] (cit. on pp. 25, 43).

[5] Amendola, L. et al. "Conditions for the Cosmological Viability of $f(R)$ Dark Energy Models". *Physical Review D*, **75**, (2007), 083504. [DOI] (cit. on p. 36).

[6] Aparicio Resco, M. et al. "On Neutron Stars in $f(R)$ Theories: Small Radii, Large Masses and Large Energy Emitted in a Merger". *Physics of the Dark Universe*, **13**, (2016), 147–161. [DOI] (cit. on pp. 52, 83, 89).

[7] Appleby, S. A. and Battye, R. A. "Do Consistent $f(R)$ Models Mimic General Relativity plus Λ?" *Physics Letters B*, **654**, (2007), 7–12. [DOI]. [arXiv:0705.3199 (astro-ph)] (cit. on p. 52).

[8] Arapoglu, A. S. et al. "Constraints on Perturbative $f(R)$ Gravity via Neutron Stars". *Journal of Cosmology and Astroparticle Physics*, **2011**, (2011), 020–020. [DOI]. [arXiv:1003.3179] (cit. on pp. 52, 83, 84).

[9] Arnett, W. D. and Bowers, R. L. "A Microscopic Interpretation of Neutron Star Structure". *The Astrophysical Journal Supplement Series*, **33**, (1977), 415. [DOI] (cit. on p. 16).

[10] Astashenok, A. V. et al. "Further Stable Neutron Star Models from $f(R)$ Gravity". *Journal of Cosmology and Astroparticle Physics*, **2013**, (2013), 040–040. [DOI]. [arXiv:1309.1978] (cit. on pp. 52, 83, 85).

[11] Astashenok, A. V. et al. "The Realistic Models of Relativistic Stars in $f(R) = R + \alpha R^2$ Gravity". *Classical and Quantum Gravity*, **34**, (2017), 205008. [DOI]. [arXiv:1704.08311] (cit. on pp. 52, 83, 85).

[12] Babichev, E. and Langlois, D. "Relativistic Stars in $f(R)$ Gravity". *Physical Review D*, **80**, (2009), 121501. [DOI] (cit. on pp. 3, 30, 32, 46, 52).

[13] Babichev, E. and Langlois, D. "Relativistic Stars in $f(R)$ and Scalar-Tensor Theories". *Physical Review D*, **81**, (2010), 124051. [DOI] (cit. on pp. 46, 52).

[14] Bahcall, J. N. et al. "New Solar Opacities, Abundances, Helioseismology, and Neutrino Fluxes". *The Astrophysical Journal*, **621**, (2005), L85–L88. [DOI]. [arXiv:astro-ph/0412440] (cit. on pp. 10, 14).

[15] Bahcall, N. et al. "The Cosmic Triangle: Revealing the State of the Universe". *Science*, **284**, (1999), 1481–1488. [DOI]. [arXiv:astro-ph/9906463] (cit. on pp. 1, 25).

[16] Bailey, D. H. et al. "High-Precision Computation: Mathematical Physics and Dynamics". *Applied Mathematics and Computation*, **218**, (2012), 10106–10121. [DOI] (cit. on pp. 56, 57).

[17] Barausse, E. et al. "Curvature Singularities, Tidal Forces and the Viability of Palatini $f(R)$ Gravity". *Classical and Quantum Gravity*, **25**, (2008), 105008. [DOI]. [arXiv:0712.1141] (cit. on p. 26).

[18] Barausse, E. et al. "A No-Go Theorem for Polytropic Spheres in Palatini $f(R)$ Gravity". *Classical and Quantum Gravity*, **25**, (2008), 062001. [DOI]. [arXiv:gr-qc/0703132] (cit. on p. 26).

[19] Berti, E. et al. "Testing General Relativity with Present and Future Astrophysical Observations". *Classical and Quantum Gravity*, **32**, (2015), 243001. [DOI] (cit. on pp. 2, 3, 25, 30).

[20] Bertotti, B. et al. "A Test of General Relativity Using Radio Links with the Cassini Spacecraft". *Nature*, **425**, (2003), 374–376. [DOI] (cit. on pp. 6, 38).

[21] Bisabr, Y. "Solar System Constraints on a Cosmologically Viable $f(R)$ Theory". *Physics Letters B*, **683**, (2010), 96–100. [DOI]. [arXiv:0907.3838 (gr-qc)] (cit. on p. 45).

[22] Bonazzola, S. et al. "Axisymmetric Rotating Relativistic Bodies: A New Numerical Approach for 'exact' Solutions". *Astronomy and Astrophysics*, **278**, (1993), 421–443 (cit. on p. 16).

[23] Brax, P. et al. "$f(R)$ Gravity and Chameleon Theories". *Physical Review D*, **78**, (2008), 104021. [DOI]. [arXiv:0806.3415] (cit. on pp. 30, 32, 38–40, 52).

[24] Brax, P. et al. "Screening Fifth Forces in K-Essence and DBI Models". *Journal of Cosmology and Astroparticle Physics*, **2013**, (2013), 020–020. [DOI]. [arXiv:1209.1293] (cit. on pp. 38, 39).

[25] Brax, P. et al. "Neutron Stars in Screened Modified Gravity: Chameleon vs Dilaton". *Physical Review D*, **95**, (2017), 083514. [DOI]. [arXiv:1702.02983] (cit. on p. 52).

[26] Buchdahl, H. A. "Non-Linear Lagrangians and Cosmological Theory". *Monthly Notices of the Royal Astronomical Society*, **150**, (1970), 1. [DOI] (cit. on p. 26).

[27] Burrage, C. and Sakstein, J. "Tests of Chameleon Gravity". *Living Reviews in Relativity*, **21**, (2018), 1. [DOI] (cit. on pp. 35, 39).

[28] Bustelo, A. J. and Barraco, D. E. "Equilibrium Hydrostatic Equation and Newtonian Limit of the Singular $f(R)$ Gravity". *Classical and Quantum Gravity*, **24**, (2007), 2333–2342. [DOI]. [arXiv:gr-qc/0611149] (cit. on p. 52).

[29] Cañate, P. et al. "Spherically Symmetric Black Holes in $f(R)$ Gravity: Is Geometric Scalar Hair Supported ?" *Classical and Quantum Gravity*, **33**, (2016), 155005. [DOI]. [arXiv:1509.01664] (cit. on pp. 34, 36, 46, 59).

[30] Capone, M. and Ruggiero, M. L. "Jumping from Metric $f(R)$ to Scalar-Tensor Theories and the Relations between Their Post-Newtonian Parameters". *Classical and Quantum Gravity*, **27**, (2010), 125006. [DOI]. [arXiv:0910.0434] (cit. on pp. 2, 30).

[31] Capozziello, S. et al. "Cosmological Viability of $f(R)$-Gravity as an Ideal Fluid and Its Compatibility with a Matter Dominated Phase". *Physics Letters B*, **639**, (2006), 135–143. [DOI]. [arXiv:astro-ph/0604431] (cit. on p. 2).

[32] Capozziello, S. et al. "A Bird's Eye View of $f(R)$-Gravity". *The Open Astronomy Journal*, **3**, (2010), 49–72. [DOI]. [arXiv:0909.4672] (cit. on pp. 1, 26).

[33] Capozziello, S. et al. "Comparing Scalar-Tensor Gravity and $f(R)$-Gravity in the Newtonian Limit". *Physics Letters B*, **686**, (2010), 79–83. [DOI]. [arXiv:1002.1364 (gr-qc)] (cit. on pp. 29, 52).

[34] Capozziello, S. et al. "Hydrostatic Equilibrium and Stellar Structure in $f(R)$ Gravity". *Physical Review D*, **83**, (2011), 064004. [DOI] (cit. on p. 52).

[35] Capozziello, S. and Francaviglia, M. "Extended Theories of Gravity and Their Cosmological and Astrophysical Applications". *General Relativity and Gravitation*, **40**, (2008), 357–420. [DOI]. [arXiv:0706.1146] (cit. on p. 1).

[36] Capozziello, S. and Tsujikawa, S. "Solar System and Equivalence Principle Constraints on $f(R)$ Gravity by the Chameleon Approach". *Physical Review D*, **77**, (2008), 107501. [DOI] (cit. on pp. 30, 37, 40, 48, 52).

[37] Capozziello, S. et al. "The Mass-Radius Relation for Neutron Stars in $f(R)$ Gravity". *Physical Review D*, **93**, (2016), 023501. [DOI]. [arXiv:1509.04163] (cit. on pp. 52, 83, 84, 87, 89).

[38] Carroll, S. M. "The Cosmological Constant". *Living Reviews in Relativity*, **4**, (2001), 1. [DOI]. [arXiv:astro-ph/0004075] (cit. on p. 1).

[39] Carroll, S. M. et al. "Is Cosmic Speed-Up Due to New Gravitational Physics?" *Physical Review D*, **70**, (2004), 043528. [DOI]. [arXiv:astro-ph/0306438] (cit. on pp. 43, 50).

[40] Chandrasekhar, S. *An Introduction to the Study of Stellar Structure*. Unabr. and corr. republ. of orig. publ. 1939 by Univ. of Chicago Pr. Dover Books on Astronomy. New York: Dover Publ, 1970 (cit. on pp. 10, 13).

[41] Chiba, T. "$1/R$ Gravity and Scalar-Tensor Gravity". *Physics Letters B*, **575**, (2003), 1–3. [DOI]. [arXiv:astro-ph/0307338] (cit. on pp. 3, 36, 37, 75).

[42] Chiba, T. et al. "Solar System Constraints to General $f(R)$ Gravity". *Physical Review D*, **75**, (2007), 124014. [DOI] (cit. on pp. 30, 37, 52).

[43] Clifton, T. et al. "Modified Gravity and Cosmology". *Physics Reports*, **513**, (2012), 1–189. [DOI]. [arXiv:1106.2476] (cit. on p. 25).

[44] Cognola, G. et al. "Class of Viable Modified $f(R)$ Gravities Describing Inflation and the Onset of Accelerated Expansion". *Physical Review D*, **77**, (2008), 046009. [DOI]. [arXiv:0712.4017 (astro-ph)] (cit. on p. 53).

[45] Cooney, A. et al. “Neutron Stars in $f(R)$ Gravity with Perturbative Constraints”. *Physical Review D*, **82**, (2010), 064033. [DOI] (cit. on pp. 52, 83, 84).

[46] Copeland, E. J. et al. “Dynamics of Dark Energy”. *International Journal of Modern Physics D*, **15**, (2006), 1753–1935. [DOI] (cit. on p. 1).

[47] Damour, T. and Esposito-Farèse, G. “Nonperturbative Strong-Field Effects in Tensor-Scalar Theories of Gravitation”. *Physical Review Letters*, **70**, (1993), 2220–2223. [DOI] (cit. on p. 16).

[48] de Aguiar, B. F. and Mendes, R. F. P. “Highly Compact Neutron Stars and Screening Mechanisms. I. Equilibrium and Stability”. *Physical Review D*, **102**, (2020), 024064. [DOI]. [arXiv:2006.10080] (cit. on pp. 35, 52).

[49] de Aguiar, B. F. “Neutron Stars and Screening Mechanisms” (2020), 117 (cit. on p. 35).

[50] De Felice, A. and Tsujikawa, S. “$f(R)$ Theories”. *Living Reviews in Relativity*, **13**, (2010), 3. [DOI]. [arXiv:1002.4928] (cit. on pp. 1, 25, 30, 34, 40, 83, 94).

[51] de la Cruz-Dombriz, A. et al. “Comment on “Viable Singularity-Free $f(R)$ Gravity without a Cosmological Constant”". *Physical Review Letters*, **103**, (2009), 179001. [DOI] (cit. on pp. 37, 45).

[52] de la Cruz-Dombriz, Á. “A Flavour on $f(R)$ Theories: Theory and Observations”. *Modified Gravity and Cosmology: An Update by the CANTATA Network*. Ed. by Saridakis, E. N. et al. Cham: Springer International Publishing, 2021, 43–78. [DOI] (cit. on p. 1).

[53] de la Cruz-Dombriz, A. et al. “Theoretical and Observational Constraints of Viable $f(R)$ Theories of Gravity”. *Physical Review D*, **93**, (2016), 084016. [DOI]. [arXiv:1511.00102] (cit. on p. 48).

[54] Degollado, J. C. et al. “On the Formation of ”Supermassive” Neutron Stars and Dynamical Transition to Spontaneous Scalarization”. *Physics Letters B*, **808**, (2020), 135666. [DOI]. [arXiv:2008.10683] (cit. on p. 16).

[55] Diaz Alonso, J. and Ibanez Cabanell, J. M. “Field Theoretical Model for Nuclear and Neutron Matter. II Neutron Stars”. *The Astrophysical Journal*, **291**, (1985), 308. [DOI] (cit. on p. 16).

[56] Dima, A. et al. “Dynamical Chameleon Neutron Stars: Stability, Radial Oscillations, and Scalar Radiation in Spherical Symmetry”. *Physical Review D*, **104**, (2021), 084017. [DOI] (cit. on p. 35).

[57] Dolgov, A. D. and Kawasaki, M. “Can Modified Gravity Explain Accelerated Cosmic Expansion?” *Physics Letters B*, **573**, (2003), 1–4. [DOI]. [arXiv:astro-ph/0307285] (cit. on pp. 36, 43).

[58] Doneva, D. D. et al. “The I-Q Relations for Rapidly Rotating Neutron Stars in $f(R)$ Gravity”. *Physical Review D*, **92**, (2015), 064015. [DOI]. [arXiv:1507.00378 (astro-ph, physics:gr-qc)] (cit. on p. 84).

[59] Douchin, F. and Haensel, P. “A Unified Equation of State of Dense Matter and Neutron Star Structure”. *Astronomy & Astrophysics*, **380**, (2001), 151–167. [DOI] (cit. on p. 84).

[60] Dunsby, P. K. S. et al. “On the LCDM Universe in $f(R)$ Gravity”. *Physical Review D*, **82**, (2010), 023519. [DOI]. [arXiv:1005.2205] (cit. on p. 2).

[61] Erickcek, A. L. et al. "Solar System Tests Do Rule out $1/R$ Gravity". *Physical Review D*, **74**, (2006), 121501. [DOI] (cit. on pp. 3, 36, 37, 52).

[62] Faraoni, V. "Scalar Field Mass in Generalized Gravity". *Classical and Quantum Gravity*, **26**, (2009), 145014. [DOI]. [arXiv:0906.1901 (gr-qc)] (cit. on pp. 30, 33).

[63] Faraoni, V. and Nadeau, S. "The (Pseudo)Issue of the Conformal Frame Revisited". *Physical Review D*, **75**, (2007), 023501. [DOI]. [arXiv:gr-qc/0612075] (cit. on p. 33).

[64] Faulkner, T. et al. "Constraining $f(R)$ Gravity as a Scalar-Tensor Theory". *Physical Review D*, **76**, (2007), 063505. [DOI] (cit. on pp. 3, 30, 37, 38, 40).

[65] Feng, W.-X. et al. "Equation of State of Neutron Stars with Junction Conditions in the Starobinsky Model". *International Journal of Modern Physics D*, **27**, (2018), 1750186. [DOI]. [arXiv:1702.05936 (gr-qc)] (cit. on p. 85).

[66] Frolov, A. V. "Singularity Problem with $f(R)$ Models for Dark Energy". *Physical Review Letters*, **101**, (2008), 061103. [DOI] (cit. on pp. 3, 28, 34, 52, 94).

[67] Ganguly, A. et al. "Neutron Stars in Starobinsky Model". *Physical Review D*, **89**, (2014), 064019. [DOI]. [arXiv:1309.3279] (cit. on pp. 35, 52, 90).

[68] Guo, J.-Q. "Solar System Tests of $f(R)$ Gravity". *International Journal of Modern Physics D*, **23**, (2014), 1450036. [DOI]. [arXiv:1306.1853] (cit. on pp. 28, 37, 38, 52, 53).

[69] Haensel, P. and Potekhin, A. Y. "Analytical Representations of Unified Equations of State of Neutron-Star Matter". *Astronomy & Astrophysics*, **428**, (2004), 191–197. [DOI] (cit. on p. 21).

[70] Haensel, P. et al. *Neutron Stars: Equation of State and Structure. 1*. Astrophysics and Space Science Library. New York, NY: Springer, 2010 (cit. on p. 15).

[71] Hairer, E. et al. *Solving Ordinary Differential Equations I: Nonstiff Problems*. 2nd rev. ed. Springer Series in Computational Mathematics. Heidelberg ; London: Springer, 2009 (cit. on p. 57).

[72] Hendry, A. W. "A Polytropic Model of the Sun". *American Journal of Physics*, **61**, (1993), 906–910. [DOI] (cit. on p. 13).

[73] Henttunen, K. et al. "Stellar Configurations in $f(R)$ Theories of Gravity". *Physical Review D*, **77**, (2008), 024040. [DOI]. [arXiv:0705.2683] (cit. on pp. 35, 52).

[74] Higuchi, Y. and Shirasaki, M. "The Imprint of $f(R)$ Gravity on Weak Gravitational Lensing I: Connection between Observables and Large Scale Structure". *Monthly Notices of the Royal Astronomical Society*, **459**, (2016), 2762–2776. [DOI]. [arXiv:1603.01325] (cit. on p. 2).

[75] Hu, W. and Sawicki, I. "Models of $f(R)$ Cosmic Acceleration That Evade Solar-System Tests". *Physical Review D*, **76**, (2007), 064004. [DOI]. [arXiv:0705.1158] (cit. on pp. 1, 2, 47, 48, 53, 81).

[76] Hull, T. E. et al. "Comparing Numerical Methods for Ordinary Differential Equations". *SIAM Journal on Numerical Analysis*, **9**, (1972), 603–637 (cit. on p. 57).

[77] Jaime, L. G. and Salgado, M. "Cosmic Acceleration in Asymptotically Ricci Flat Universe". *Physical Review D*, **98**, (2018), 084045. [DOI]. [arXiv:1711.08026] (cit. on pp. 3, 25).

[78] Jaime, L. G. et al. “Robust Approach to $f(R)$ Gravity”. *Physical Review D*, **83**, (2011), 024039. [DOI]. [arXiv:1006.5747] (cit. on pp. 2–4, 26, 28, 33, 35, 45, 47, 52, 53, 57, 58).

[79] Jaime, L. G. et al. “$f(R)$ Cosmology Revisited”. *arXiv:1206.1642* (2012). [arXiv:1206.1642 (astro-ph)] (cit. on pp. 1, 3, 34, 44–47, 64).

[80] Jaime, L. G. et al. “Note on the Equation of State of Geometric Dark-Energy in f(R) Gravity”. *Physical Review D*, **89**, (2014), 084010. [DOI]. [arXiv:1312.5428] (cit. on p. 27).

[81] Jana, S. and Mohanty, S. “Constraints on $f(R)$ Theories of Gravity from GW170817”. *Physical Review D*, **99**, (2019), 044056. [DOI]. [arXiv:1807.04060] (cit. on p. 2).

[82] Joyce, A. et al. “Beyond the Cosmological Standard Model”. *Physics Reports*, **568**, (2015), 1–98. [DOI]. [arXiv:1407.0059] (cit. on pp. 3, 25).

[83] Kainulainen, K. et al. “Spherically Symmetric Spacetimes in $f(R)$ Gravity Theories”. *Physical Review D*, **76**, (2007), 024020. [DOI]. [arXiv:0704.2729] (cit. on pp. 26, 35, 52).

[84] Kainulainen, K. et al. “The Interior Spacetimes of Stars in Palatini $f(R)$ Gravity”. *Physical Review D*, **76**, (2007), 043503. [DOI]. [arXiv:gr-qc/0611132] (cit. on pp. 26, 29).

[85] Kase, R. and Tsujikawa, S. “Neutron Stars in $f(R)$ Gravity and Scalar-Tensor Theories”. *Journal of Cosmology and Astroparticle Physics*, **2019**, (2019), 054–054. [DOI]. [arXiv:1906.08954] (cit. on pp. 30, 52, 83, 84).

[86] Khoury, J. and Weltman, A. “Chameleon Cosmology”. *Physical Review D*, **69**, (2004), 044026. [DOI]. [arXiv:astro-ph/0309411] (cit. on pp. 28, 29, 31, 35, 37, 39, 40).

[87] Khoury, J. and Weltman, A. “Chameleon Fields: Awaiting Surprises for Tests of Gravity in Space”. *Physical Review Letters*, **93**, (2004), 171104. [DOI]. [arXiv:astro-ph/0309300] (cit. on pp. 37, 39, 40).

[88] Kobayashi, T. and Maeda, K.-i. “Relativistic Stars in $f(R)$ Gravity, and Absence Thereof”. *Physical Review D*, **78**, (2008), 064019. [DOI]. [arXiv:0807.2503] (cit. on pp. 3, 28, 46, 52, 53, 57, 63).

[89] Kobayashi, T. and Maeda, K.-i. “Can Higher Curvature Corrections Cure the Singularity Problem in $f(R)$ Gravity?” *Physical Review D*, **79**, (2009), 024009. [DOI] (cit. on p. 52).

[90] Lattimer, J. M. and Prakash, M. “Neutron Star Observations: Prognosis for Equation of State Constraints”. *Physics Reports*, **442**, (2007), 109–165. [DOI]. [arXiv:astro-ph/0612440] (cit. on p. 15).

[91] Legred, I. et al. “Implicit Correlations within Phenomenological Parametric Models of the Neutron Star Equation of State”. *Physical Review D*, **105**, (2022), 043016. [DOI]. [arXiv:2201.06791 (astro-ph, physics:gr-qc, physics:nucl-th)] (cit. on p. 20).

[92] Levi, M. E. et al. *The Dark Energy Spectroscopic Instrument (DESI)*. 2019. [DOI]. [arXiv:1907.10688 (astro-ph)] (cit. on p. 92).

[93] Liddle, A. R. and Lyth, D. H. *Cosmological Inflation and Large-Scale Structure*. Cambridge: Cambridge University Press, 2000. [DOI] (cit. on p. 1).

[94] Liu, T. et al. "Constraining $f(R)$ Gravity in Solar System, Cosmology and Binary Pulsar Systems". *Physics Letters B*, **777**, (2018), 286–293. [DOI] (cit. on pp. 30, 37, 40, 52).

[95] Martin, J. "Everything You Always Wanted To Know About The Cosmological Constant Problem (But Were Afraid To Ask)". *Comptes Rendus Physique*, **13**, (2012), 566–665. [DOI]. [arXiv:1205.3365 (astro-ph)] (cit. on p. 25).

[96] Miranda, V. et al. "Viable Singularity-Free $f(R)$ Gravity Without a Cosmological Constant". *Physical Review Letters*, **102**, (2009), 221101. [DOI]. [arXiv:0905.1941] (cit. on pp. 2, 28, 34, 44, 45, 50, 52, 53, 58).

[97] Miranda, V. et al. "Miranda et al. Reply:" *Physical Review Letters*, **103**, (2009), 179002. [DOI] (cit. on pp. 45, 57).

[98] Motohashi, H. et al. "$f(R)$ Gravity and Its Cosmologicals Implications". *International Journal of Modern Physics D*, **20**, (2011), 1347–1355. [DOI] (cit. on pp. 2, 25, 46).

[99] Multamaki, T. and Vilja, I. "Static Spherically Symmetric Perfect Fluid Solutions in $f(R)$ Theories of Gravity". *Physical Review D*, **76**, (2007), 064021. [DOI]. [arXiv:astro-ph/0612775] (cit. on pp. 35, 52).

[100] Multamaki, T. and Vilja, I. "Constraining Newtonian Stellar Configurations in $f(R)$ Theories of Gravity". *Physics Letters B*, **659**, (2008), 843–846. [DOI]. [arXiv:0709.3422] (cit. on pp. 35, 52).

[101] Multamaki, T. and Vilja, I. "Spherically Symmetric Solutions of Modified Field Equations in $f(R)$ Theories of Gravity". *Physical Review D*, **74**, (2006), 064022. [DOI]. [arXiv:astro-ph/0606373] (cit. on p. 35).

[102] Navarro, I. and Van Acoleyen, K. "$f(R)$ Actions, Cosmic Acceleration and Local Tests of Gravity". *Journal of Cosmology and Astroparticle Physics*, **2007**, (2007), 022–022. [DOI]. [arXiv:gr-qc/0611127] (cit. on pp. 35, 40).

[103] Negrelli, C. et al. "Solar System Tests and Chameleon Effect in $f(R)$ Gravity". *Physical Review D*, **101**, (2020), 064005. [DOI]. [arXiv:2002.12073] (cit. on pp. 3, 37, 38, 40, 44–46, 48, 52, 53, 81).

[104] Nojiri, S. et al. "Modified Gravity Theories on a Nutshell: Inflation, Bounce and Late-time Evolution". *Physics Reports*, **692**, (2017), 1–104. [DOI]. [arXiv:1705.11098] (cit. on pp. 1, 30, 34).

[105] Nojiri, S. and Odintsov, S. D. "Can $f(R)$-Gravity Be a Viable Model: The Universal Unification Scenario for Inflation, Dark Energy and Dark Matter". *arXiv:0801.4843 [astro-ph]* (2008). [arXiv:0801.4843 (astro-ph)] (cit. on p. 25).

[106] Odintsov, S. D. et al. "Quantitative Predictions for $f(R)$ Gravity Primordial Gravitational Waves". *arXiv:2108.11231 [astro-ph]* (2022). [arXiv:2108.11231 (astro-ph)] (cit. on p. 2).

[107] Olmo, G. J. "Limit to General Relativity in $f(R)$ Theories of Gravity". *Physical Review D*, **75**, (2007), 023511. [DOI]. [arXiv:gr-qc/0612047] (cit. on p. 29).

[108] Olmo, G. J. "Re-Examination of Polytropic Spheres in Palatini f(R) Gravity". *Physical Review D*, **78**, (2008), 104026. [DOI]. [arXiv:0810.3593] (cit. on p. 26).

[109] Orellana, M. et al. "Structure of Neutron Stars in R-squared Gravity". *General Relativity and Gravitation*, **45**, (2013), 771–783. [DOI]. [arXiv:1301.5189 (astro-ph, physics:gr-qc)] (cit. on pp. 52, 84).

[110] Pearson, J. M. et al. "Inner Crust of Neutron Stars with Mass-Fitted Skyrme Functionals". *Physical Review C*, **85**, (2012), 065803. [DOI]. [arXiv:1206.0205] (cit. on p. 85).

[111] Perlmutter, S. et al. "Measurements of Omega and Lambda from 42 High-Redshift Supernovae". *The Astrophysical Journal*, **517**, (1999), 565–586. [DOI]. [arXiv:astro-ph/9812133] (cit. on p. 1).

[112] Poisson, E. and Will, C. M. *Gravity: Newtonian, Post-Newtonian, Relativistic*. Cambridge ; New York: Cambridge University Press, 2014 (cit. on pp. 5–7, 13).

[113] Potekhin, A. Y. et al. "Analytical Representations of Unified Equations of State for Neutron-Star Matter". *Astronomy & Astrophysics*, **560**, (2013), A48. [DOI]. [arXiv:1310.0049] (cit. on p. 85).

[114] Press, W. H., ed. *Numerical Recipes: The Art of Scientific Computing*. 3rd ed. Cambridge, UK ; New York: Cambridge University Press, 2007 (cit. on p. 9).

[115] Quiros, I. et al. "The Conformal Transformation's Controversy: What Are We Missing?" *General Relativity and Gravitation*, **45**, (2013), 489–518. [DOI]. [arXiv:1108.5857 (gr-qc, physics:hep-th)] (cit. on p. 33).

[116] Rackauckas, C. and Nie, Q. "DifferentialEquations.Jl – A Performant and Feature-Rich Ecosystem for Solving Differential Equations in Julia". *Journal of Open Research Software*, **5**, (2017), 15. [DOI] (cit. on p. 57).

[117] Read, J. S. et al. "Constraints on a Phenomenologically Parameterized Neutron-Star Equation of State". *Physical Review D*, **79**, (2009), 124032. [DOI]. [arXiv:0812.2163] (cit. on pp. 15, 19–23).

[118] Read, J. S. et al. "Measuring the Neutron Star Equation of State with Gravitational Wave Observations". *Physical Review D*, **79**, (2009), 124033. [DOI]. [arXiv:0901.3258] (cit. on p. 20).

[119] Rezzolla, L. and Zanotti, O. *Relativistic Hydrodynamics*. First edition. Oxford: Oxford University Press, 2013 (cit. on p. 7).

[120] Riess, A. G. et al. "Observational Evidence from Supernovae for an Accelerating Universe and a Cosmological Constant". *The Astronomical Journal*, **116**, (1998), 1009–1038. [DOI]. [arXiv:astro-ph/9805201] (cit. on p. 1).

[121] Sakstein, J. "Astrophysical Tests of Modified Gravity". *arXiv:1502.04503 [astro-ph]* (2015). [arXiv:1502.04503 (astro-ph)] (cit. on p. 39).

[122] Salgado, M. et al. "High Precision Rotating Neutron Star Models. I. Analysis of Neutron Star Properties." *Astronomy and Astrophysics*, **291**, (1994), 155–170 (cit. on pp. 15–17).

[123] Sami, M. and Myrzakulov, R. "Late-Time Cosmic Acceleration: ABCD of Dark Energy and Modified Theories of Gravity". *International Journal of Modern Physics D*, **25**, (2016), 1630031. [DOI] (cit. on p. 25).

[124] Santos, E. "Neutron Stars in Generalized $f(R)$ Gravity". *Astrophysics and Space Science*, **341**, (2012), 411–416. [DOI]. [arXiv:1104.2140] (cit. on pp. 52, 89).

[125] Sbisà, F. et al. "Pressure Effects in the Weak-Field Limit of f(R) = R + Alpha R2̂ Gravity". *Physical Review D*, **99**, (2019), 104046. [DOI]. [arXiv:1811.01322] (cit. on p. 37).

[126] Sbisà, F. et al. "Neutron Star Masses in R^2-Gravity". *Physics of the Dark Universe*, **27**, (2020), 100411. [DOI] (cit. on p. 85).

[127] Seifert, M. D. "Stability of Spherically Symmetric Solutions in Modified Theories of Gravity". *Physical Review D*, **76**, (2007), 064002. [DOI] (cit. on p. 35).

[128] Shampine, L. F. "Some Practical Runge-Kutta Formulas". *Mathematics of Computation*, **46**, (1986), 135–150. [DOI] (cit. on p. 57).

[129] Shapiro, S. L. and Teukolsky, S. A. *Black Holes, White Dwarfs, and Neutron Stars: The Physics of Compact Objects*. First. Wiley, 1983. [DOI] (cit. on pp. 5, 7).

[130] Shtanov, Y. "On the Conformal Frames in $f(R)$ Gravity". *Universe*, **8**, (2022), 69. [DOI]. [arXiv:2202.00818 (astro-ph, physics:gr-qc)] (cit. on p. 33).

[131] Silvestri, A. and Trodden, M. "Approaches to Understanding Cosmic Acceleration". *Reports on Progress in Physics*, **72**, (2009), 096901. [DOI] (cit. on pp. 1, 2, 25, 34).

[132] Song, Y.-S. et al. "Cosmological Constraints on $f(R)$ Acceleration Models". *Physical Review D*, **76**, (2007), 063517. [DOI]. [arXiv:0706.2399] (cit. on p. 2).

[133] Sotiriou, T. P. *$F(R)$ Gravity and Scalar-Tensor Theory*. 2006. [DOI]. [arXiv:gr-qc/0604028] (cit. on p. 30).

[134] Sotiriou, T. P. and Faraoni, V. "$F(R)$ Theories Of Gravity". *Reviews of Modern Physics*, **82**, (2010), 451–497. [DOI]. [arXiv:0805.1726] (cit. on pp. 1, 2, 25, 30).

[135] Sotiriou, T. P. and Liberati, S. "Metric-Affine $f(R)$ Theories of Gravity". *Annals of Physics*, **322**, (2007), 935–966. [DOI]. [arXiv:gr-qc/0604006] (cit. on p. 26).

[136] Starobinsky, A. A. "A New Type of Isotropic Cosmological Models without Singularity". *Physics Letters B*, **91**, (1980), 99–102. [DOI] (cit. on pp. 25, 35, 83).

[137] Starobinsky, A. A. "Disappearing Cosmological Constant in $f(R)$ Gravity". *JETP Letters*, **86**, (2007), 157–163. [DOI] (cit. on pp. 1–3, 33, 45, 93).

[138] Staykov, K. V. et al. "Slowly Rotating Neutron and Strange Stars in R^2 Gravity". *Journal of Cosmology and Astroparticle Physics*, **2014**, (2014), 006–006. [DOI]. [arXiv:1407.2180] (cit. on p. 84).

[139] Stergioulas, N. "Rotating Stars in Relativity". *Living Reviews in Relativity*, **6**, (2003), 3. [DOI]. [arXiv:gr-qc/0302034] (cit. on p. 5).

[140] Straumann, N. "Problems with Modified Theories of Gravity, as Alternatives to Dark Energy". *arXiv:0809.5148 [astro-ph, physics:gr-qc]* (2008). [arXiv:0809.5148 (astro-ph, physics:gr-qc)] (cit. on p. 1).

[141] Sultana, J. and Kazanas, D. "A No-Hair Theorem for Spherically Symmetric Black Holes in R^2 Gravity". *General Relativity and Gravitation*, **50**, (2018), 137. [DOI]. [arXiv:1810.02915 (gr-qc)] (cit. on p. 29).

[142] Tamaki, T. and Tsujikawa, S. "Revisiting Chameleon Gravity: Thin-shell and No-Shell Fields with Appropriate Boundary Conditions". *Physical Review D*, **78**, (2008), 084028. [DOI] (cit. on pp. 39, 40).

[143] Thongkool, I. et al. "Constraining $f(R)$ Gravity Models with Disappearing Cosmological Constant". *Physical Review D*, **80**, (2009), 043523. [DOI]. [arXiv:0906.2460 (astro-ph, physics:gr-qc, physics:hep-ph, physics:hep-th)] (cit. on pp. 48, 50).

[144] Tsujikawa, S. et al. "Constraints on Scalar-Tensor Models of Dark Energy from Observational and Local Gravity Tests". *Physical Review D*, **77**, (2008), 103009. [DOI]. [arXiv:0803.1106 (astro-ph)] (cit. on p. 40).

[145] Upadhye, A. and Hu, W. "Existence of Relativistic Stars in $f(R)$ Gravity". *Physical Review D*, **80**, (2009), 064002. [DOI] (cit. on pp. 3, 28, 35, 46, 52, 53, 65).

[146] Velasquez, J. and Castaneda, L. "Equivalence between Scalar-Tensor Theories and $f(R)$-Gravity: From the Action to Cosmological Perturbations". *Journal of Physics Communications*, **4**, (2020), 055007. [DOI]. [arXiv:1808.05615] (cit. on pp. 2, 29).

[147] Verner, J. H. "Explicit Runge-Kutta Methods with Estimates of the Local Truncation Error". *SIAM Journal on Numerical Analysis*, **15**, (1978), 772–790 (cit. on p. 57).

[148] Wald, R. M. *General Relativity*. Chicago: University of Chicago Press, 1984 (cit. on pp. 1, 4, 5, 7, 11, 31, 33).

[149] Weinberg, D. H. et al. "Observational Probes of Cosmic Acceleration". *Physics Reports*, **530**, (2013), 87–255. [DOI]. [arXiv:1201.2434] (cit. on pp. 1, 25).

[150] Weinberg, S. "Infrared Photons and Gravitons". *Physical Review*, **140**, (1965), B516–B524. [DOI] (cit. on p. 2).

[151] Will, C. M. "The Confrontation between General Relativity and Experiment". *Living Reviews in Relativity*, **9**, (2006), 3. [DOI]. [arXiv:gr-qc/0510072] (cit. on pp. 2, 6, 40).

[152] Woodard, R. P. "Avoiding Dark Energy with 1/R Modifications of Gravity". Vol. 720. 2007, 403–433. [DOI]. [arXiv:astro-ph/0601672] (cit. on p. 25).

[153] Yazadjiev, S. S. et al. "Non-Perturbative and Self-Consistent Models of Neutron Stars in R-squared Gravity". *Journal of Cosmology and Astroparticle Physics*, **2014**, (2014), 003–003. [DOI]. [arXiv:1402.4469] (cit. on pp. 52, 83, 84, 90).

[154] Yu, S. et al. "On Static and Spherically Symmetric Solutions of Starobinsky Model". *Research in Astronomy and Astrophysics*, **18**, (2018), 157. [DOI]. [arXiv:1711.04064] (cit. on p. 35).

[155] Zhang, P. "The Behavior of $f(R)$ Gravity in the Solar System, Galaxies and Clusters". *Physical Review D*, **76**, (2007), 024007. [DOI]. [arXiv:astro-ph/0701662] (cit. on p. 37).